DESIGN, FABRICATION AND TESTING OF A WEARABLE COOLING SYSTEM

A Thesis
Presented to
The Academic Faculty

By

Timothy C. Ernst

In Partial Fulfillment
Of the Requirements for the Degree
Masters of Science in Mechanical Engineering

Georgia Institute of Technology
February 2005

DESIGN, FABRICATION AND TESTING OF A WEARABLE COOLING SYSTEM

Approved by:

Dr. Srinivas Garimella, Chair
School of Mechanical Engineering
Georgia Institute of Technology

Dr. Samuel Shelton
School of Mechanical Engineering
Georgia Institute of Technology

Dr. David Rosen
School of Mechanical Engineering
Georgia Institute of Technology

Date Approved: February 2005

To my wife Terri who provided me with the much needed support and love throughout this endeavor. And also to my parents who have always encouraged and supported me.

ACKNOWLEDGEMENTS

I would like to thank the members of the Sustainable Thermal Systems Laboratory at Georgia Institute of Technology, namely the director Dr. Srinivas Garimella who provided this research opportunity to me and served as my advisor. The students in the laboratory also helped in many ways by offering advice and help whenever asked. I especially thank Jesse Killion, Matt Determan and David Falkowski for their input and for their willingness to discuss the many aspects of the project that proved difficult to resolve. I also appreciate the help of Lalit Bohra as he answered the many questions I had throughout the process of writing and formatting my thesis.

Timothy C. Ernst

TABLE OF CONTENTS

Page

ACKNOWLEDGEMENTS iv

LIST OF TABLES ix

LIST OF FIGURES x

LIST OF SYMBOLS xiii

SUMMARY xviii

Chapter

1. INTRODUCTION 1

    1.1 Background 1

        1.1.1 System Power 2

        1.1.2 Thermodynamic Cycle of the Portable Cooling System 6

        1.1.3 Heat Removal to the Ambient 8

    1.2 Scope of Current Research 13

    1.3 Thesis Organization 14

2. LITERATURE REVIEW 15

    2.1 Portable Cooling Systems 15

        2.1.1 Phase-Change Materials 15

        2.1.2 Adsorption Systems 16

        2.1.3 Absorption Cycle 16

        2.1.4 Brayton Cycle 17

    2.2 Cooling Garments 20

    2.3 Summary 23

3. EXPERIMENTAL SETUP 25
3.1 Compressor Testing 25
3.1.1 Compressor Description 25
3.1.2 Compressor Housing 29
3.1.3 Vapor-Compression System Description 31
3.1.4 Coolant System Description 36
3.1.5 Auxiliary Components 38
3.1.6 System Operation 41
3.1.7 Compressor Testing Results 42
3.2 Finalized Overall System 43
3.2.1 Finalized System Component Description 43
3.2.2 Finalized System Testing 50
4. DATA ANALYSIS 58
4.1 System Overview 58
4.2 Cycle Diagrams 61
4.3 Sample Calculations 62
4.3.1 Thermodynamic Cycle Analysis 62
4.3.2 Air-Side Analysis 66
4.3.3 Coolant-Side Analysis 68
4.3.4 System Performance 69
4.3.5 Error Analysis 70
4.3.6 Ambient Heat Loss/Gain Calculations 72
5. RESULTS 78

5.1 Cooling System Performance 78
5.1.1 Performance at Constant Ambient Temperature 80
5.1.2 Performance at Constant Engine Speed 82
5.1.3 Performance at Constant Evaporator Temperature 84
5.1.4 Effect of Increased Engine Speed 86
5.2 Fuel Consumption 87
6. WEARABLE SYSTEM 91
6.1 Wearable Evaporator 91
6.1.1 Wearable Evaporator Modeling 91
6.1.2 Cooling Garment Description 92
6.2 System Mass 97
7. CONCLUSIONS AND RECOMMENDATIONS 98
7.1 Conclusions 98
7.2 Recommendations 99
7.2.1 Engine and Gear Train Modifications 100
7.2.2 Compressor Modifications 101
7.2.3 Condenser Modifications 102
7.2.4 User Comfort Characterization 103
APPENDIX A - THERMODYNAMIC CYCLE ANALYSIS 104
A.1 System Inputs 104
A.2 Vapor Compression Cycle Analysis 106
A.2.1 State Points 106
A.2.2 Energy and Mass Balances 108

APPENDIX B – CONDENSER DESIGN 111
B.1 Condenser Description 111
B.2 Condenser Geometry 112
B.3 Air-Side Calculations 114
B.3.1 Air-Side Heat Transfer 115
B.3.2 Air-Side Pressure Drop 117
B.4 Refrigerant-Side Heat Transfer and Pressure Drop 118
B.5 Condenser Selection 121
APPENDIX C – EVAPORATOR MODELING 123
C.1 Evaporator Description 123
C.2 Energy Balance 124
C.3 Heat Gain from the Environment 128
C.4 Refrigerant-Side Heat Transfer and Pressure Drop 131
APPENDIX D – ANALYSIS OF A REPRENTATIVE DATA POINT 134
D.1 Sample Point - Heat Duty Calculation 134
APPENDIX E – FAN CORRELATION 142
E.1 Fan Measurements 142
REFERENCES 146

LIST OF TABLES

Table		Page
1.1	Refrigerant Selection Matrix (Calm and Hourahan, 2001)	7
2.1	Portable Cooling Systems Summary	19
3.1	Condenser Geometry and Performance	34
4.1	Measured Data	60
4.2	Heat Transfer with the Ambient	77
5.1	Fuel Consumption Rates	89
6.1	Evaporator Geometry	95
6.2	Component and System Mass	97
A.1	Thermodynamic Cycle Inputs	104
B.1	Condenser Geometry	112
D.1	Measured Data	134
D.2	Thermodynamic Cycle Calculations	136
D.3	Air-Side Analysis	137
D.4	Coolant-Side Analysis	138
D.5	System Performance Analysis	138
D.6	Error Analysis Calculation	139
D.7	Ambient Heat Gain/Loss Calculation	140
E.1	Air Flow Readings	144

LIST OF FIGURES

Figure		Page
1.1	Energy Density Comparison……	3
1.2	Volumetric Energy Density Comparison……	4
1.3	Condenser Comparison – Wearable vs. Pack-Mounted……..	10
1.4	Insulation Heat Gain Percentage……	11
1.5	Input Power Versus Mass Flow Rate of Air……..	12
2.1	Brayton Cycle Cooling System Schematic (Rahman, 1996)……..	18
3.1	Air Compressor Details……	26
3.2	Compressor – Intake Stroke……..	27
3.3	Compressor – Compression Stroke……	27
3.4	Compressor Enclosure……	29
3.5	Compressor Enclosure Layout……	30
3.6	Compressor Testing Configuration……	31
3.7	Representative Condenser Section……..	32
3.8	Refrigerant Condenser……	33
3.9	Test Evaporator Coolant Tank……	36
3.10	Plexiglas Enclosure Surrounding Test Facility……..	38
3.11	Compressed Air Motor……..	39
3.12	Reduction Gearing to Compressor……	40
3.13	Compressor Testing Arrangement……	42
3.14	Finalized Portable Cooling System Configuration……	43
3.15	CAD Model of System……..	44
3.16	Isometric Views of the System……	45

Figure		Page
3.17	Reduction Gear Train……	45
3.18	Gear Layout and Ratios…….	46
3.19	Compressor Layout……	48
3.20	Cooling System Test Configuration……...	50
3.21	Cooling System Being Tested at Controlled Elevated Temperatures……	52
3.22	Plexiglas Enclosure Inside Air Handler (2 Views)……	53
3.23	Test Evaporator……..	55
3.24	Test Loop Schematic……..…	56
4.1	Portable Cooling System Schematic……..…	59
4.2	Temperature-Entropy Diagram for the Representative Data Point…….....	61
4.3	Pressure-Enthalpy Diagram for the Representative Data Point…….	62
4.4	Ambient Heat Transfer Locations……..	73
5.1	Pressure versus Enthalpy Diagram Across the Test Matrix……...	78
5.2	Full Test Results…….	79
5.3	Heat Duty versus Engine Speed…….	80
5.4	Heat Duty versus Ambient Temperature……	83
5.5	Heat Duty versus Engine Speed…….	85
5.6	Heat Duty versus Engine Speed ($T_{evap,coolant}$ = 28°C, T_{amb} = 43.3°C)……	86
5.7	Variation of Fuel Consumption Rate with Ambient Air Temperature……..	88
6.1	Representative Section of Wearable Evaporator Garment…….	91
6.2	Cooling Garment Exterior……..	93
6.3	Cooling Garment Construction……...	93
6.4	Cooling Garment Interior……	94
6.5	Portable Cooling System Testing……	96

Figure **Page**

A.1 Simplified Thermodynamic Cycle……106

A.2 Pressure-Enthalpy Diagram of Thermodynamic Cycle……108

B.1 Representative Condenser Section……111

B.2 Frontal View of Simplified Condenser Geometry……112

B.3 Condenser Multi-Louver Fin……113

B.4 Multi-Louver Fin Cross-Section……113

C.1 Representative Section of Wearable Evaporator Garment……123

C.2 Heat Transfer to Evaporator……...124

C.3 Differential Element of Evaporator Fin……126

C.4 Foil Temperature Profile……128

E.1 Turbine Anemometer Path……143

E.2 Condenser Face Air Velocity……144

LIST OF SYMBOLS

A	area (m^2)
a	fan constant
C	flow coefficient
CAT	closest approach temperature (°C)
c_p	specific heat (J/kg-K)
Co	convection number
D_h	hydraulic diameter (m)
$\dot{E}$	energy usage rate (W)
F	view factor
f	flow coefficient, friction factor
F_d	flow depth (m)
F_p	fin pitch (m)
g	gravity (m/s^2)
h	enthalpy (J/kg), height (m), convection coefficient (W/m^2-K)
$\bar{h}$	average convection coefficient (W/m^2-K)
I	current (A)
ID	inner diameter (m)
j	convective heat transfer factor
k	thermal conductivity (W/m-K)
l	length (m)
L	length (m), louver

LHV	lower heating value (J/kg)
LMTD	log mean temperature difference (°C)
M	physical activity level (MET)
m	mass (kg), thermal resistance ratio
$\dot{m}$	mass flow rate (kg/s)
N	quantity
$\overline{Nu}$	average Nusselt number
OD	outer diameter (m)
P	perimeter (m), pressure (kPa)
Pr	Prandtl number
p_r	pressure ratio
$\dot{Q}$	thermal energy transfer (W)
R	thermal resistance (K/W), effective temperature (°C)
Ra	Rayleigh number
RPM	rotational speed (revolutions/minute)
T	temperature (°C), tube
t	time (s), thickness (m)
U	uncertainty
V	voltage (V)
$\dot{V}$	volumetric flow rate (m^3/s)
v	velocity (m/s)
vol	volume (m^3)
$\dot{vol}$	volumetric flow rate (m^3/s)

$\dot{W}$	work input (W)
w	width (m)
X	flow coefficient
x	refrigerant quality, position (m)
z	length (m)

Greek Letters

α	thermal diffusivity (m^2/s)
β	thermal expansion coefficient (1/K)
Δ	amount of change
δ	difference
δ_{fin}	fin thickness (m)
ε	emissivity
η	efficiency, system performance coefficient
μ	dynamic viscosity ($N\text{-}s/m^2$)
ν	kinematic viscosity (m^2/s)
ρ	density (kg/m^3)
σ	Boltzman's constant ($W/m^2\text{-}K^4$)
ϕ	flow coefficient
ψ_s	convection number function

Sub-scripts and Super-scripts

amb	ambient

c	cross-sectional, compressor
comp	compressor
cond	condenser
conv	convection
D	diameter
evap	evaporator
exp	expansion valve
F	flow
f	fins
fr	frontal
G	gas
i	in
inf	infinity
ins	insulation
int	internal
isen	isentropic
L	liquid
liq	liquid
L_p	louver pitch
m	mean
o	out
p	pitch
rad	radiation

ref	refrigerant
s	surface
surf	surface
t	tube
tot	total
tpm	two-phase mean
x=0	quality of zero
x=1	quality of one

SUMMARY

A wearable cooling system was developed in this study for use in elevated temperature environments by military, fire-fighting, chemical-response, and other hazardous duty personnel. Such a system is expected to reduce heat-related stresses, increasing productivity and allowable mission duration, reduce fatigue, and lead to a safer working environment. The cooling system consists of an engine-driven vapor-compression system assembled in a backpack configuration, coupled with a cooling garment containing refrigerant lines worn in close proximity to the skin. A 2.0 L fuel tank in the backpack powers a small-scale engine that runs a compressor modified from the original air compression application to the refrigerant compression application here. A centrifugal clutch and reduction gear train system was designed and fabricated to couple the engine output to the refrigerant compressor and heat rejection fan. The overall cooling system, including the wearable evaporator, had a total mass of 5.31 kg (11.7 lb) and measured 0.318 × 0.273 × 0.152 m (12.5 × 10.75 × 6 inches).

Testing was conducted in a controlled environment to determine system performance over a wide range of expected ambient temperatures (37.7-47.5°C), evaporator refrigerant temperatures (22.2-26.1°C), and engine speeds (10,500-13,300 RPM). Heat removal rates of up to 300 W, which is the cooling rate established in the literature as being required for maintaining comfort at an activity level comparable to calisthenics or moderate exercise, were demonstrated at a nominal ambient temperature of 43.3°C (110°F). Modeling the fuel as 88 percent methanol (LHV ~ 1.992×10^7 J/kg) and 12 percent oil, the system consumed 1750 W at an average fuel mass flow rate of 0.316 kg/hr to provide a nominal cooling rate of 178 W for 5.7 hrs between refueling.

1. INTRODUCTION

1.1 Background

Reducing thermal stresses for hazardous-duty personnel can increase productivity and allowable durations of missions, reduce fatigue, and lead to a safer working environment. Thermal stresses can be reduced by means of portable cooling systems in elevated temperature environments. Potential users of such systems include the military, fire-fighters, and other hazardous duty and chemical-spill response personnel. Semi-portable cooling systems that connect to centralized cooling systems are available, however this requires the user to be tethered to a fixed point at a certain radius, thus restricting the range of motion. Therefore, a completely self-contained, portable cooling system was developed in this study.

The three major challenges in the development of such portable cooling systems are as follows:

- the method of providing input power
- the miniaturization of the cooling system components
- the method of heat dissipation to the ambient air

Because this system is to be used in a portable manner, developing a system that is as lightweight and compact as possible is a key concern. The system is intended to be used independently from any external (stationary) power or input, which requires that the cooling system be capable of providing the required input power, as well as operating independently in the environment in which the user functions. This environment is often at an elevated temperature, which further increases the challenge of heat removal and rejection.

1.1.1 System Power

As mentioned earlier, one of the greatest challenges in developing such a system is that, like any air conditioning system, transferring heat against the direction of its natural flow requires significant input power. In addition, to achieve an acceptably long cooling duration (and thus length of mission), this power must be supplied for a commensurate amount of time, increasing in turn, the total energy supply carried by the user. There are several portable sources of power to choose from, including batteries, fuel cells, compressed air tanks, miniature-scale engines, and so on. All have certain benefits and limitations that must be taken into account when determining the appropriate power source. One of the more important factors is the energy density of the source: higher energy densities lead to a lower weight and volume requirement for the power source. The best choice for the particular application depends on the required mission duration.

To evaluate the various power source options, a comparison of the estimated mass of the power source versus the required duration of cooling was conducted for a nominal cooling load of 400 W. To perform this comparison, it was assumed at the outset that a vapor-compression cycle would be used to supply the cooling. A preliminary thermodynamic cycle analysis for this vapor-compression cycle was conducted using *Engineering Equation Solver* (EES) software (Klein, 2004). The cycle analysis description and detailed equations can be found in Appendix A. The analysis showed that approximately 200 W of input power would be required to provide the cooling. The three sources of power evaluated were: lithium-ion batteries, a hydrogen fuel cell and a miniature-scale engine. The lithium-ion batteries were estimated to have an energy density of 137.5 W-hr/kg (Buchmann, 2001) and result in a linear scaling of power

system weight versus time. The fuel cell alone was estimated to be 6 kg (ElectroChem, 2005), plus the necessary fuel to provide the 200 W of input power. The mass flow rate of the hydrogen to the fuel cell was estimated to be 0.054 kg/hr: this mass flow rate was approximated using the enthalpy of formation of the reactants and products along with an estimated fuel cell efficiency of 50 percent. Finally, the engine weight was estimated to be 1 kg, with a fuel mass flow rate of 0.314 kg/hr (Bair, 2003). According to Bair, a representative estimate of the fuel consumption for small-scale engines is typically 2.6 lb/hp-hr (1.58×10^{-3} kg/W-hr). Figure 1.1 shows the resulting comparison of power source weight versus the cooling duration.

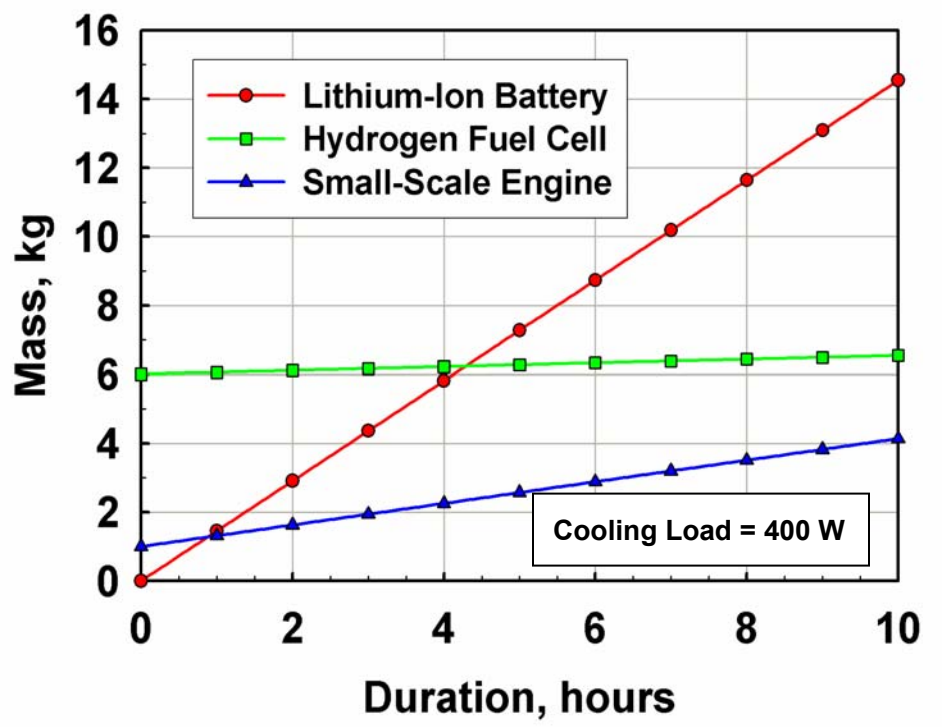

Figure 1.1 Energy Density Comparison

As displayed in Figure 1.1, the use of batteries results in essentially a linear profile based on cooling duration, since the amount of energy batteries can deliver depends on the mass

of batteries being used. For the graph of the engine and the fuel cell, both have an initial mass equal to the individual component's mass, in addition to the mass of fuel required for operation. The mass of fuel for the fuel cell and engine both scale proportionately with time. The fuel cell starts with a relatively high mass, however, the mass flow rate of the fuel is much lower than that of the engine due to the higher efficiency of fuel cells in converting fuel to useful mechanical energy. This would result in a more gradual increase in overall mass with duration compared to the overall mass of the engine-based system. However, the considerable difference in initial mass renders the engine lighter than the fuel cell for durations well past the longest anticipated duration of ten hours. For durations shorter than one hour, Figure 1.1 shows that based on system mass considerations, batteries would be the appropriate choice for the power source.

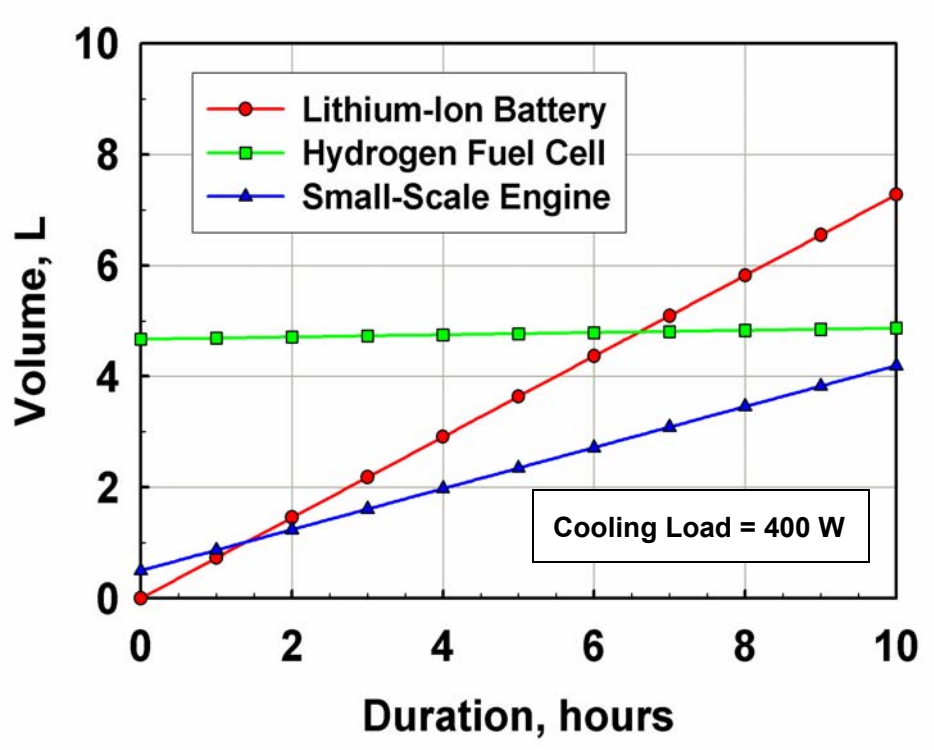

Figure 1.2 Volumetric Energy Density Comparison

Figure 1.2 shows the variation of the volume of the batteries, fuel cell and engine with cooling duration. Volumetric energy density is another important consideration, because it determines the compactness of the fuel source, and in turn, the overall system. Again, the tare volume of the power source is taken into account, as well as the variation based on the desired cooling duration, when the different options are compared.

The volumetric variation shows trends similar to the variation of the mass of the system for the three options shown. Again, the initial crossover point for the optimum is at a duration of approximately 1 hour, where the batteries require a larger volume than the engine. It is shown that even past a duration of 10 hours, the engine-driven system would result in the lowest volume system among these options.

Based on the above discussion, considering only the energy density and volumetric energy density, the optimum power source for the application under consideration is the small-scale engine. However, there are other factors to take into account including reliability, noise, exhaust, ease of refueling or replacing the energy source, and the availability of external power or fuel. The batteries would yield the most reliable and predictable power source of the three options considered; however, they quickly become bulky and heavy for longer durations, rendering them useful only for shorter periods. They also require recharging, which can take several hours, and also the availability of an electrical power source.

The hydrogen fuel cell would also deliver reliable power to the system and the required fuel itself does not add significantly to the mass; however, its base weight and volume are large. The fuel cell was found to be least attractive for this application and

therefore no further analysis was considered. Both the fuel cell and batteries would require a DC motor to drive the system; this additional weight was not accounted for.

As previously mentioned, the drawbacks of the engine are that it produces high noise levels and exhaust, and it is potentially the least reliable of the three types of input power systems analyzed. The noise level can possibly be reduced by muffling the exhaust and shielding the engine, however it still produces significant noise. Exhaust from the engine also implies that the system must be operated either outside or in areas with proper ventilation. Despite the drawbacks of the small-scale engine, it was chosen as the power source for this project due to its significant advantages in energy density, which enables long duration missions.

1.1.2 Thermodynamic Cycle of the Portable Cooling System

Absorption and vapor compression systems were the options initially considered for the cooling system in this study. The absorption cycle uses heat input from a gas burner, and requires a liquid pump (with a small electrical power input) to circulate the working fluid. As this is a first-generation system, an R134a-based vapor compression cycle was chosen for the present study based on the fewer components required and the lower complexity.

The use of R134a as the refrigerant for the cycle was determined by examining several factors including predicted performance, ozone depletion potential (ODP), global warming potential (GWP), cost, physical properties and availability. Several refrigerants were examined using EES software to determine the performance of each, and were ranked according to their predicted efficiency for use in the portable cooling system (Table 1.1). A commonly used refrigerant was desirable, since parts would be readily

available that would be compatible with the refrigerant. The environmental impact of the refrigerant was also taken into account with the intention of minimizing this effect. The following table shows the refrigerants analyzed and displays the required system input power for each working fluid in descending order of efficiency.

Table 1.1 Refrigerant Selection Matrix (Calm and Hourahan, 2001)

Refrigerant	Ozone Depletion Potential	Global Warming Potential	Input Power (W)	Efficiency Rank
R141b	0.09	700	146	1
R11	1.00	4600	147	2
R123	0.01	120	148	3
R114	0.85	9800	151	4
R717 (Ammonia)	0	< 1	151	5
R152a	0	120	152	6
R12	0.82	10600	154	7
R134a	0	1300	155	8
R500	0.61	7900	155	9
R22	0.03	1700	157	10
R290 (Propane)	0	20	158	11
Note: A cooling load of 400 W was imposed for this analysis.				

Refrigerants R11, R114, R12 and R500 were eliminated due to their large values of ozone depletion potential. Ammonia (R717) was also eliminated due to safety and material compatibility issues with aluminum, a lightweight metal used for heat exchangers. Of the remaining refrigerants, R134a had the fourth best efficiency and differed in input power required by only 9 W from R141b, which gave the best performance. Since R134a is commonly used and is relatively inexpensive (~11 $/kg),

the difference in performance was small enough to neglect for the first generation system, representing approximately a 5.8 percent difference in performance.

The decision to use a vapor compression cycle resulted in the need for developing a miniaturized compressor, since it is the key component in the system and serves as the driving force for the entire cycle. The availability of small-scale refrigerant compressors is limited, and proved to be a design challenge for the project, as discussed in greater detail in subsequent chapters. Most readily available small-scale refrigerant compressors are hermetically sealed and driven by an enclosed motor. The sealed shell however causes the entire compressor to be too large to use. Readily available sealed compressors that were investigated generally had an oval-like shaped enclosure with a minor diameter of approximately 13 cm (5 inches), a major diameter of approximately 18 cm (7 inches) and a height of 13 cm (5 inches). Without the hermetically sealed enclosure, the compressor system could be significantly reduced in size. In order to eliminate the need for the sealed enclosure, modifications to the compressor were designed and fabricated, as described later in Chapter 3. The compressor used for this experiment was an off-the-shelf air compressor that was significantly modified in-house for this application. The remaining components of the thermodynamic cycle such as heat exchangers, valves and tubing were readily available in small sizes.

1.1.3 Heat Removal to the Ambient

As part of the thermodynamic cycle, the condenser serves the role of desuperheating and condensing the refrigerant by transferring the heat from the refrigerant to the surroundings. Two methods of heat removal to the ambient were examined for use in this project. They included an air-coupled heat exchanger that would

be mounted on the backpack, and a wearable condenser. For the wearable condenser, the exterior of the garment being worn would serve as the condenser. Located inside the garment, the wearable evaporator would be separated from the condenser on the outside by a layer of insulation. The use of a wearable condenser could potentially enable the heat from the refrigerant to be transferred to the surrounding air in a passive manner. This type of condenser would not require a fan, and hence would not place additional loading on the power source for air movement. On the other hand, an air-coupled tube-and-fin heat exchanger functioning as the condenser would necessitate the use of a fan to draw air across the condenser, requiring additional input power.

Despite the additional load placed on the power source by the fan and the added complexity, the air-coupled pack-mounted condenser proved to be more practical. This was due to the fact that the wearable condenser would cause significantly increased parasitic heat loss to the evaporator. This is because the hottest and coolest portions of the system would be in close proximity to each other and would only be separated by a thin insulating layer of approximately 6.4 mm (¼ inch); thicker layers would make the system awkward and bulky. The heat gain through the insulation to the evaporator is much larger for the wearable condenser since the temperature of the condenser is much higher than that of the ambient air. For example, in an ambient of 43.3°C and a body heat rejection of 400 W, preliminary analyses showed that the condenser temperature would be 60.4°C for the wearable condenser (Appendix A and B). This would result in a higher surface temperature of the insulation than that of the pack-mounted system where the surrounding air temperature would be 43.3°C.

For a full-body suit, the predicted increased temperature of the insulation surface would result in a heat gain through the insulation of about 109 W for the pack-mounted condenser system and 290 W for the wearable condenser. The resulting unwanted heat gain to the evaporator would be 21 percent of the total heat duty of the evaporator for the pack-mounted system and 42 percent for the wearable system. The parasitic heat gain from the condenser to the evaporator would cause the required system input power to

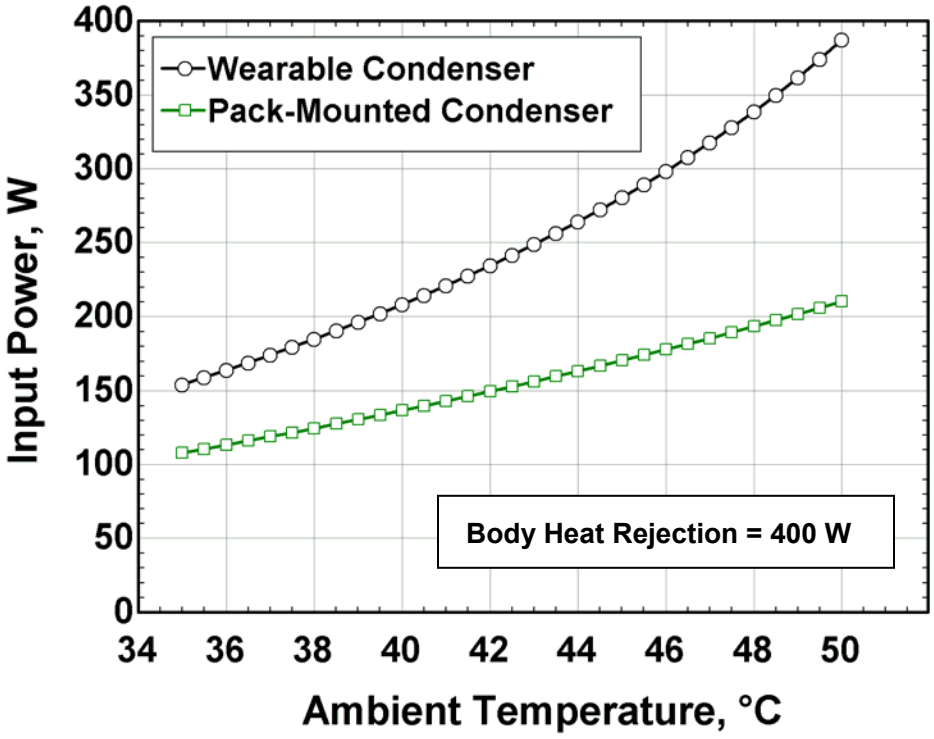

Figure 1.3 Condenser Comparison – Wearable vs. Pack-Mounted

increase significantly, as shown in Figure 1.3. This graph is a comparison of the required input power versus temperature for a system using the wearable condenser and also the pack-mounted condenser.

The advantage of the elimination of fan power input in the passive cooling approach is lost due to the increased heat load placed on the evaporator, resulting in an increased

refrigerant flow rate requirement and therefore greater compressor work input. At an ambient temperature of 43.3°C and a body cooling load of 400 W, the compressor work would increase from 138 W for the pack-mounted condenser option to 251 W for the wearable condenser. The work input to drive the fan for the pack-mounted system would add an additional 22 W, resulting in a total input work of 159 W. The required work input for the wearable condenser would simply be the 251 W to run the compressor (i.e., 58 percent more than the total power input for the pack-mounted system), since the condenser would use a passive approach for heat rejection and would require no fan.

The insulation thickness and thermal conductivity also have a significant impact on the input power requirement of the cooling system. Figure 1.4 shows the effect of insulation thickness and conductivity on the heat gain through the insulation for both the

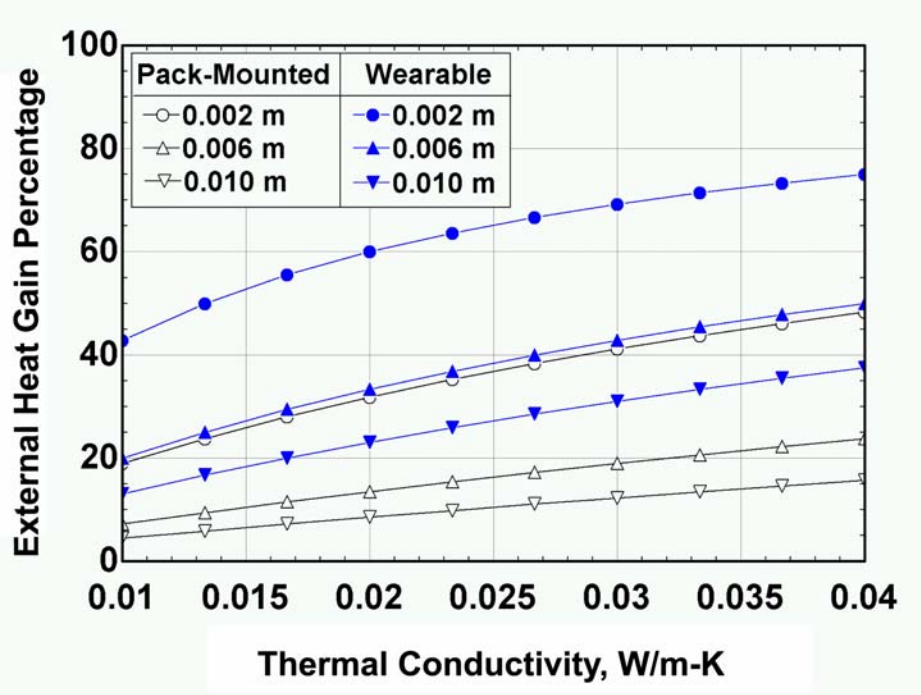

Figure 1.4 Insulation Heat Gain Percentage

wearable and the pack-mounted condensers as a percentage of the total heat duty of the evaporator, which combines both the body heat rejection and the heat gain through the insulation.

Based on the preliminary analyses discussed above, a system with a fan-cooled condenser built into the backpack structure was chosen. Use of the air-coupled heat exchanger for the condenser resulted in the need to optimize the air flow rate through the condenser. There is a tradeoff in power consumption between the fan work and compressor work, as mentioned earlier. Higher fan work results in higher air flow rates and a decrease in the condenser temperature and pressure. This leads to a lower compressor work input requirement. The optimum air mass flow rate was found to be around 0.12 kg/s (225 cfm), using the overall system modeling tool described in detail in Appendices A, B and C. Figure 1.5 shows the work input of the fan, compressor and total work input required versus the mass flow rate of air over the condenser.

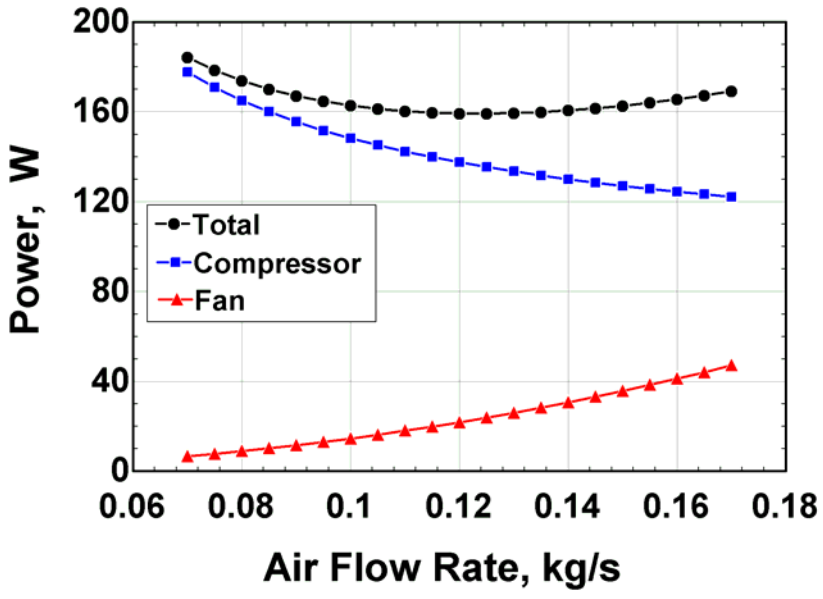

Figure 1.5 Input Power Versus Mass Flow Rate of Air

1.2 Scope of Current Research

As discussed earlier, there were several challenges associated with the development of a portable/wearable cooling system. During the course of this research, these multi-faceted challenges were investigated and analyzed, and a prototype system was fabricated and tested. Throughout the design process, many alternatives were examined for each component and also for the system configuration. The resulting system is the combination of the most promising alternatives realized during this process. In order to achieve the final results, the system was first modeled using thermodynamic cycle calculations and heat exchanger design calculations in the EES platform, which enabled the determination of system sizing and energy input requirements. This included modeling of the compressor, condenser and evaporator in the refrigeration cycle, as well as the condenser fan and other system components. From the analysis in EES, the appropriately sized air compressor was selected and modified in-house into a refrigerant compressor.

Testing was conducted in two major steps. Because the compressor represents such a significant part of the system, validation tests were first conducted on a specially fabricated, stand-alone compressor test stand. This testing helped ascertain that the modified compressor would perform as required; i.e., compressing the refrigerant in an efficient manner while delivering sustained performance. When it was determined that the modified compressor would perform satisfactorily, the finalized overall system was assembled and tested. The prototype was built as closely as possible to the actual system; the main difference being the installation of the instrumentation required to measure the cycle performance, such as thermocouples and pressure gages. The prototype was then

tested over a matrix of test conditions to determine system performance at various combinations of ambient temperature, evaporator temperature and engine speed. The results of the system testing were then analyzed and the system performance was evaluated. Finally, the system developed in this manner was assembled into a compact, wearable cooling system.

1.3 Thesis Organization

The thesis is organized as follows:

- Chapter 2 discusses the research that has been done previously in areas related to personal cooling.
- Chapter 3 provides detailed information about the experimental set-up and the testing that was performed in this research.
- Chapter 4 describes the analyses of the results using a representative data point for illustrative purposes.
- Chapter 5 presents the results of the testing and shows the influence of the key parameters on system performance.
- Chapter 6 describes the development of the wearable evaporator and the integration of the system into a wearable device.
- Chapter 7 provides a summary of the conclusions obtained from the study, and recommendations for future development.

2. LITERATURE REVIEW

2.1 Portable Cooling Systems

A variety of methods have been investigated to provide portable cooling of personnel working in high thermal stress conditions. These systems range from very simple methods to much more complicated ones, with corresponding variations in cooling duration, size and weight.

2.1.1 Phase-Change Materials

One of the simplest methods is the use of ice packs or other phase-change materials worn in close contact with the body located in pockets throughout a garment interior. This provides a reliable means of cooling the body without the use of a complicated cycle or methodology. Heat from the body is transferred to the phase-change material as it melts; this provides cooling for a limited duration. The main drawback of such a system is the need for additional packs to be readily available for replacement whenever the material has melted and the liquid has warmed to the point where cooling of the individual is no longer sufficient. If the cooling system is to be used for extended periods of time, the transportation of replacement cooling packs would be cumbersome. Providing cooling for a longer duration would require amounts of phase-change material that make this system impractical. The main advantage of using ice is the reliability of cooling and the simplicity. In the research performed by Epstein et al. (1986), it was seen that ice had the greatest cooling capability of several cooling methods tested, but was impractical due to the replacement requirement. Based on a simple calculation involving

the latent heat of fusion for water (335 kJ/kg), the mass of ice needed to provide 300 W of cooling for a mission duration of only 2 hours was found to be 6.4 kg.

2.1.2 Adsorption Systems

Another method of cooling involves the use of an adsorption device. In this method, evaporation of water provides the cooling to the system. This is accomplished by means of a desiccant bed which adsorbs the vaporized water into the desiccant. This lowers the vapor pressure of the water, resulting in evaporation at the lowered pressure, which in turn provides cooling at the desired temperature. An adsorption system of this type was developed by Grzyll and Balderson (1997) and used calcium oxide as the desiccant.

The use of adsorption is another reliable and simple method that does not require any excessively loud or complicated components. An electrically driven pump is needed to circulate water, as well as tanks for holding the desiccant and water. One of the drawbacks of such a system is that it requires components for the storage of both desiccant and water to operate. To provide cooling for extended periods of time, the system becomes heavy and large. The adsorption system developed by Grzyll and Balderson (1997) weighed 19.9 kg (43.9 lb) and had overall dimensions of 0.602 m × 0.188 m × 0.335 m. Another drawback is the lag time associated with the startup of the system and the beginning of any cooling effect. Reaching peak cooling can take approximately 30-45 minutes with an adsorption system (Grzyll and Balderson, 1997).

2.1.3 Absorption Cycle

Another method that could be used for portable cooling involves the use of an absorption cycle. This method of cooling could use ammonia-water or water-lithium

bromide solutions as the working fluid pairs. Using this method would require heat input from a fuel source, as well as electrical input to drive a liquid pump. The advantage of an absorption cycle is that the shaft work input to the pump is much less than that required for vapor compression. The main energy input to the cycle is heat input, which can easily be obtained using combustion of a liquid fuel. The energy density of fuel is much higher than that of batteries, which makes absorption an attractive alternative. Such a system has been designed by Drost and Friedrich (1997) of Pacific Northwest National Laboratory using a water-lithium bromide combination. Based on their research, they predict that a 4-5 kg system could be built to provide 350 W of cooling. The overall dimensions of the system are not given in their paper.

The absorption cycle makes use of relatively few moving parts, however there is the need for additional heat exchangers and a more complicated overall cycle than vapor compression. Also, the heat that is input to the system from the fuel source must be removed to the surrounding atmosphere in addition to the heat rejected from the user. This requires that a significant amount of heat be rejected to the surroundings through air-coupled heat exchange. This in turn leads to the need for considerable air flow across the condenser and the corresponding fan power input.

2.1.4 Brayton Cycle

Finally, another potential method to provide portable cooling is the Brayton cycle cooling system. This method uses an air-cycle that compresses atmospheric air and separates the air stream into two parts as shown in Figure 2.1. The first air stream passes through a combustion chamber and expander to provide input power to the system. The second stream passes through a heat exchanger to remove heat to the surroundings, and is

then expanded back to a lower pressure and temperature to provide cooled air. The Brayton cycle used by Rahman (1996) is shown in Figure 2.1.

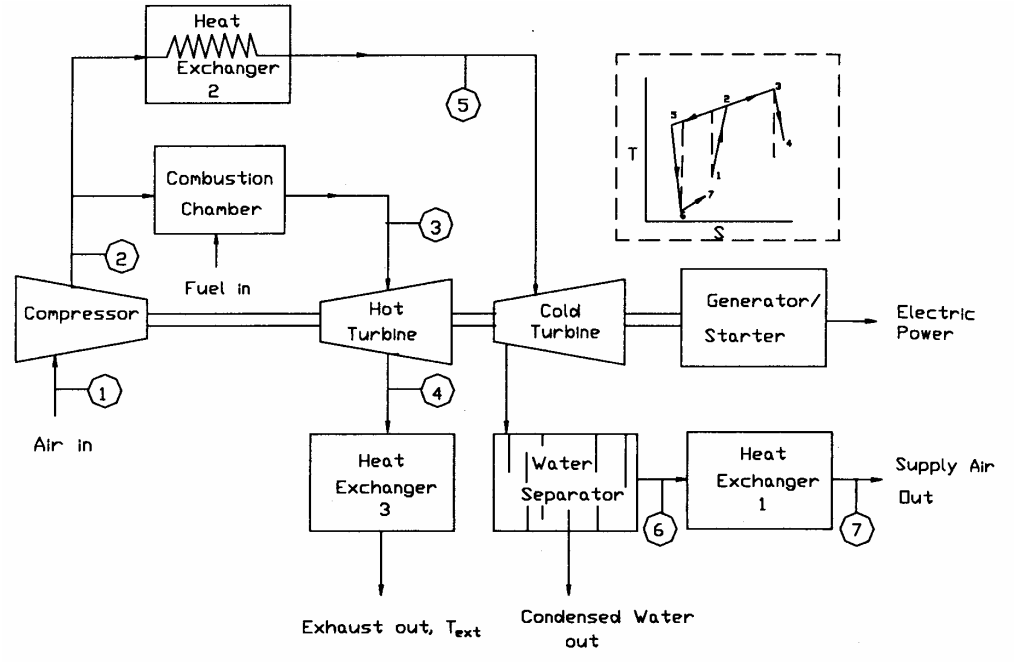

Figure 2.1 Brayton Cycle Cooling System Schematic (Rahman, 1996)

The cooled air stream is passed inside the garment being worn to provide cooling to the user. This method was employed by Rahman (1996) in the development of a cooling system for soldiers, and also provided power for electric devices being used by the soldiers. A generator was attached inline with the compressor and expander shaft to provide the electrical power. The disadvantage of such a system is the overall complexity. It requires many components, including several heat exchangers, a compressor, a combustion chamber, two expansion turbines, a generator and a water separator. The system is also capable, however, of providing drinkable water and electrical energy, so the added complexity may be warranted (Rahman, 1996). Rahman does not provide information regarding the overall weight of the system or the cooling

duty obtained. However, the overall dimensions of the system were stated to be 0.47 m × 0.279 m × 0.368 m.

A summary and comparison of the different cooling systems discussed above is provided in Table 2.1.

Table 2.1 Portable Cooling Systems Summary

Portable Cooling System	Advantages	Disadvantages
Phase-Change Materials	Simplicity – Uses only ice-packs or other phase change materials to cool the body. No moving parts or complicated thermodynamic cycles.	Offers only short mission duration since the amount of phase-change materials needed for extended duration would be too heavy. To provide 300 W of cooling, 3.2 kg/hr of ice would be required.
Adsorption System	Simplicity – Water vapor is adsorbed by desiccant and used to cool a circulating fluid.	Requires replacement of desiccant material after use. Provides limited duration and is bulky and heavy, overall system is 19.9 kg (Grzyll and Balderson, 1997). There is also a lag time between system startup and the beginning of cooling.
Absorption Cycle	Uses a high energy density liquid fuel to provide the main input power to the system. System has few moving parts. A 4-5 kg system could provide 350 W of cooling (Drost and Friedrich, 1997).	More complicated than many other systems, requires additional heat exchangers and components. Heat input to system from both the body and combustion must be rejected to the ambient, causing a high airflow requirement.
Brayton Cycle	Uses a high energy density fuel to operate. Delivers cooled air to the garment to cool the user, which aids in body heat and perspiration removal. The system can also provide electrical power and drinkable water (Rahman, 1996).	Overall system is complicated, requiring several heat exchangers, a combustor, two expansion turbines and a compressor.
Vapor Compression Cycle	Thermodynamic cycle is relatively simple and can be driven by a variety of power sources including batteries, fuel cell, or engine.	Vapor compression requires significant shaft work input. Power source must have a high energy density to be practical.

2.2 Cooling Garments

Research has also been conducted on various types of cooling garments for heat removal from the body. This can be accomplished by a variety of methods including air passing inside the garment across the user's body, individual ice-packs or phase change materials, and finally, tubing carrying water or refrigerant. The temperature of the cooling garment near the skin is of importance when designing a personal cooling system. The temperature must be low enough to enable the necessary heat transfer from the body, but not so low as to feel uncomfortable to the user. Research has been done to determine the average comfortable skin temperature. Nunneley (1970) states that for individuals at rest, this temperature is approximately 33°C. The desired skin temperature to remain comfortable declines as the activity level of the individual increases, as this aids in removal of an increasing amount of heat from the body, which requires a larger thermal gradient. As the required heat removal rate from the body approaches 400 W, the average comfortable skin temperature is approximately 30°C (Nunneley, 1970). The decline in comfortable skin temperature continues at a rate of approximately 1°C per 100 W of additional heat rejection.

Cooling of the body using airflow inside a garment is useful because the air is capable of removing heat by convection and also through the evaporation of perspiration, if the air has sufficiently low humidity. The system developed by Rahman (1996) using the Brayton cycle (described above) would produce cooled air delivered to the garment. The other cycles discussed would typically use tubing carrying water or refrigerant as the means of heat removal. The disadvantage of using air in these systems is the need for an additional air-coupled heat exchanger to cool the air before traveling to the garment,

which requires an additional temperature difference and leads to lower cycle performance as opposed to routing the cooling fluid directly to the garment. Some pressurized air-cooled garments are also difficult to work in, as stated by Nunneley (1970) in her comparison of cooling garments. This can cause the user to work harder to perform the same tasks, adding to the required cooling duty. There are also some flow distribution problems associated with uniformly distributing the cooled air over the body.

Garments that use tubing with water flowing inside have been analyzed extensively for use in cooling systems in many applications. They include astronauts working in space suits, aircraft pilots, workers using chemical response suits, and those using other protective gear that inhibits heat transfer. Epstein et al. (1986) analyzed several suits, as well as various methods of cooling such as air, water and ice. They explain two methods of describing the performance of a cooling suit, namely the efficiency and the effectiveness. The efficiency is the amount of cooling per unit area, or heat flux, and the effectiveness is the total cooling of a particular area of the body. Their findings showed that cooling of the torso was more effective than other parts of the body, due primarily to the larger surface area. The head was shown to be the most efficient area to cool; however, due to the limited area, it was a less effective area to cool. One drawback of using cooling vests with incorporated tubing found by Epstein et al. (1986) was the condensation of the subjects' perspiration on the tubing. Differences in the performance of cooling suits that use refrigerants versus those that use water as the working fluid were found to be negligible by White et al. (1991). They performed experiments using a chemical response suit and various cooling schemes and found both to be beneficial in reducing the effects of thermal stress.

A review by Shvartz (1972) compared several different cooling suits, ranking them in efficiency and effectiveness. The study agreed with Epstein et al. (1986) that the head is the most efficient place to cool. However, it does not provide as much cooling overall as the significantly larger area of the torso. Shvartz recommended percentages of tubing to be allotted to various portions of the body for maximum effectiveness if using a full body cooling suit. He recommends that the torso should receive 30 percent, the head and neck 25 percent, the thighs 17 percent, upper arms 15 percent, the calves 8 percent, and the forearms 5 percent (Shvartz, 1972).

Nag et al. (1998) performed testing to determine the body's response to heat removal while in a high temperature environment by means of a water cooled garment. For this research, a three-layer cotton vest was lined with 2 mm diameter latex tubes. A vest that covered approximately 20 percent of the total body area was used during this study. The research used a closed water loop that was cooled by an insulated ice-pack to provide approximately 2 hours of cooling. The study found that the cooling suit itself can impede some of the body's natural cooling through the evaporation of perspiration and recommended that any suit used should work with the body's own natural temperature regulation as much as possible. The cooling garment itself should be capable of wicking away any perspiration that is generated inside. Nag et al. (1998) found that the cooling vest tested was successful at providing cooling, and would help maintain body core and skin temperatures that were comfortable to the user.

Recently, Pourmohamadian et al. (2004) conducted research on a thin, flexible, non-metallic heat exchanger that could provide an alternative to the standard tubing currently used for cooling garments. The micro-channel heat exchangers are made from a heat-

sealable polyimide film and have a thickness of 0.2 mm. These heat exchangers are very thin and therefore do not have significant mass, are flexible, and can handle pressures up to 2.07 MPa (300 psi). The fact that they are thin and flexible means they would lend themselves well to being used as heat exchangers for a cooling garment. They are also capable of withstanding the pressures associated with a vapor compression refrigeration cycle using R-134a, which means that the refrigerant could be directly routed to the cooling garment without the need for an additional closed water loop. The flexible heat exchangers are also compatible with refrigerant R-134a. Currently, research is being done to develop connections from the polyimide heat exchanger to standard connections. This needs to be accomplished prior to being used in conjunction with a cooling garment.

2.3 Summary

The above review of the literature shows that portable cooling systems are needed for those working in ambient conditions that are likely to cause heat-related fatigue. Those who would benefit from such cooling systems include military, firefighters, factory workers, and hazardous duty workers in chemical response suits and other protective garments. There have been many variations in the methods used to provide portable cooling, each method with its own benefits and limitations. Phase-change materials used by firefighters only provide cooling for a limited duration. Adsorption systems lower the vapor pressure of water and essentially boil off the water at the desired temperature, resulting in a cooling effect. However, the amount of desiccant and water needed causes these systems to be excessively heavy for extended-duration use. Absorption cycles require higher complexity than other systems, and also require large heat rejection rates to the surrounding atmosphere. Brayton cycle based systems are useful for applications

that require personal cooling as well as portable electrical power and drinkable water supply. However, these systems are complex, with many components that add to the overall size and weight of the system.

The system developed in the present study used a vapor-compression refrigeration cycle powered by a small-scale engine. Some of the papers analyzed for the literature review discuss this method of providing personal cooling, however they found such systems unattractive due to various reasons such as the inefficiency of small-scale engines, the overall weight of the resulting system and the sound level produced. However, in the absence of systematic results from actual experiments on such systems, it was deemed appropriate to investigate and develop engine-driven vapor-compression systems for personal cooling. It should be noted that recent advances in the efficiency of small-scale engines make them more attractive for use in such systems. The predicted fuel consumption rate and the weight of such systems appear to be overestimated in the literature. For example, Rahman (1996) predicted that a system employing an engine-driven vapor compression cycle would weigh approximately 25 pounds (11.3 kg), with a fuel consumption rate of at least 1 lb/hr (0.454 kg/hr). Methods of noise reduction may also be used to render the system more practical. The present study attempts to take advantage of these advances to design, fabricate and test a compact and practical engine-driven vapor-compression system for portable cooling applications.

3. EXPERIMENTAL SETUP

This chapter is divided into two major sections: the first discusses the development and testing of the proposed compressor, while the second discusses the configuration and testing of the overall system. Thus, the focus of the first stage of the development was to establish whether the proposed air compressor could be satisfactorily modified to function as a refrigerant compressor of the desired capacity. After it was determined that the performance of the modified compressor was satisfactory, the overall system was built and tested to determine its performance characteristics.

3.1 Compressor Testing

As discussed in the introduction, one of the difficulties in developing a portable cooling system is the need for components of small size and mass. One of the key components of the refrigeration cycle is the compressor, which drives the entire thermodynamic cycle. Compressors of the size and style required for this project were not readily available. Therefore, an off-the-shelf air compressor was modified considerably to function as a refrigerant compressor for the portable cooling system. A description of the compressor development and testing follows.

3.1.1 Compressor Description

A small-scale air compressor was used as an initial prototype for the refrigerant compressor. The model HC-5320284 12-volt DC portable air compressor (Target Corporation) was chosen as a starting point for the refrigerant compressor development. Components of this compressor that required modification included the intake manifold, crankcase, crankshaft and the overall structure of the compressor housing. The

compressor had a piston diameter of 19 mm (0.75 inches) and a stroke of 17 mm (0.675 inches), yielding a total displacement of 4.92×10^{-6} m³ (0.30 cubic inches). The compressor is shown in Figure 3.1.

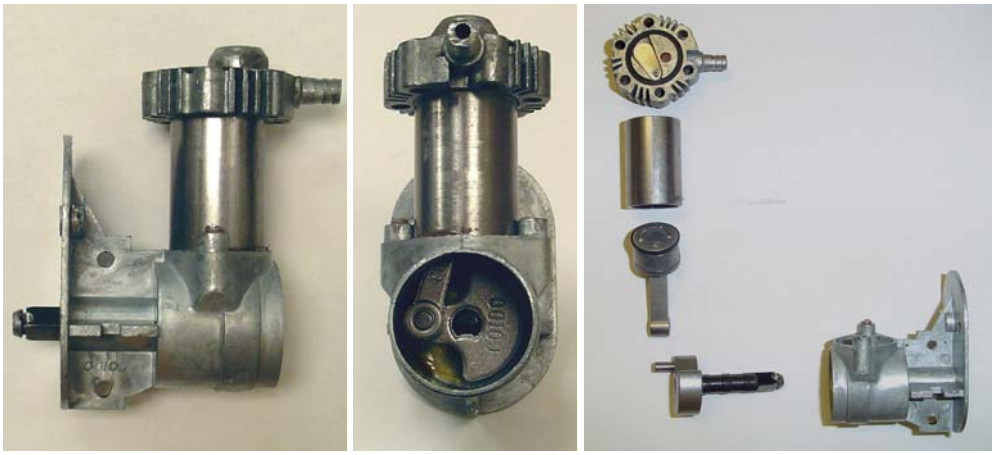

Figure 3.1 Air Compressor Details

In order to use the air compressor with refrigerant rather than air, the three main areas that needed to be addressed included:

- the requirement for a pressurized crankcase
- a modified intake manifold
- the addition of a rotating seal

The crankcase required pressurization to provide the necessary backside pressure during startup. Without equalization of pressure on both sides of the piston, the starting torque would be too high for the crankshaft to be rotated. Backside pressure also helps during operation as there is an equalization of forces on both sides of the piston (Figures 3.2 and 3.3). This leads to smoother operation since the variation of torque on the crankshaft is not as large. Theoretically, the average input power should not be affected; however, the crankshaft lacked a sufficiently large flywheel to enable smooth operation.

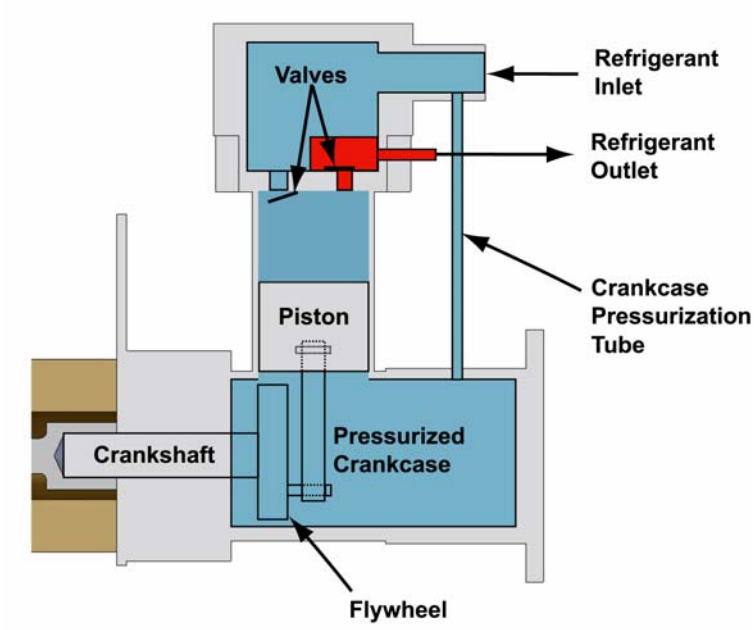

Figure 3.2 Compressor - Intake Stroke

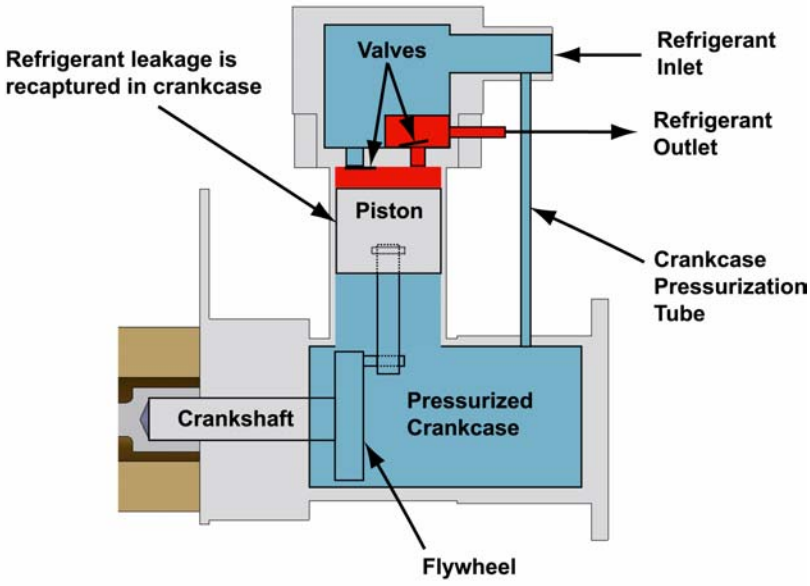

Figure 3.3 Compressor - Compression Stroke

A flywheel serves as an energy storage and supply device by smoothing out variations in torque and speed. With the presence of backside pressure on the piston from the refrigerant in the crankcase, the average pressure differential is lower, minimizing the need for a larger flywheel.

As shown in Figures 3.2 and 3.3, the presence of refrigerant on the backside of the piston also alleviates the problem of any refrigerant leaking past the piston seal. As with any compression system, there would be a small amount of leakage past the piston during operation. Any refrigerant that leaks by enters the crankcase, which is connected to the low pressure side of the system, thus recapturing the refrigerant.

With the addition of a pressurized crankcase comes the need for a rotating seal between the crankcase housing and the input shaft. There is a limited selection of small-scale rotating seals available for this size of rotating shaft. A Teflon rotating seal was found that delivered the required size, pressure and seal rotational velocity combination for the input shaft. The seal had an outer diameter of 9.5 mm (0.375 inches) and an inner diameter of 6.4 mm (0.25 inches), with a width of 3.2 mm (0.125 inches) and satisfied the size and performance requirements for this application.

The compressor modifications required to convert the air compressor into a refrigerant compressor allowed the testing of the compressor to commence. These modifications are described in a subsequent section (3.1.2). The goal was to initially test the compressor head, valves and rotating seal and determine whether changes would be required, based on system performance. The structural integrity of the compressor was also evaluated during the testing to ensure that the crankshaft, connecting rod, piston and bearing surfaces were of sufficient strength to enable compression of refrigerant instead

of air. The refrigerant is approximately 15 times denser than air at the temperatures and pressures being tested. Since the refrigerant compressor was operated at approximately the same rotational speed as the original air compressor design speed, the theoretical volumetric flow would be the same for both, because it is a positive displacement compressor. This resulted in higher flow losses through the valves for an equivalent volumetric flow of refrigerant as compared to air. The result was a greater differential pressure from flow losses, in addition to the nominal pressure difference, and therefore an increased stress level on the system components. In view of these considerations, the initial compressor testing allowed verification that the compressor would be capable of performing as required in a refrigerant compression application.

3.1.2 Compressor Housing

In order to meet the previously stated requirements for backside pressure and proper sealing of the rotating seal, a vessel that completely enclosed the compressor and head assembly was fabricated to enable testing of the compressor. This was accomplished by using a rectangular aluminum channel (d, Figure 3.4) that measured 50.8 mm × 102 mm (2 inches × 4 inches). A section was cut to a length of 76.2 mm (3 inches) to provide the necessary volume for the compressor (c).

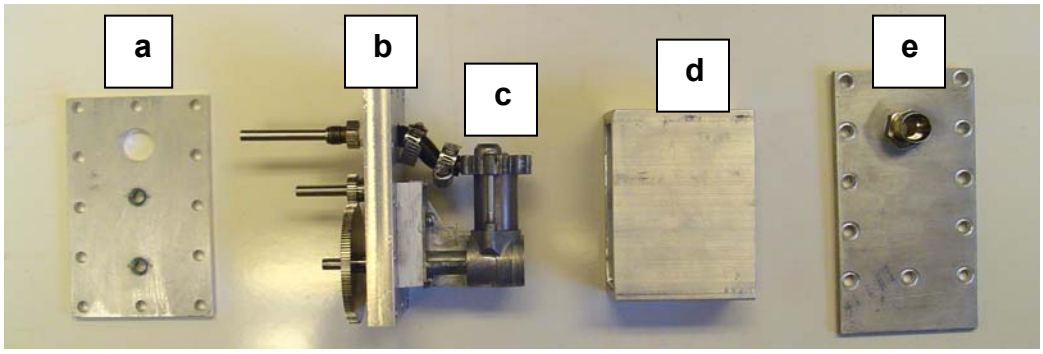

Figure 3.4 Compressor Enclosure

Two flanges were machined, which enabled sealing of the ends of the rectangular channel (d). The front and back flanges (b and e) were made from 12.7 mm and 6.4 mm (½ inch and ¼ inch) thick aluminum plates, respectively. The back flange (e) was used to seal the end of the enclosure and also for an inlet port from the evaporator. The front flange (b) served two purposes: it provided the front face of the rectangular enclosure for sealing purposes and it also held the rotating seals and bearings for the shaft, thus requiring the 12.7 mm (½ inch) thickness. The two endplates (b and e) were then bolted together with the rectangular channel (d) in between to form the complete enclosure. The additional bearing plate (a) was used to support the bearings for the rotational shafts. Twelve 6.4 mm (¼ inch) bolts were used to provide the uniform sealing force required to seal the enclosure. The seams were sealed using 1.5 mm (0.06 inch) thick rubber gaskets between the plates and the rectangular channel.

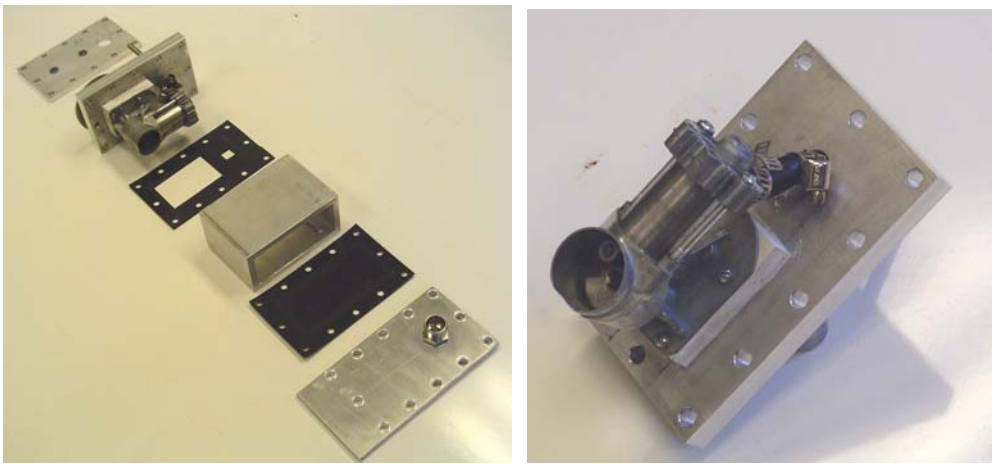

Figure 3.5 Compressor Enclosure Layout

As shown in Figure 3.5, the compressor was mounted to the 12.7 mm (½ inch) thick aluminum plate and driven by the input shaft passing through the plate.

3.1.3 Vapor-Compression System Description

To begin the cycle, the refrigerant was drawn into the compressor inlet valve on the top of the head. The surrounding low-pressure refrigerant gas inside the rectangular enclosure was free to flow into the compressor during the intake stroke. As the crankshaft turned, it expelled the refrigerant through the outlet valve into the high-pressure discharge hose. This hose was routed out of the aluminum enclosure and to the condenser using a 6.4 mm (¼ inch) copper tube.

Wherever possible, the system was designed to simulate the actual layout of the proposed portable cooling system. Extra instrumentation required for testing purposes was also included in the test facility, which added significantly to the size and weight of the overall system. Figure 3.6 shows the configuration of the compressor enclosure, as well as the instrumentation, condenser and air motor, as discussed later.

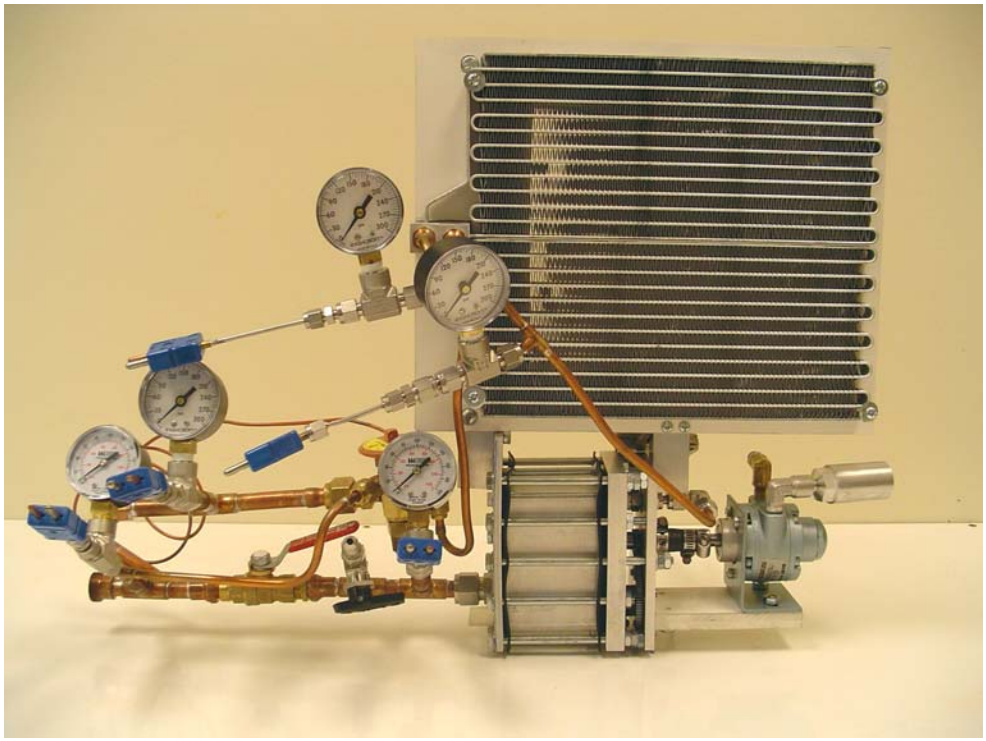

Figure 3.6 Compressor Testing Configuration

The computer program which was developed to model the overall thermodynamic cycle was used to predict the required condenser size. The multi-louver fin microchannel condenser chosen for this purpose is depicted schematically in Figure 3.7. Such a configuration offers high refrigerant-side heat transfer coefficients, enhances air-side heat transfer due to the interrupted fins, and provides a large surface-to-volume ratio, all of which lead to the compact geometry essential for this application.

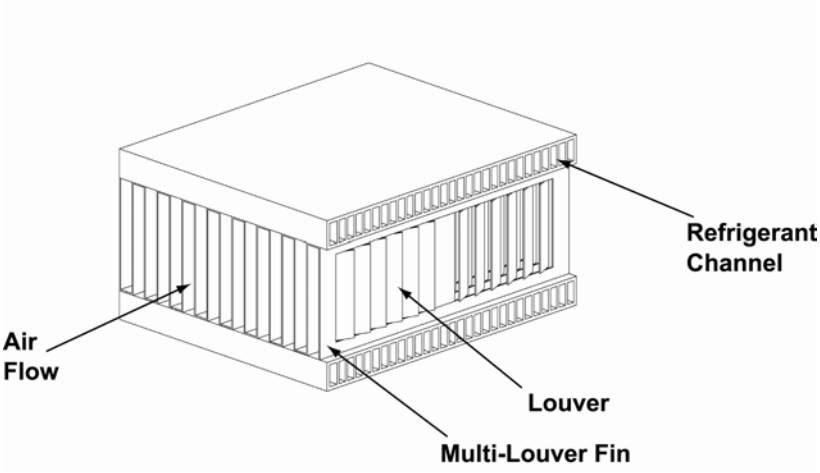

Figure 3.7 Representative Condenser Section

A preliminary design calculation was performed to estimate the size of the condenser required for this application, keeping in mind that the dominant thermal resistance is on the air side. Kim and Bullard's (2002) empirical correlations for heat transfer in multi-louver fins were used for the air-side calculation. Details of these calculations can be seen in Appendix B. The heat transfer from the refrigerant inside the tubing was also analyzed, despite having less of an impact on the overall thermal resistance of the condenser. The Shah (1979) correlation for condensation inside tubes was used for computing the tube-side heat transfer coefficient, as explained in detail in Appendix C. These analyses showed that the average condensation coefficient across the condenser

was 3945 W/m²-K for a refrigerant mass flow rate of 3.04×10^{-3} kg/s, in a configuration where the refrigerant flowed in series along consecutive tubes. Similarly, the air-side heat transfer coefficient was 145 W/m²-K. Details of the geometric features of the condenser that yielded these values are shown in Table 3.1. With a tube-side surface area of 0.177 m² and an air-side effective surface area of 0.83 m², the respective thermal resistances of the two sides were 1.4×10^{-3} K/W and 8.3×10^{-3} K/W, yielding an overall thermal conductance (UA) of 100 W/K.

Figure 3.8 Refrigerant Condenser

The actual condenser used for testing (Figure 3.8) was an aluminum microchannel, multi-louver fin heat exchanger supplied by Modine Manufacturing Company. This condenser approximated the modeled heat exchanger as closely as possible and had the advantage of being readily available. Although it was slightly larger than desired from space utilization concerns, it was used for the fabrication of the system. The face area of this condenser was 0.0620 m² (96.1 square inches) with dimensions of 0.260 m (10.25 inches) wide by 0.238 m (9.375 inches) tall. The airflow depth was 0.0211 m (0.83

inches). The condenser consisted of 24 rows of microchannels with 615 louvered fins per meter. Table 3.1 summarizes the geometric details of the modeled and the actual condenser. This condenser is expected to reject 554 W at a condensation temperature of 46.1°C and an ambient temperature of 37.7°C.

Figure 3.8 displays the condenser and air shroud (fabricated in-house from an acetate sheet.) The air shroud routed the air from the rectangular cross-section of the condenser to the circular cross-section of the axial flow fan. The refrigerant temperature and pressure were measured at the condenser inlet and outlet to determine the thermodynamic states entering and exiting the condenser. The refrigerant flowed out of the condenser through a 6.4 mm (¼ inch) copper tube to the expansion valve.

Table 3.1 Condenser Geometry and Performance

	Modeled	**Actual**
Face Area (m²)	0.0388	0.0620
Width (m)	0.199	0.260
Height (m)	0.195	0.238
Flow Depth (mm)	15	21
Rows	20	24
Fins/meter	839	615
Tube Pitch (mm)	10.2	9.9
Fin Pitch (mm)	1.2	1.5
Louvers per Fin	9	10
Louver Pitch (mm)	1.6	1.5
Tube Side Surface Area (m²)	0.177	0.26
Air-Side Effective Surface Area (m²)	0.83	1.33
Air-Side Convection Coefficient (W/m²-K)	145	-
Tube-Side Convection Coefficient (W/m²-K)	3945	-
UA (W/K)	100	-

After exiting the condenser, the refrigerant entered the Sporlan model FFE-1/4-C thermostatic expansion valve with external equalization where it expanded to the low side pressure as a two-phase fluid with a quality of approximately 0.2, typically. Using a valve of this type allowed for automatic regulation of the refrigerant flow based on the amount of superheat (3°C) of the refrigerant leaving the evaporator, eliminating the need for manual control. The refrigerant pressure and temperature were measured before entering the evaporator; however, since it was in a two-phase state, an isenthalpic expansion assumption was required to estimate its thermodynamic state. Sight glasses at both the inlet and outlet of the evaporator allowed visual examination of the refrigerant to ensure that the refrigerant was entering as a two-phase fluid and leaving as a superheated gas. The refrigerant temperature and pressure were also measured at the evaporator outlet. The refrigerant was routed back to the compressor enclosure to complete the cycle.

Inside the compressor enclosure, polyol ester refrigerant oil (National Refrigeration Products) was used to lubricate the moving parts of the compressor. The crankcase was located toward the bottom of the enclosure so that the crankshaft and connecting rod were in contact with the oil at the bottom of the stroke. This allowed the crankshaft to lubricate the compressor by distributing the oil throughout the enclosure.

The evaporator was also modeled in the EES program, however the evaporator used for testing was significantly different than that of the model. The modeled evaporator was intended to simulate the configuration used in the cooling garment, as this would represent the actual use of the system. For testing purposes, an evaporator that would allow straightforward measurement of the cooling duty of the system was constructed.

Wherever possible, the test evaporator was built as closely as possible to the cooling garment configuration; such as the length and diameter of tubing. The evaporator used for testing is described in Section 3.1.4. The description of the cooling garment evaporator and system modeling in EES is described in Chapter 6.

3.1.4 Coolant System Description

The coolant system served as a means of providing the desired heat input to the

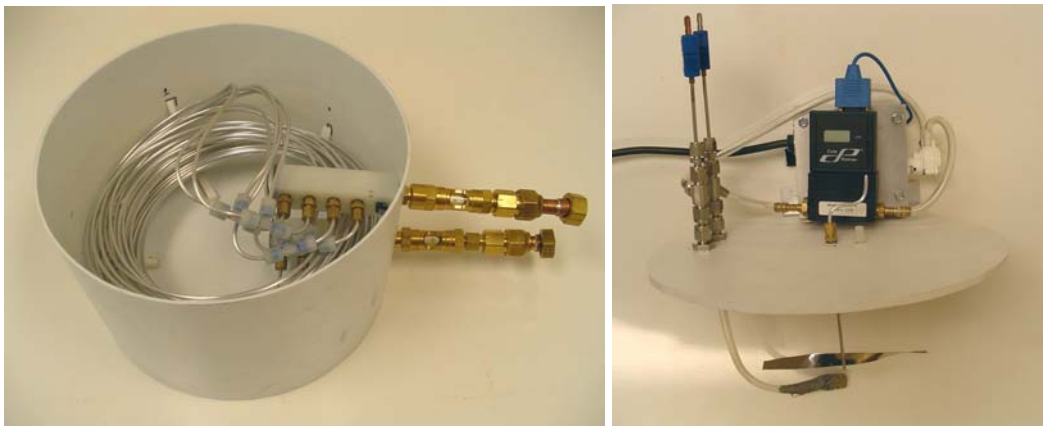

Figure 3.9 Test Evaporator Coolant Tank

evaporator. For testing purposes, the evaporator consisted of a coiled tube-in-shell heat exchanger (Figure 3.9) with coolant on the shell side and the refrigerant flowing inside eight aluminum tubes. Refrigerant was distributed in these tubes from a common header. The outer diameter of the aluminum tubing was 3.2 mm (0.125 inches), with an inner diameter of 1.9 mm (0.075 inches). Each tube was cut to 3.05 m (120 inches) length and wrapped in a spiral pattern before returning to the exit header. The refrigerant and coolant were designed to be in a largely counterflow orientation. Thus, the refrigerant entered these tubes in parallel at the bottom of the tank and spiraled upward in a

clockwise direction to the top refrigerant header, while coolant entered from the top and was directed in a counterclockwise direction by means of the discharge tube. The coolant suction hose was located at the bottom of the tank, oriented in a manner to aid in counterclockwise rotation as well. The tubes were placed in an 8 Liter container of coolant that was used to measure the heat duty of the evaporator.

A Greylor model LGP-115 variable speed pump circulated the coolant during testing, as shown on the right side of Figure 3.9 (the silver box located behind the flow meter). Coolant was drawn from the bottom center of the tank by the suction side of the pump and flowed through the Cole-Parmer digital flow meter model 32916-16. The coolant then flowed to a 1000 W Firerod Model 9745 cartridge heater that heated the coolant to the desired inlet temperature for the evaporator, which allowed a predetermined heat input to be set. The coolant was then discharged into the top of the tank horizontally to promote a counterclockwise flow with respect to the refrigerant to aid in heat transfer. The coolant temperature was measured at the inlet and outlet of the shell side of the evaporator.

The temperature of the evaporator coolant was selected to provide a comfortable range for cooling of the body, since the heat exchanger would be in direct contact with the skin in the actual system. The evaporator refrigerant-side temperature was slightly below the desired skin temperature to allow heat transfer while remaining comfortable for the user. The coolant flow rate (~1 LPM) was maintained at a level high enough to prevent significant temperature variation (< 2°C) between the inlet and outlet of the tank, which provided an almost constant temperature for the evaporator.

3.1.5 Auxiliary Components

To simulate the ambient conditions in which the portable cooling system would operate, the system was surrounded in a Plexiglas enclosure (Figure 3.10) of dimensions 0.610 m wide by 0.381 m deep by 0.508 m tall (24 inches × 15 inches × 20 inches).

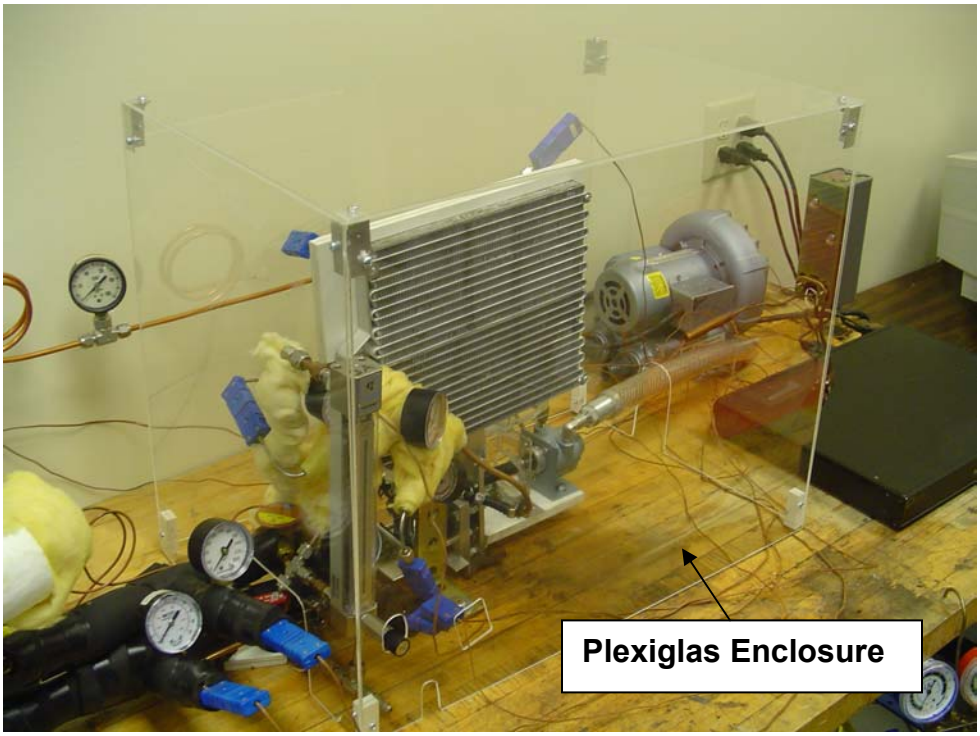

Figure 3.10 Plexiglas Enclosure Surrounding Test Facility

The Plexiglas enclosure allowed the air to be maintained at an elevated temperature surrounding the condenser and compressor assemblies, and also enabled viewing of the overall system. Prior to testing, the air temperature was raised to approximately 37.7°C-43.3°C (100-110°F) inside the enclosure by means of a 1500 W VS Appliances model VS523 air heater that was controlled by a thermostat (Honeywell Model L6006A) mounted directly to the Plexiglas enclosure. The enclosure was not insulated and

therefore lost heat to the surrounding air, which was at room temperature. During testing, the air heater did not need to operate to maintain the interior temperature, because the heat rejected by the condenser maintained the desired surrounding air temperature.

System power during testing was supplied by a 0.35 horsepower Gast model 16AM compressed air-driven motor capable of speeds ranging from 0 to 10,000 RPM (Figure 3.11). This allowed the rotational speed of the compressor to be varied by adjusting the supply air pressure.

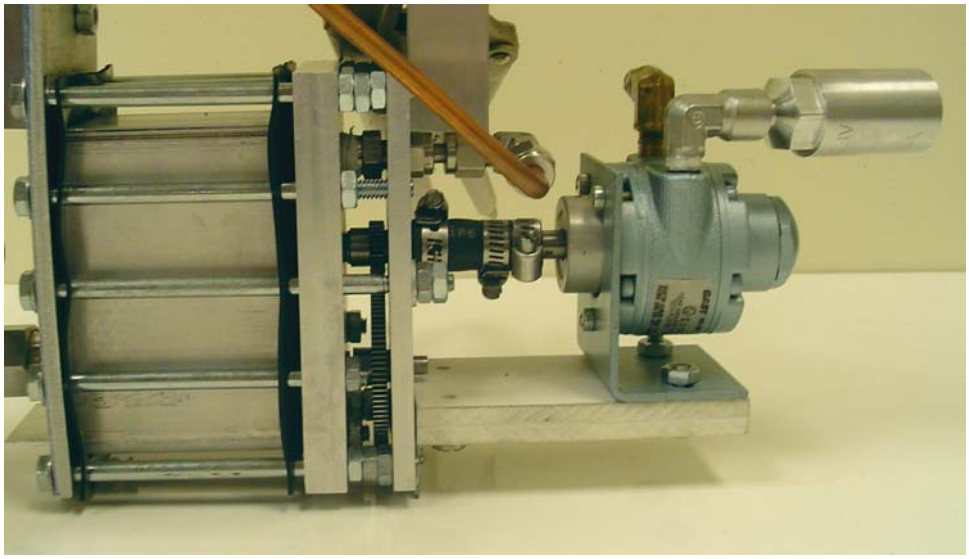

Figure 3.11 Compressed Air Motor

The output of the air-driven motor was geared in a 4:1 ratio to reduce the rotational speed to that required by the compressor. This was accomplished through the use of two stainless steel gears with a diametral pitch of 48. The gear had a pitch diameter of 63.5 mm (2.5 inches) and 120 teeth, whereas the pinion had a pitch diameter of 15.9 mm (0.625 inches) and 30 teeth. The air motor was connected to the pinion by means of a flexible coupling and a 6.4 mm (¼ inch) diameter shaft. Power was then transmitted to the input of the compressor through the gear assembly. This is shown in Figure 3.12.

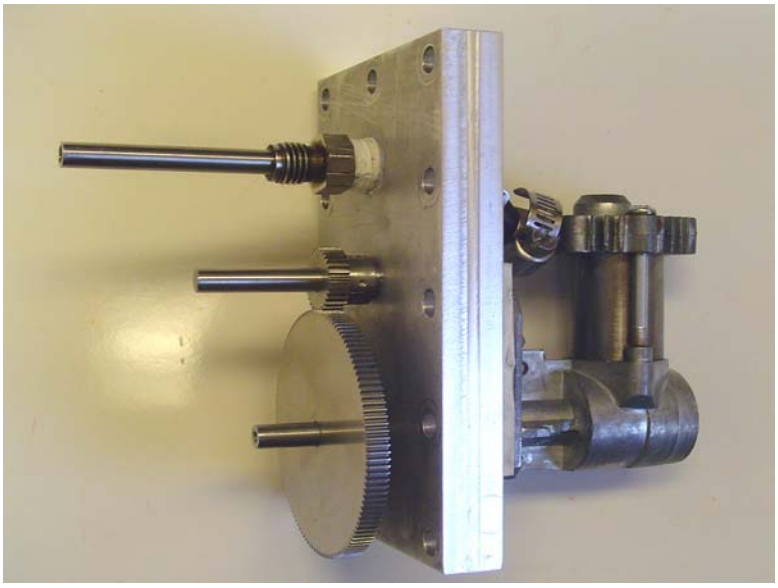

Figure 3.12 Reduction Gearing to Compressor

Airflow across the condenser was provided by an electric motor-driven axial flow fan (Master Airscrew MAS0740). (For the purposes of testing, an electric motor was used so that independent control of the fan speed would be possible). For the actual system, the fan drive was connected to the input of the overall system, eliminating the need for an electric motor. The fan blade was a high-speed axial flow propeller used for small model airplanes, with a diameter of 0.178 m (7 inches). During testing, the propeller was generally driven between 3000 and 5000 RPM.

Initially, a centrifugal fan was used that mounted directly on the input shaft to the compressor; however, the fan was not large enough to generate the airflow required to adequately cool the refrigerant at the desired condenser pressure. There is a trade off between fan work and compressor work. With lower fan work, the condenser refrigerant temperature increases, causing a higher refrigerant pressure in the condenser. This in turns leads to greater compressor work input. Conversely, as the fan work (and therefore

the airflow rate) is increased, the condenser pressure is lowered, requiring less compressor work. An optimal value of airflow of about 0.12 kg/s yields the best system efficiency, as discussed in Chapter 1 from the program used to model the overall system. The centrifugal fan initially used had an airflow rate of approximately 20 percent of the desired airflow. With the redesigned system using an axial airflow fan, the aiflow was increased to the desired level of approximately 0.12 kg/s and the condenser pressure decreased significantly to the intended design pressure of 1193 kPa (176 psia).

3.1.6 System Operation

Testing of the system began by setting the appropriate ambient (37.7-47.5°C) and coolant (26-30°C) temperatures. Next, the refrigeration cycle was started by allowing compressed air to enter the air motor, thus rotating the compressor. As the system approached steady state, the expansion valve began noticeably regulating the refrigerant flow, and therefore the pressure, to the evaporator. The system would continue to operate as it approached the desired conditions. The heat input was increased during this time to the desired level and the system pressures, temperatures, flow rate, and heat input were recorded.

The pressure, flow rate, and heat input were manually recorded by reading values from the various gauges in intervals of approximately 2-3 minutes, whereas the temperature data from the thermocouples were recorded using an IOTech data acquisition system (TempScan 1100) and a personal computer. Temperatures at nine locations were recorded throughout the cycle at an interval of ten seconds. They included five refrigerant temperatures at the condenser inlet and outlet, the evaporator inlet and outlet, and the compressor inlet downstream of the suction regulation valve. These same

locations were used to record the refrigerant pressures as well. Two thermocouples were used on the coolant loop at the inlet and outlet to the evaporator shell-side and two were used for the air flowing into and out of the condenser. TempView software was used to track and record the data. Onscreen charts were used to determine steady state conditions as well as responses to step changes in conditions such as compressor speed, evaporator heat input, and air temperature changes. Figure 3.13 provides an overview of the test facility and the corresponding instrumentation and data acquisition system.

Figure 3.13 Compressor Testing Arrangement

3.1.7 Compressor Testing Results

The compressor was able to deliver an average of 330 Watts of cooling in an ambient temperature of 37.7°C. As stated earlier, the purpose of the compressor testing was to determine whether the modified *air* compressor was capable of satisfactory operation under the required loads and flow conditions when used with *refrigerant*. Based on these compressor tests, the results described above demonstrated that it was capable of being

used as a refrigerant compressor for the system under consideration. After establishing feasibility, several modifications (described in subsequent sections) were made to the system to enable it to perform more reliably and efficiently, while being more compact and lightweight. Testing of the overall system and data analysis were conducted after the finalized system was fabricated.

3.2 Finalized Overall System

3.2.1 Finalized System Component Description

Upon completion of compressor testing, the final system was designed and built to operate as a personal cooling system. Figure 3.14 following shows the overall layout of the components of the system arranged for use in a portable cooling system.

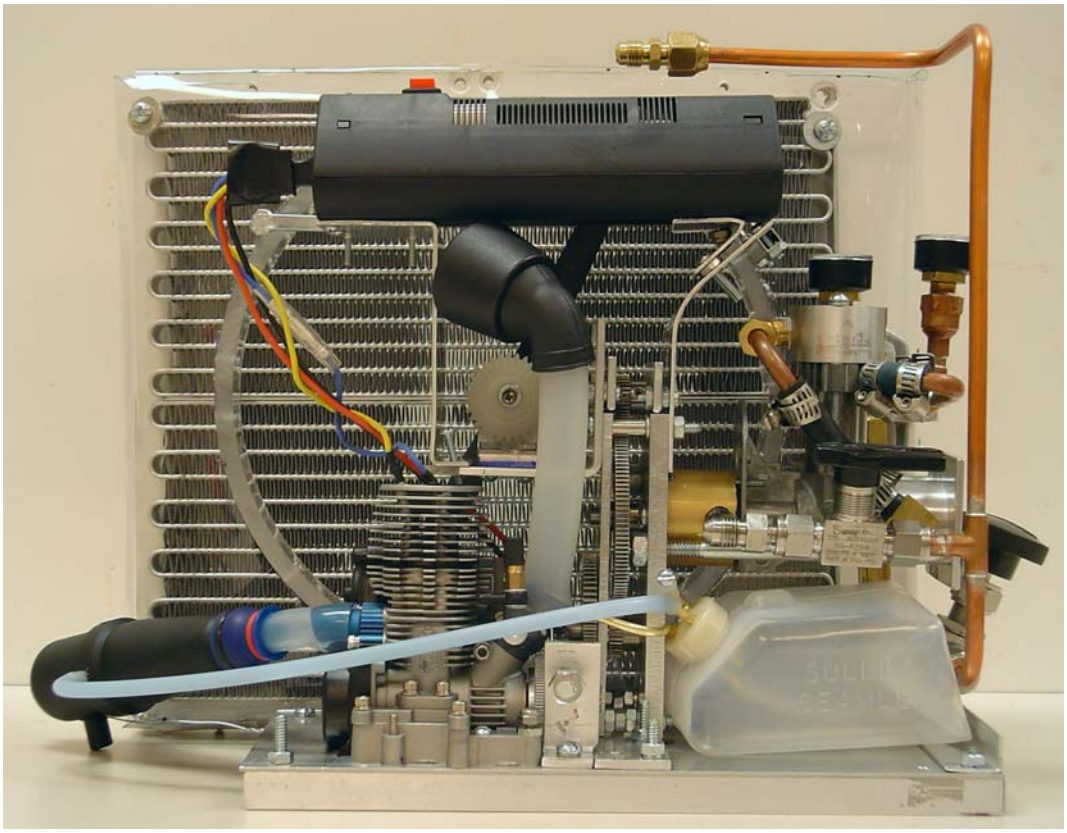

Figure 3.14 Finalized Portable Cooling System Configuration

Figure 3.15 shows the components required for engine starting, power generation, refrigerant compression and flow control, air flow control and fuel storage. The layout of the system components was initially established using Solidworks (2003) CAD modeling software.

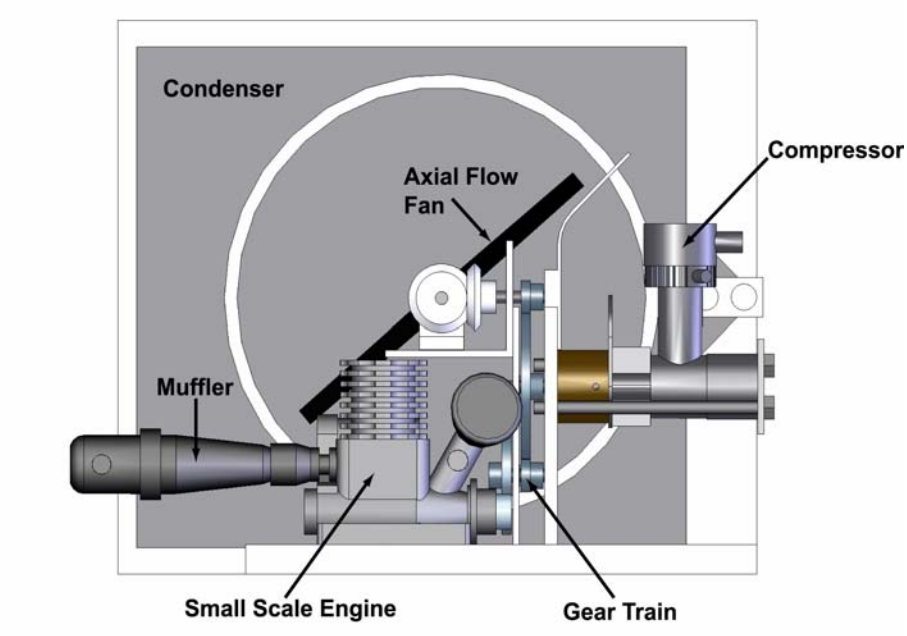

Figure 3.15 CAD Model of System

Figure 3.15 shows the CAD renderings of the system with the major components labeled. Toward the bottom center is the engine, which provides input power to the entire system. On the right is the refrigerant compressor with the modifications to the intake manifold and crankcase. The condenser is shown in the back, and establishes the overall cross-sectional profile of the system. Power to the compressor was delivered by means of a gear train (Figure 3.17) that reduced the engine speed at a 15.4:1 ratio. It also delivered power to the fan, which drew air across the condenser. Figure 3.16 provides two isometric views of the system.

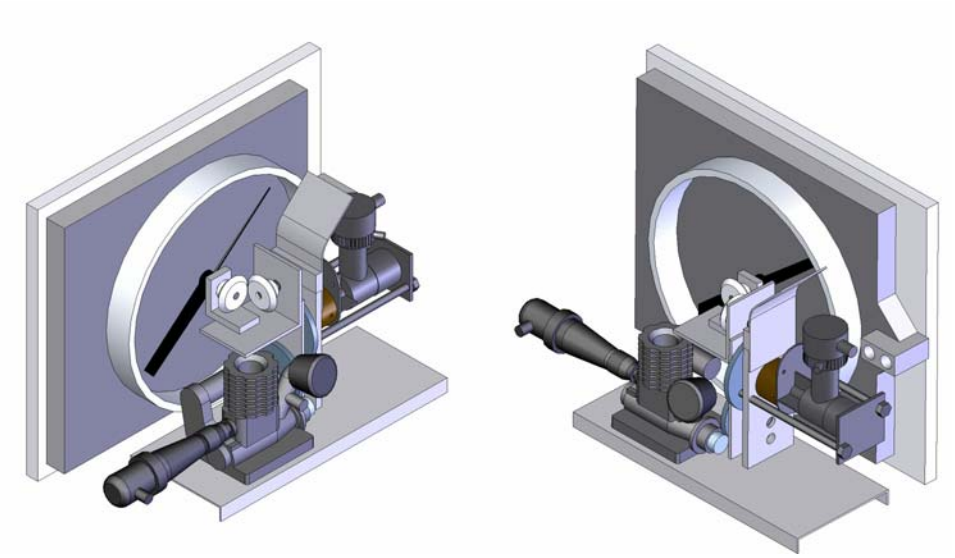

Figure 3.16 Isometric Views of the System

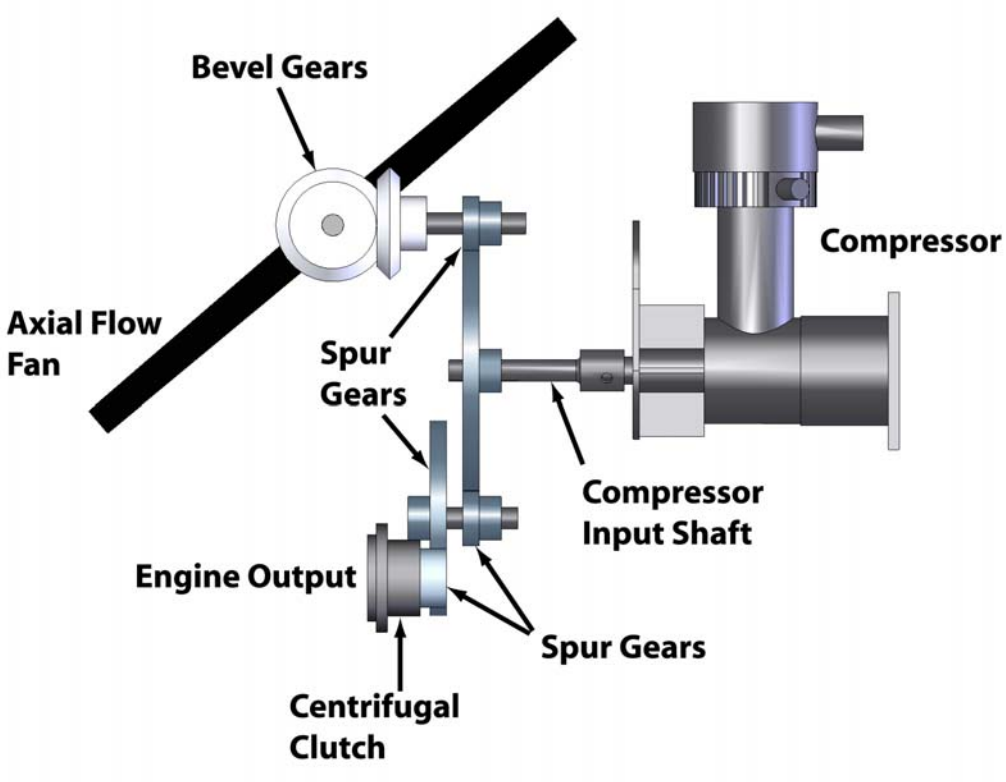

Figure 3.17 Reduction Gear Train

3.2.1.1 Engine and Reduction Gear Train

The input power to the cooling system was supplied by a Traxxas Model TRX-2.5, 2-stroke compression ignition engine, which had a displacement of 2.5 cubic centimeters and was capable of rotational speeds of up to 30,000 RPM. It delivered its power to the gear train by means of a centrifugal clutch. This allowed the engine to be started independent of the gear train and the associated load of the compressor and fan. The engine generally started quickly when the start button was depressed on the battery pack included with the engine which energized the electric starter and glow plug.

After the engine started and was allowed to operate for a short period of time, the engine throttle was increased causing the centrifugal clutch to engage, which also caused the drive train to rotate. The drive train was composed of three parallel and one perpendicular shafts as shown in Figure 3.18.

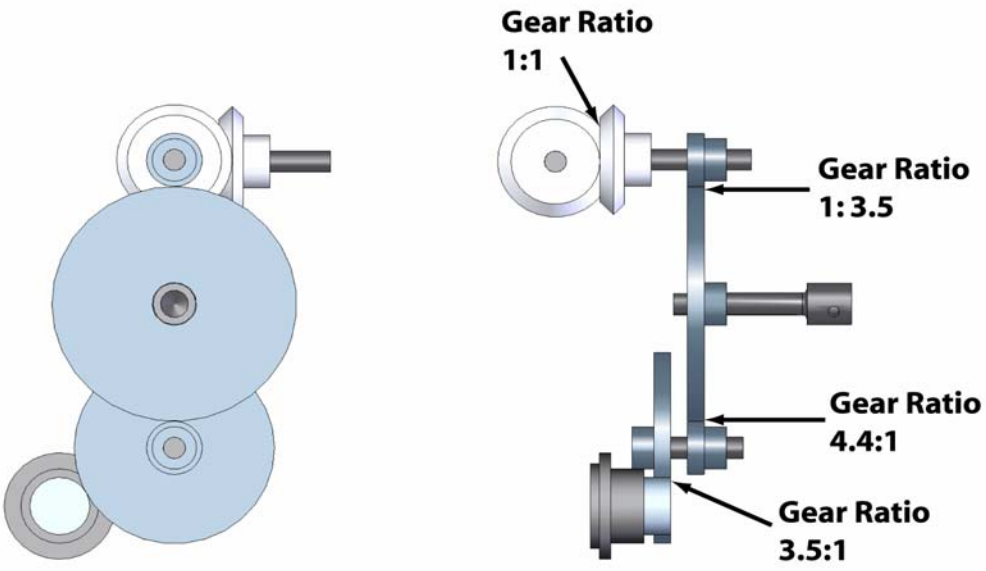

Figure 3.18 Gear Layout and Ratios

The input was first geared down in a 3.5:1 ratio from the engine to a shaft that was subsequently geared down in a 4.4:1 ratio; this low speed shaft rotated the compressor. This resulted in a speed reduction from the engine to the compressor of 15.4:1. From the compressor shaft speed, a gearing ratio of 1:4.4 was used to increase the speed for the condenser fan. The required location of the fan dictated the drive train configuration: the fan needed to be centered on the face of the condenser and the axis of the fan normal to it. This required using the gears to place it in the proper location and orientation. Two bevel gears were also used in a 1:1 ratio to change the axis of rotation by 90 degrees.

The gear train was held in place by means of two plates that held high speed bearings and provided the necessary distance and orientation to transmit power between the high and low speed shafts. The parallel plates were attached to the base and were part of the overall integrated structure that supported the entire system. The thick and thin aluminum plates are 6.4 and 3.2 mm (0.25 and 0.125 inches), respectively. The compressor hub was mounted directly on the thick aluminum plate, as shown later.

The engine was run on a mixture of fuel containing methane (78%), nitro-methane (10%), and castor oil (12%). As it was a two-stroke engine, the fuel contained the lubrication oil (castor oil) for the moving components. The fuel tank is slightly pressurized by the engine exhaust to maintain fuel flow to the engine, as shown by the 3.2 mm (⅛ inch) diameter flexible hose connecting the muffler and fuel tank in Figure 3.14.

3.2.1.2 Refrigeration System

The refrigeration system consisted of many of the same components that were used for the compressor testing, with modifications where necessary. The condenser remained unchanged except for the shroud used to direct airflow from the condenser to the fan,

which was made from a clear acetate sheet that was heated and formed to the desired shape.

Several modifications were made to the compressor after the initial feasibility testing was completed. Most notable was the elimination of the compressor enclosure that served as a reservoir of refrigerant vapor for the intake valve. Rather than using an enclosure to completely surround the compressor, the problems described earlier regarding the need for a pressurized crankcase were solved by other means.

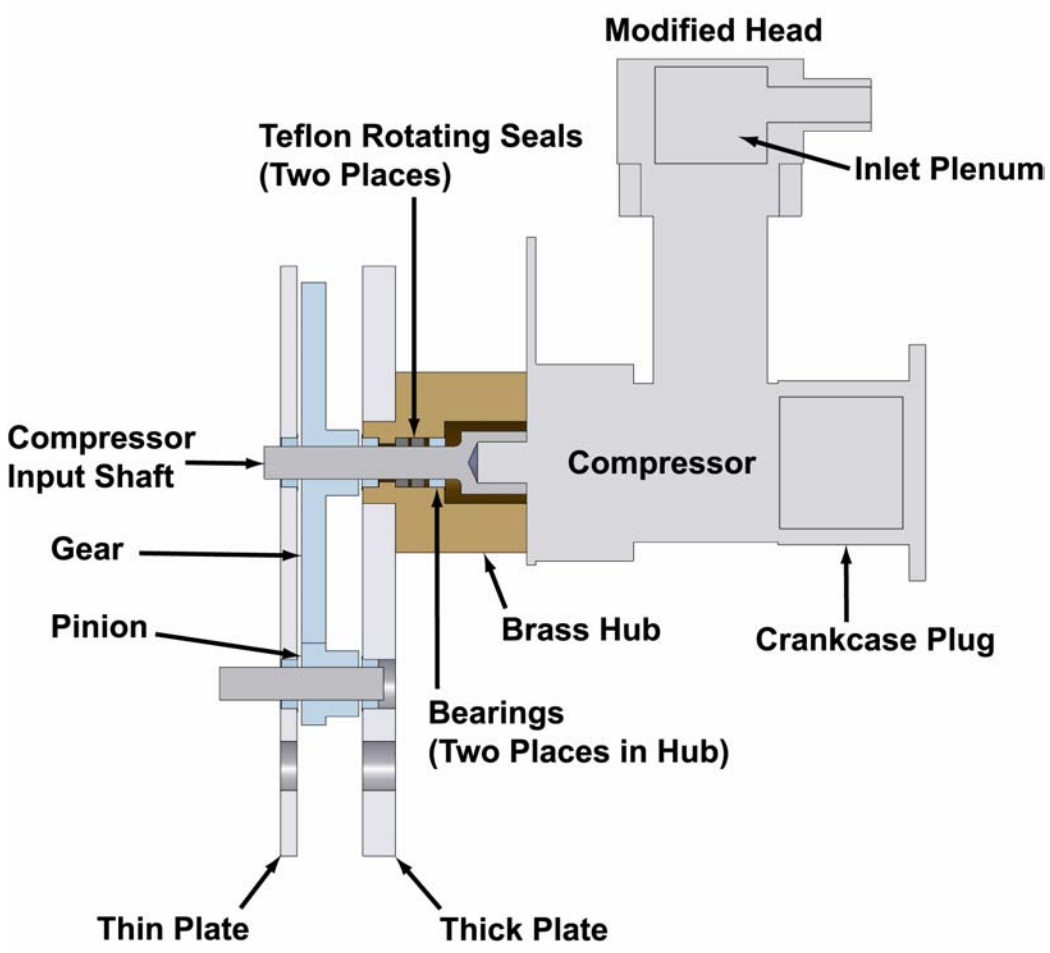

Figure 3.19 Compressor Layout

To provide back pressure to the piston, as described earlier, the crankcase was sealed using an aluminum plug that was clamped on the opening of the crankcase as shown in Figure 3.19. This plug allowed the crankcase to be extended outward for additional volume for lubricating oil as well as refrigerant. Sealing of the rotating crankshaft was accomplished using the Teflon rotating seals, as described earlier. The compressor input shaft traveled through a brass hub which held the two bearings and two Teflon seals which prevented leakage during rotation of the shaft.

The second change was to the compressor head, since the compressor was no longer contained inside the enclosure, a different method of delivering refrigerant to the intake valve was required. This was accomplished using a cylindrical plenum sealed to the compressor head. The plenum had a ⅛ inch NPT threaded port at the top for a small pressure gauge (Ashcroft 0-200 psi) and a ¼ inch NPT tap on the side for the refrigerant to flow from the evaporator. A ⅛ inch NPT port that allowed the crankcase to be pressurized was also provided. This tube connected to the crankcase plug, enabling the piston to have the required backside pressure for proper operation.

The aforementioned modifications to the refrigeration system had several advantages over the original configuration, including the reduction in weight and size, added simplicity, ease of compressor change out, and increased ability for heat rejection to the surrounding air directly from the compressor. The reconfiguration allowed the elimination of the rectangular enclosure and associated endplates, gaskets and bolts. Rather than sealing the entire volume surrounding the compressor, the crankcase was sealed and the compressor body itself became the pressure vessel. This allowed for significant reductions in weight and overall size of the compressor system. Change out

of the compressor also required less disassembly, and these changes enabled easier access.

Heat generated from the friction of the piston and the cylinder wall, as well as the compression of refrigerant gases, heated the head and walls of the cylinder significantly. With the redesigned system, the compressor itself was exposed to the surrounding air which enabled increased heat removal, rather than being absorbed by the refrigerant that was originally surrounding it inside the enclosure.

3.2.2 Finalized System Testing

Testing of the portable cooling system was initiated after the final system was built.

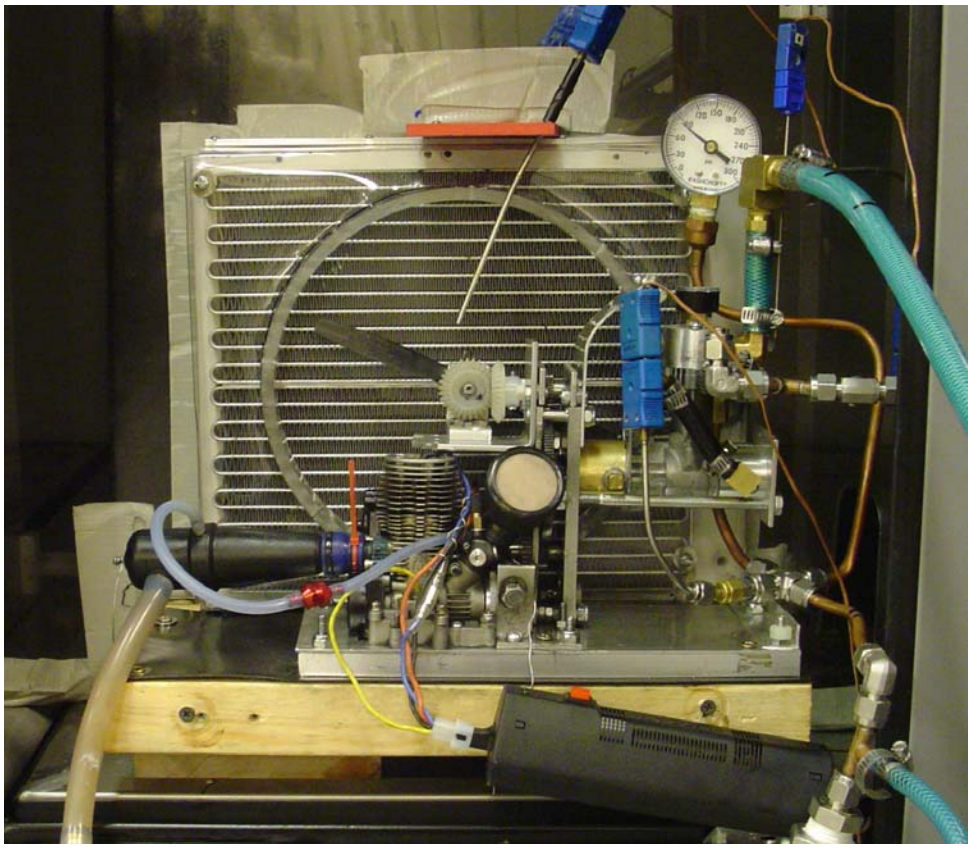

Figure 3.20 Cooling System Test Configuration

In these tests, the engine was used as the source of power for both the fan and the reconfigured compressor. The testing configuration included additional instrumentation to allow system and component performance measurements throughout the cycle. (It should be noted that for a portable version of the cooling system, much of the instrumentation would not be used.) Also, some components such as the battery pack and fuel tank were removed from the overall structure for ease of use during testing.

The entire system was placed inside an air handler (Figure 3.21) that was used to provide air at the controlled elevated temperatures necessary for testing. The system was shielded from the effect of the air handler's own air movement by means of a Plexiglas enclosure to ensure that condenser airflow was generated solely by the fan integral to the cooling system. A Mannix model DCFM 8906 digital turbine anemometer was used in front of the condenser to ensure that the effect of the air handler's own air movement was negligible compared to the fan's air movement. This was accomplished by testing the air flow rate across the condenser with the air handler both operating and while shut off; the difference in the air flow rate between the two cases was found to be negligible.

Figure 3.21 shows three photographs which display the details of the air handler used to simulate the elevated temperature environment (a), as well as the testing configuration (b) and also a close up of the cooling system (c).

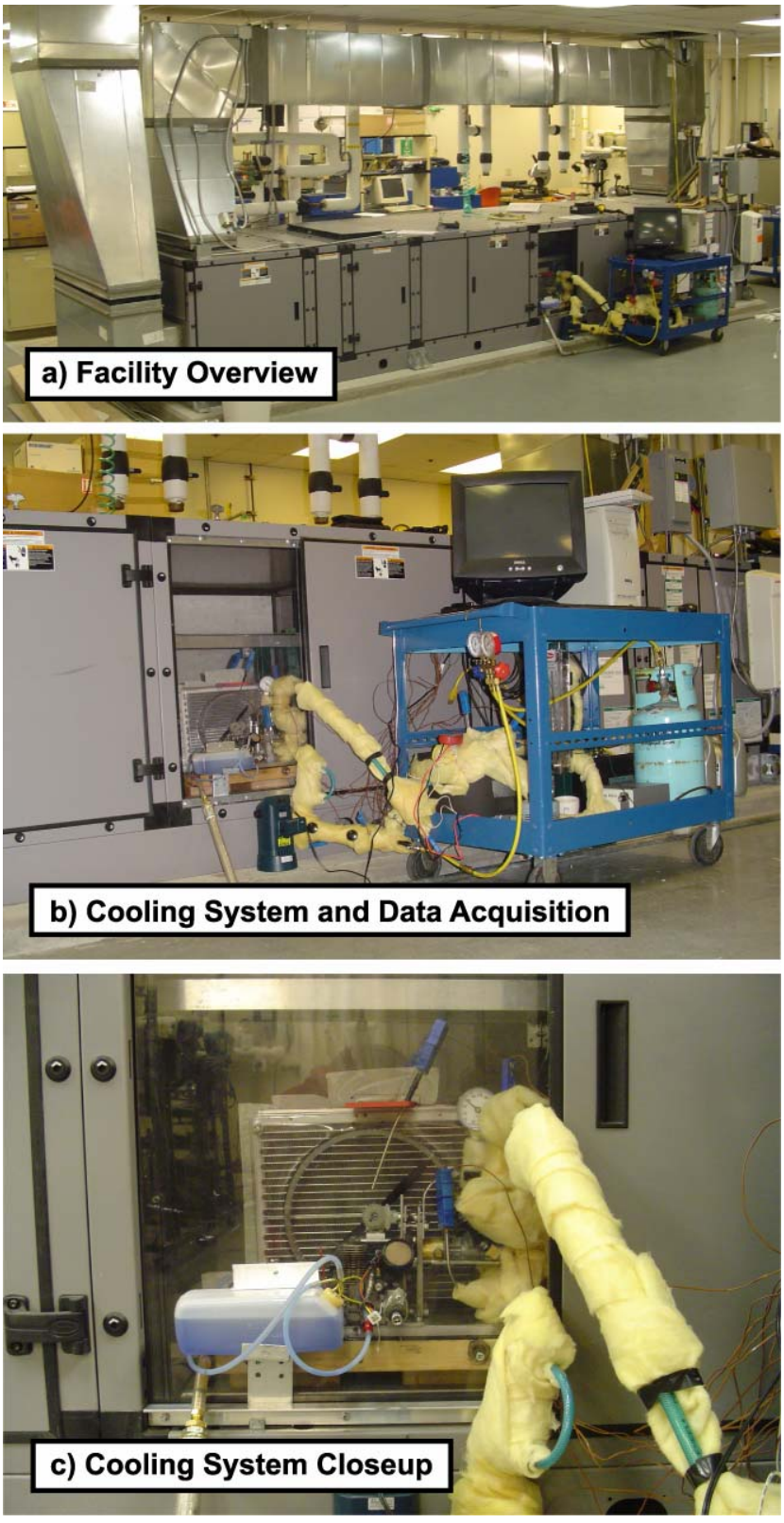

Figure 3.21 Cooling System Being Tested at Controlled Elevated Temperatures

As shown in Figure 3.22, the Plexiglas enclosure cross section was larger than the condenser face. For this reason, an internal barrier was used to separate the regions of air toward the front and back of the condenser. The air was drawn in the face of the condenser and discharged across the compressor and engine, which allowed both

Figure 3.22 Plexiglas Enclosure Inside Air Handler (2 Views)

components to be cooled by the passing air. The barrier prevented cycling of the air back to the front of the condenser inside the enclosure. This allowed the condenser to draw air from the air handler at the desired temperature and discharge it without recirculation. The entire enclosure was located approximately 10 cm (4 inches) away from the wall of the air handler; this gap allowed the heated air discharged from the condenser to flow out of and away from the enclosure.

The engine speed was controlled by means of a throttle linkage that extended outside the Plexiglas enclosure. The fuel tank was also located outside to enable refilling of the tank when necessary. The engine exhaust was routed out of the air handler and to a fume hood. The electrical connections were also routed to the exterior to allow the battery pack to be connected to the starting circuit of the engine.

As described above, the majority of the cooling system components were contained inside the air handler. This is a more realistic configuration since the entire system would be at the elevated ambient temperature during use. However, to allow measurement and control of the evaporator duty, refrigerant lines were routed out of the air handler to a test evaporator, as shown in Figure 3.23. The evaporator had the same configuration as described previously in the compressor testing. The expansion valve was also located outside the air handler, which allowed adjustments to be made as necessary during testing. The expansion valve was a 6.4 mm (¼ inch) Swagelock needle valve, which allowed control of the low-side pressure to the desired value. A section of transparent hose was used in-line upstream of the expansion valve to enable a visual check of the refrigerant leaving the condenser. This allowed verification that the system had a sufficient refrigerant charge and that the refrigerant exited the condenser as a subcooled

liquid. The lines to and from the evaporator were insulated with fiberglass to minimize unwanted heat transfer.

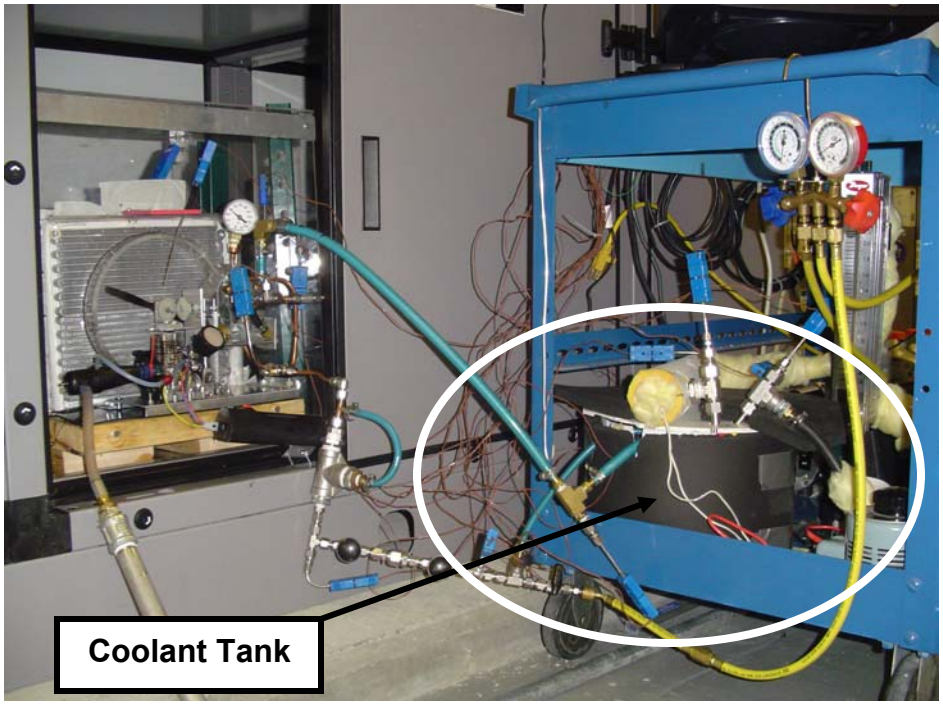

Figure 3.23 Test Evaporator

As mentioned previously, the test evaporator was similar to the evaporator used during compressor testing. The three differences were the method of heat input measurements, the use of a different coolant flow meter, and the use of a 50/50 mixture of water and ethylene glycol for the coolant. The heat duty of the evaporator was obtained by measuring the voltage and current to the cartridge heater using an Omega model HHM93 digital voltmeter and an Amprobe model ACD-10 TRMS digital clamp-on ammeter. The voltage to the heater was varied using a Powerstat model 116 variable transformer capable of an output of up to 1000 W. In addition, the evaporator duty computed from the coolant temperature difference and flow rate was used as a means of validating this measured heater input. The coolant flow meter was a 0-2.2 GPM Dwyer

model RMC-142-SSV rotameter. The coolant was circulated using a Barnant Model 75225-12 variable speed pump, typically at a flow rate of approximately 1500 mL/min. Inside the 8 liter coolant tank, the refrigerant tubing had the same spirally wound pattern as described earlier, with the coolant flowing in a counter flow arrangement to the refrigerant. The refrigerant leaving the evaporator flowed through a flexible transparent hose to ensure that it was in a superheated state upon exiting the evaporator. It then returned to the suction side of the compressor inside the air handler via another flexible hose.

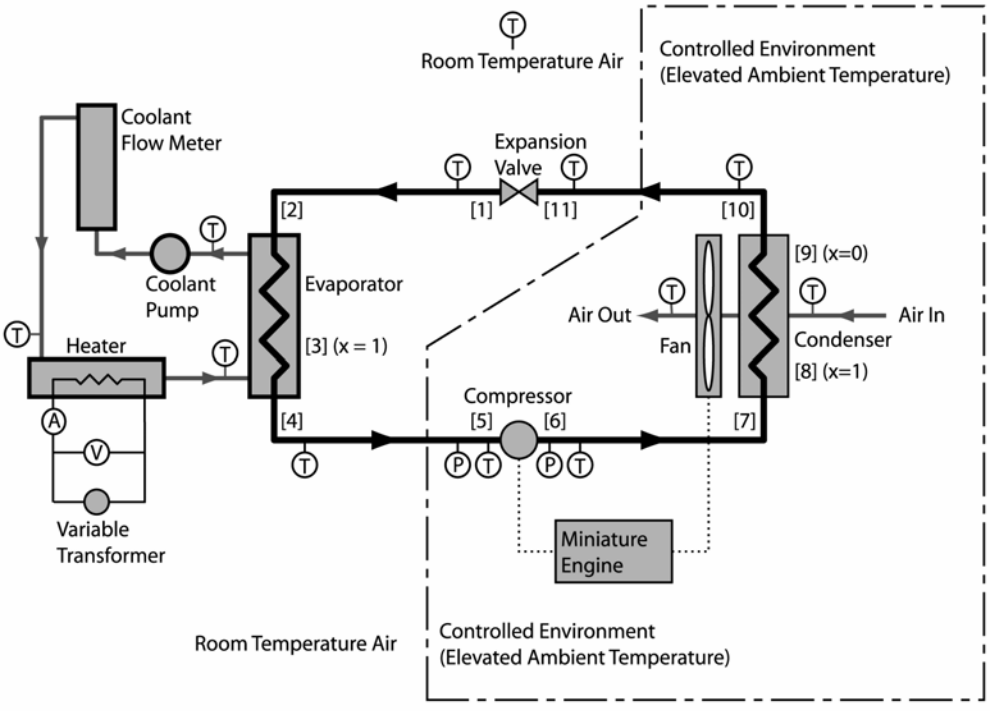

Figure 3.24 Test Loop Schematic

As shown in Figure 3.24, twelve temperatures and two pressure measurements were taken around the test loop during testing to monitor the system performance. The refrigerant temperature was measured and recorded using type T thermocouples in 6

locations in the cycle, the water side was measured in 3 locations, and the air temperature was measured in 3 locations. These measurements are described in Chapter 4, where the analysis of the data is presented in detail. The high and low side refrigerant pressures were also measured using Ashcroft 0-200 psig and 0-300 psig pressure gauges, respectively. In addition to this, the coolant flow rate was measured along with the heater voltage and current. To determine the engine speed, a Monarch Instrument digital stroboscope model BA-115 was employed.

Three parameters were varied during the testing of the portable cooling system: the ambient air temperature, the engine speed and the evaporator temperature. Testing was performed over an ambient temperature range of 37.7-47.5°C (100-117.5°F), evaporator temperatures were varied from 22.2-26.1°C (72-79°F), and the engine speed was varied from 10,500-13,300 RPM. Some additional testing was also done outside these ranges to investigate the maximum potential performance of the system.

During each test, the system was allowed to achieve steady state operation at the desired combination of test conditions. Temperatures were recorded at a scan rate of one scan per second over the entire duration of testing. The pressures, heater voltage and current, and water flow rate were recorded periodically throughout the testing, typically every 2-3 minutes. The system was generally allowed to operate at a steady state condition for approximately 5-10 minutes while data were taken. These data were analyzed to obtain component and system performance measures, described in Chapter 4.

4. DATA ANALYSIS

The tests of the portable cooling system described in the previous chapter were conducted to examine the effect of three primary parameters on system performance. Three values each of the ambient air temperature, the evaporator water temperature, and the engine speed were investigated, for a total of 27 combinations of conditions. An additional four conditions outside the test matrix were investigated to establish the effects of increased engine speed. The analysis of the data obtained in these tests is explained in detail in this chapter (and also in Appendix D), using a representative data point at the following conditions for illustrative purposes:

- Ambient Air Temperature = 43.5°C (110.3°F)
- Evaporator Average Coolant Temperature = 29.9°C (85.8°F)
- Engine Speed = 13,300 RPM

4.1 System Overview

A schematic of the portable cooling system test facility (presented earlier in Chapter 3), is shown in Figure 4.1. The facility can be divided into two major portions – the high ambient temperature region inside the air handler, and the cooled components region. Thus, the compressor, condenser and engine were placed inside the air handler with a controlled elevated temperature. The dashed line spanning the circumference of the condenser, compressor and engine indicates the components located inside the elevated-temperature environment. The evaporator and associated tubing were at room temperature air of nominally 25.6°C (78.1°F). The refrigerant temperatures and

pressures were measured at the various locations around the refrigerant system as shown in Figure 4.1 to measure the operating conditions.

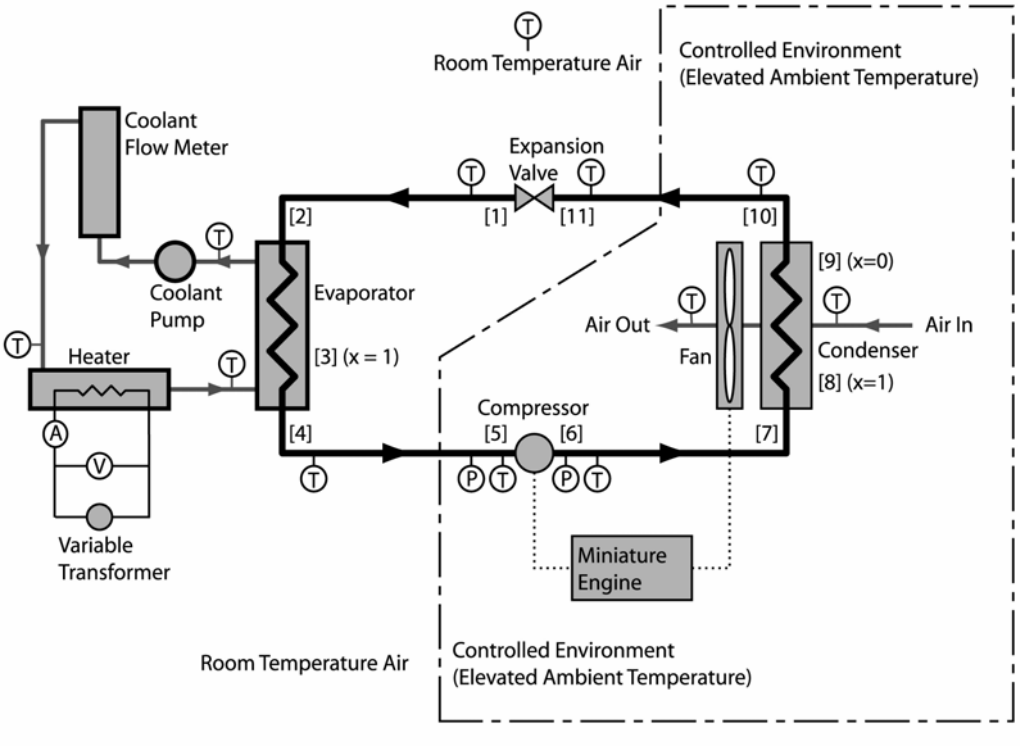

Figure 4.1 Portable Cooling System Schematic

The refrigerant cycle is shown in bold lines, and the evaporator coolant loop in gray lines. The coolant loop is used to provide the desired heat load to the evaporator. Toward the right-hand side is the air-coupled refrigerant condenser used to remove heat from the refrigerant. Table 4.1 shows the values of the measured test conditions for a representative data point.

Table 4.1 Measured Data

Refrigerant Cycle:	***SI Units***	***British Units***
Evaporator refrigerant inlet temperature [2]	24.9°C	76.8°F
Evaporator refrigerant outlet temperature [4]	29.1°C	84.4°F
Condenser refrigerant inlet temperature [7]	68.9°C	156.0°F
Condenser refrigerant outlet temperature [10]	50.4°C	122.7°F
Compressor refrigerant inlet temperature [5]	28.3°C	82.9°F
Compressor refrigerant outlet temperature [6]	68.9°C	156.0°F
Expansion valve refrigerant inlet temperature [11]	50.4°C	122.7°F
Expansion valve refrigerant outlet temperature [1]	24.9°C	76.8°F
Low-side refrigerant pressure [5]	663.8 kPa	96.3 psia
High-side refrigerant pressure [6]	1370 kPa	198.7 psia
Condenser Air-Side:		
Condenser air inlet temperature	43.5°C	110.3°F
Condenser air outlet temperature	46.0°C	114.8°F
Engine speed	13,300 RPM	
Evaporator Coolant-Side:		
Evaporator coolant inlet temperature	30.9°C	87.6°F
Evaporator coolant outlet temperature	28.8°C	83.8°F
Coolant volumetric flow rate	2.555×10^{-5} m^3/s	0.405 GPM
Heater voltage	58.2 Volts	
Heater amperage	3.86 Amps	
Heater coolant inlet temperature	28.7°C	83.7°F
Heater coolant outlet temperature	30.9°C	87.6°F
Other Variables:		
Coolant	50% Prestone coolant, 50% water	
Coolant specific heat	3412 J/kg-K	Coolant Manual (Prestone, 2001)
Coolant density	1069 kg/m^3	Coolant Manual (Prestone, 2001)
Coolant Volume	0.008 m^3	2.11 gallon
Room Air Temperature	25.6 °C	78.1°F

4.2 Cycle Diagrams

The thermodynamic cycle for the representative test condition presented in Table 4.1 is shown in Figure 4.2 on a temperature-entropy diagram for R134a. For reference, the condenser air temperatures and the evaporator coupling fluid temperatures are also shown, although the entropy scale does not apply to these fluids.

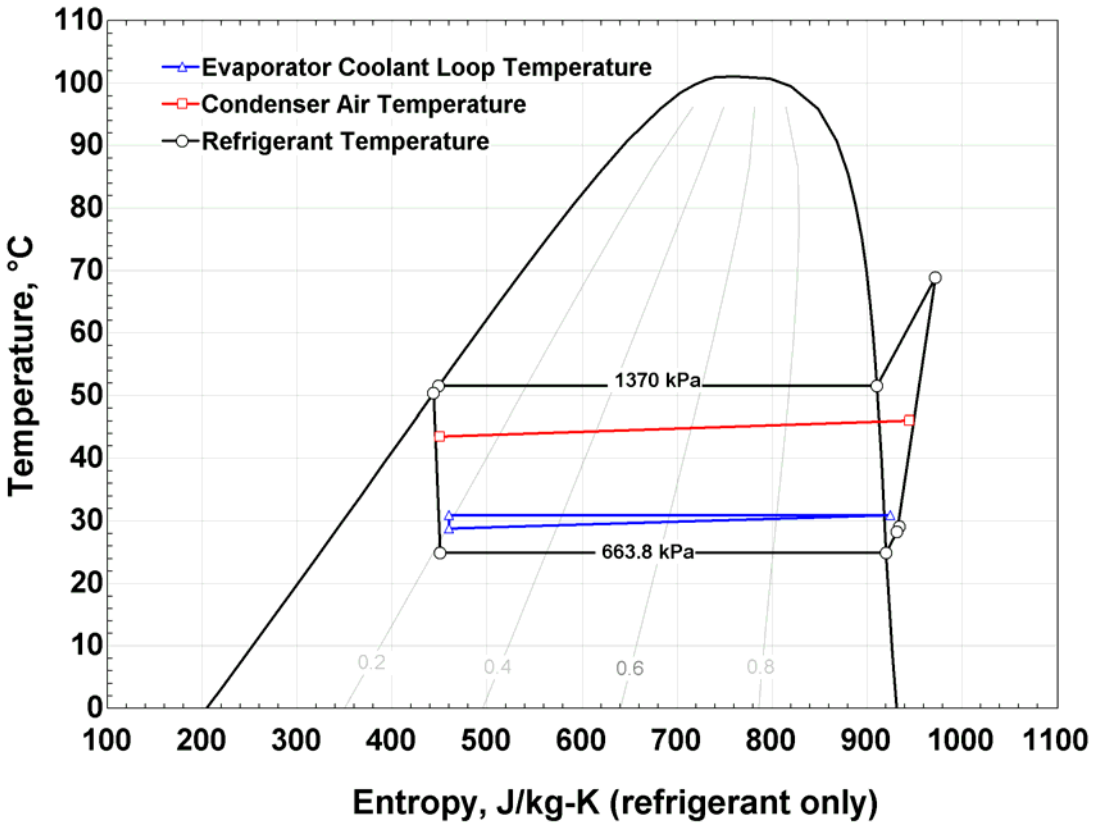

Figure 4.2 Temperature-Entropy Diagram for the Representative Data Point

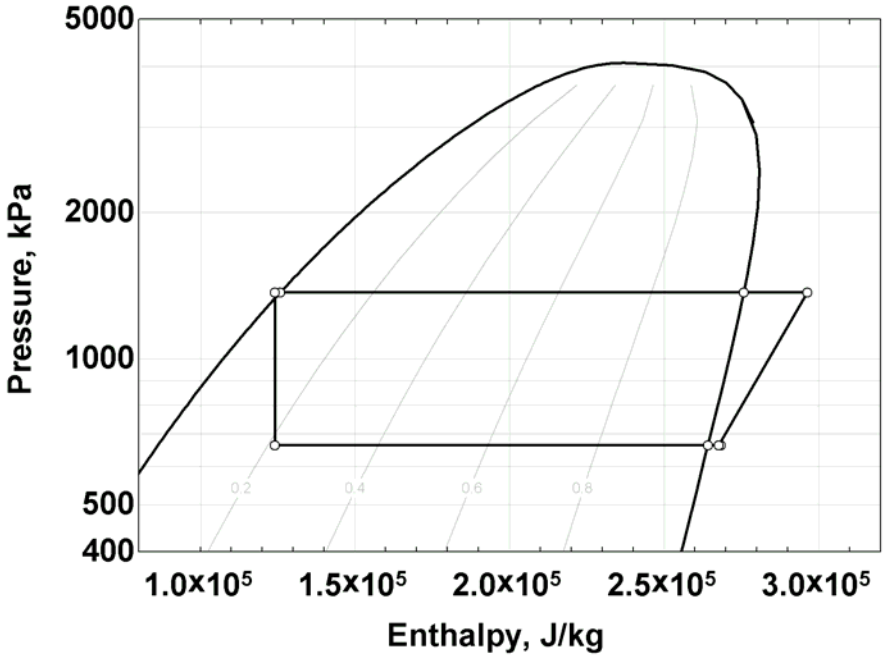

Figure 4.3 Pressure-Enthalpy Diagram for the Representative Data Point

The data were also plotted on a pressure-enthalpy diagram using EES software, as shown in Figure 4.3.

4.3 Sample Calculations

4.3.1 Thermodynamic Cycle Analysis

The calculations begin by first determining the heat input to the system. This yields the key indicator of system performance and is also used to calculate the refrigerant mass flow rate. The flow rate of the refrigerant is used to determine several different cycle values throughout the refrigerant loop. The evaporator heat load is calculated using the input voltage and current to the heater as follows:

$$\dot{Q}_{evap,heater} = V \cdot I \tag{4.1}$$

For this test case, the heater voltage and amperage were measured to be 58.2 Volts and 3.86 Amps, respectively, resulting in a heater input of 225 Watts. Of this heat input, the amount supplied to the coolant was computed by accounting for any potential thermal storage in the loop during the test. This is because, during testing, it was desired to keep the coolant tank temperature constant; however, slight variations occurred over time if the heat input did not exactly match the evaporator duty. To account for this, the change in temperature of the coolant tank was taken into account. The calculation proceeds as follows. The total mass of coolant in the tank is measured using:

$$m_{coolant} = \rho_{coolant} \cdot vol_{coolant} \tag{4.2}$$

where $vol_{coolant}$ is the total volume of coolant in the system, and is equal to 0.008 m^3 (8 L). With a coolant density of 1069 kg/m^3, as obtained from the Prestone coolant manual (Prestone, 2001) for a 50/50 mixture of ethylene glycol and water, the coolant mass is 8.552 kg. Using this mass of coolant along with the specific heat of coolant, 3412 J/kg-K, the energy stored in the coolant loop is estimated as follows:

$$\dot{Q}_{storage} = m_{coolant} \cdot c_{p,coolant} \cdot \frac{-dT_{average}}{dt} \tag{4.3}$$

The coolant tank temperature was taken as the average of the incoming and outgoing coolant. The change in the value of the average tank temperature was computed over the interval of time over which the specific data point was taken. For the representative case, $dT_{average}/dt$ was -1.88×10^{-4}°C/s. This duty due to thermal storage generally represented only a small fraction of the total evaporator duty. Thus, for the case shown, the heat duty associated with the change in coolant tank temperature was 5.5 W, compared to the heater input of 225 W. Over the range of experiments conducted in this study, the

thermal storage portion of the evaporator load typically varied from 1 to 12 percent with an average across the test matrix of 8 percent. The total indicated evaporator duty is the sum of the heater input power and the duty associated with the change (in this case, due to the negative change in temperature, the additional cooling of the storage tank) in internal energy of the tank:

$$\dot{Q}_{evap,total} = \dot{Q}_{evap,heater} + \dot{Q}_{storage} \tag{4.4}$$

This results in a total evaporator duty of 230 W, and will later be compared with the value calculated from the coolant side using the flow rate and temperature difference. With the evaporator heat duty calculated, the refrigerant mass flow rate is determined next, which allows the calculation of the various heat and work inputs/outputs to the refrigerant system. The refrigerant flow rate is calculated using the evaporator heat duty and the refrigerant inlet and outlet enthalpies:

$$\dot{m} = \frac{\dot{Q}_{evap,total}}{\left(h_{evap,out} - h_{evap,in}\right)} \tag{4.5}$$

The refrigerant enthalpies are obtained using the temperatures, pressures and qualities (as appropriate) throughout the system; EES software (Klein, 2004) was used for determining the enthalpies. The evaporator outlet and inlet enthalpies were 268,418 J/kg and 124,082 J/kg respectively. The refrigerant outlet enthalpy was determined from the measured temperature of 29.1°C and pressure of 663.8 kPa because of its superheated state ($\Delta T_{superheat}$ = 4.2°C). The inlet enthalpy of the evaporator was obtained by setting it equal to the enthalpy at the inlet of the expansion valve, i.e., 124,082 J/kg, which

assumes an isenthalpic expansion. With the total evaporator duty of 230 W, the refrigerant mass flow rate was calculated to be 1.60×10^{-3} kg/s.

With the refrigerant mass flow rate known, the condenser heat rejection based on the refrigerant side can also be calculated as follows:

$$\dot{Q}_{cond,refrigerant} = \dot{m}\left(h_{cond,in} - h_{cond,out}\right) \tag{4.6}$$

At a condenser pressure of 1370 kPa, the refrigerant saturation temperature is 51.5°C. The refrigerant entered the condenser at 68.9°C, i.e., a superheat of 17.4°C, which yielded an enthalpy of 297,405 kJ/kg. At a refrigerant exit temperature of 50.4°C ($\Delta T_{subcool}$ = 1.1°C), the enthalpy was 124,082 kJ/kg. With these enthalpies and the mass flow rate calculated above, the condenser heat rejection based on the refrigerant side was 275 W. This heat rejection will be compared later with the measured value obtained from the air side of the condenser. The compressor work input was also calculated using the compressor inlet and outlet enthalpies as follows:

$$\dot{W}_{comp} = \dot{m}\left(h_{comp,out} - h_{comp,in}\right) \tag{4.7}$$

The compressor inlet and outlet enthalpies were evaluated at the temperatures of 28.3°C and 68.9°C, respectively, and low and high side pressures of 663.8 kPa and 1370 kPa, respectively. The outlet and inlet enthalpies of 296,405 J/kg and 267,606 J/kg, respectively, yield a compressor work input of 46 W. Using the measured outlet and inlet enthalpies of the compressor along with the compressor isentropic outlet enthalpy, the compressor efficiency η_{comp} was determined as follows:

$$\eta_{comp} = \frac{h_{comp,out,isen} - h_{comp,in}}{h_{comp,out} - h_{comp,in}} \tag{4.8}$$

For this representative point, the isentropic outlet enthalpy of the compressor was 282,790 J/kg, which yields a compressor efficiency η_{comp} of 0.5273. The refrigerant temperature was measured prior to entering the intake plenum of the compressor and after exiting the discharge tube from the compressor. Heat exchange took place from the discharge tube as it passed through the intake plenum to the lower temperature refrigerant surrounding it. This results in the compressor efficiency appearing slightly higher than the actual efficiency due to the effect of the measurement location.

4.3.2 Air-Side Analysis

The condenser heat duty obtained by using the refrigerant flow rate and enthalpies was compared with the heat duty determined from the measured air flow rate and the inlet and outlet air temperatures. To determine the airflow rate across the condenser, a correlation for air flow rate as a function of fan speed was developed. The fan speed was measured using a stroboscope and the air velocity was measured with a turbine anemometer, averaging over the face of the condenser. The following second order polynomial curve-fit yielded a correlation coefficient of 0.996 over the range 2400 - 4000 RPM:

$$V_{air} = a_0 \cdot rpm_{fan}{}^2 + a_1 \cdot rpm_{fan} + a_2 \tag{4.9}$$

where $a_0 = 4.40\times10^{-8}$ m/s-RPM², $a_1 = 0.000219$ m/s-RPM, and $a_2 = 0.0774$ m/s. Additional details of the development of this correlation are shown in Appendix E. For the case under consideration, at a fan speed of 3800 RPM (engine speed = 13,300 RPM), the measured air velocity was 1.545 m/s (304.1 ft/min). The air flow rate was calculated

using this flow velocity and the condenser flow area. The face area of the condenser with a width and height of 0.2223 m and 0.2413 m respectively is:

$$A_{face} = width \cdot height \tag{4.10}$$

which results in a face area of 0.05363 m². The corresponding air flow rate is 0.0829 m³/s (175.6 cfm). The air-side condenser duty is given by:

$$\dot{Q}_{cond,air-side} = \mathrm{V}_{\mathrm{air}} \cdot A_{face} \cdot \rho_{air} \cdot c_{p,air} \left(T_{air,out} - T_{air,in} \right) \tag{4.11}$$

where the air density is 1.098 kg/m³, the specific heat of air is 1007 J/kg-K and the outlet and inlet air temperatures are 46.0°C and 43.5°C, respectively. This yields a value of 232 W for the air-side duty compared with the value obtained from the refrigerant side of 275 W: a difference of 43 W, or 18 percent. A potential source of this error may have been variation of the air temperature across the face of the condenser, since it was measured in only one inlet and one outlet location. Variations in the air outlet temperature due to differences in the refrigerant temperature (in the superheated, saturated and subcooled regions) are not appropriately accounted for in this measurement. Any variation in air temperature across the face of the condenser would cause errors in the calculated duty. The discrepancy in the measurements of the air-side and refrigerant-side condenser duty was typically between 1-20 percent, with an average of 9 percent across the entire test matrix.

The engine speed is also calculated from the measured fan speed, using the ratio of the gears between the two components, $\mathrm{ratio}_{\mathrm{gear1}} = 3.5{:}1$, as follows:

$$rpm_{engine} = rpm_{fan} \cdot ratio_{gear1} \tag{4.12}$$

The fan speed for this case was 3800 RPM, which yields an engine speed of 13,300 RPM. The compressor rotational speed was also computed from the fan speed, using a gear ratio of 4.4:1:

$$rpm_{compressor} = \frac{rpm_{fan}}{ratio_{gear2}} \tag{4.13}$$

The resulting compressor rotational speed is 864 RPM for this data point.

4.3.3 Coolant-Side Analysis

The evaporator duty was also measured using coolant side parameters of flow rate and the temperature at the inlet and outlet of the evaporator tank. The coolant mass flow rate was calculated as follows:

$$\dot{m}_{coolant} = \rho_{coolant} \cdot v\dot{o}l_{coolant} \tag{4.14}$$

where $\rho_{coolant}$ is the coolant density (1069 kg/m³ for the representative data point). The volumetric flow rate of the coolant $v\dot{o}l_{coolant}$, as measured with the rotameter, was 2.555×10^{-5} m³/s (0.405 GPM), which results in a coolant mass flow rate of 0.02731 kg/s. The coolant-side heat duty can be represented as follows:

$$\begin{aligned}\dot{Q}_{evap,coolant} &= \dot{m}_{coolant} \cdot c_{p,coolant}\left(T_{coolant,in} - T_{coolant,out}\right) \\ &+ m_{coolant} \cdot c_{p,coolant} \cdot \frac{-dT_{average}}{dt}\end{aligned} \tag{4.15}$$

The first part of the equation indicates the duty calculated from the change in temperature of the coolant at the inlet and outlet of the evaporator tank and the second half of the equation accounts for the change in temperature of the entire tank of coolant over time, as explained earlier. With the total mass of coolant in the system of 8.552 kg, a coolant

specific heat of 3412 J/kg-K, tank inlet and outlet temperatures of 30.9°C and 28.8°C, respectively, and the average rate of change in temperature of the coolant ($dT_{average}/dt$) of -1.88×10^{-4}°C/s, the coolant-side duty was found to be 211 W (with 5.5 W of the duty due to thermal storage). The corresponding heat duty based on heater input calculations was 230 W, i.e., a difference of 19.5 W. The difference was typically between 1-15 percent, with an average difference of 5 percent.

4.3.4 System Performance

The work input to the system could not be readily measured because of the use of the small-scale engine, as compared to an electric motor. Therefore, the coefficient of performance of the system (COP) on the basis of the input power from the engine could not be determined precisely. The compressor work is obtained as shown in the previous analysis; however the fan work could not be measured. In lieu of this, the system performance was quantified in two ways: the first was a pseudo-coefficient of performance which took into account only the compressor work input (neglecting the fan work) and the second was by using the measured evaporator duty and fuel energy usage. The pseudo-coefficient of performance (COP_{pseudo}) was calculated as follows:

$$COP_{pseudo} = \frac{\dot{Q}_{evap,total}}{\dot{W}_{comp}} \tag{4.16}$$

where the total evaporator heat duty was 230 W and the compressor work input was 46 W. This results in a pseudo-coefficient of performance of 5.0, neglecting the fan work input.

The fuel used was Traxxas TRX 2.5 racing engine fuel. It consisted of 78 percent methanol (methyl alcohol), 10 percent nitro-methane and 12 percent lubricating oil

(Traxxas, 2004). The fuel was modeled as having a content of 88 percent methanol and 12 percent oil. This is because the nitro-methane does not add significantly to the energy content of the methanol fuel, but rather adds additional oxygen used during combustion, and therefore can be modeled as methanol (Chemlink, 2004). The oil was assumed to have no effect on the combustion process other than lubricating the moving parts. For the case shown, the average fuel mass flow rate was measured to be 0.316 kg/hr (8.78×10^{-5} kg/s). The corresponding energy consumption rate is calculated as:

$$\dot{E}_{fuel} = \dot{m}_{fuel} \cdot LHV \tag{4.17}$$

where LHV is the lower heating value of liquid methanol (1.992×10^{7} J/kg). This results in an energy consumption rate of 1749 W from the fuel. This is then compared to the evaporator cooling duty of 230 W. The system performance comparing the evaporator cooling duty to the fuel energy usage is:

$$\eta = \frac{\dot{Q}_{evap,total}}{\dot{E}_{fuel}} \tag{4.18}$$

The resulting system efficiency (η) is 0.132.

4.3.5 Error Analysis

Uncertainties in the key performance parameters due to measurement uncertainties were estimated using an error propagation approach. An estimate of the uncertainty in the electrical heat input representing the evaporator load is presented first. The heater input is given by:

$$\dot{Q}_{evap,heater} = V \cdot I \tag{4.19}$$

The uncertainty associated with this input power is given by:

$$U^2_{\dot{Q}_{evap,heater}} = \left(\frac{\partial \dot{Q}_{evap,heater}}{\partial V} U_V \right)^2 + \left(\frac{\partial \dot{Q}_{evap,heater}}{\partial I} U_I \right)^2 \tag{4.20}$$

where the partial derivatives of the evaporator heater duty with respect to voltage and current are given by:

$$\frac{\partial \dot{Q}_{evap,heater}}{\partial V} = I \tag{4.21}$$

$$\frac{\partial \dot{Q}_{evap,heater}}{\partial I} = V \tag{4.22}$$

The uncertainties in the voltage and current were obtained from the vendor specifications. The voltmeter had an uncertainty (U_v) of 1.5 percent of the reading and the ammeter had an uncertainty (U_A) of 1.9 percent of the reading. At 58.2 volts and 3.86 amps for the representative data point, the uncertainties were 0.873 volts and 0.0733 amps, respectively. This results in the following equation for the uncertainty in the heater input measurement:

$$U_{\dot{Q}_{evap,heater}} = \sqrt{\left(I \cdot U_V\right)^2 + \left(V \cdot U_I\right)^2} \tag{4.23}$$

The resulting uncertainty is 5.4 W, i.e., $\dot{Q}_{evap,heater}$ = 224.6 ± 5.4 W, which represents an error of approximately 2.4 percent. Similar analyses were conducted on the coolant-side evaporator duty. Using the values of uncertainty for the thermocouples (U_T) of 0.5°C and the uncertainty in the coolant flow rate (U_F) of 8.8 percent (0.135 L/min), the coolant-side uncertainty was 68.1 W (32.2 percent). It should be noted that this uncertainty does not take into account the small portion of the heat duty associated with the thermal storage of the coolant tank, because this represented only a small fraction (2.6 percent) of the

evaporator load of 211 W. Thus, the evaporator duty based on the coolant-side is 211 ± 68 W, i.e., an uncertainty of 32.3 percent compared to the uncertainty in the electrical input measurement of 2.4 percent. Therefore, the evaporator duty reported in this study is based on the heater measurements.

4.3.6 Ambient Heat Loss/Gain Calculations

The heat losses and gains between the system and the ambient were computed to obtain an estimate of the parasitic heat load on the system. The components most likely to affect system performance include the following (as also shown in Figure 4.4):

- the refrigerant tube connecting the condenser outlet to the expansion valve inlet in room temperature air [1]
- the refrigerant tube connecting the expansion valve outlet to the evaporator inlet in room temperature air [2]
- the evaporator coolant tank in room temperature air [3]
- the portion of the refrigerant tube connecting the evaporator outlet to the compressor inlet in room temperature air [4]
- the portion of the refrigerant tube connecting the evaporator outlet to the compressor inlet in the elevated temperature air [5]

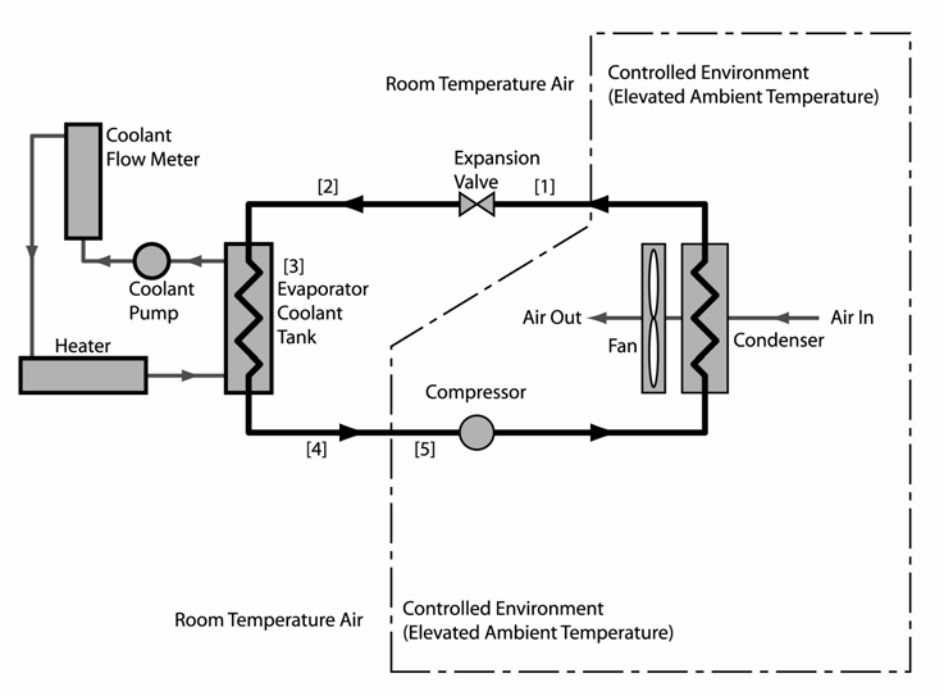

Figure 4.4 Ambient Heat Transfer Locations

A sample calculation is shown for the refrigerant tube connecting the expansion valve outlet to the evaporator inlet. The calculation begins with determining the dimensions of the portion under consideration. The inside diameter of the insulation is set equal to the outside diameter of the tube:

$$ID_{ins} = OD_{tube} \tag{4.24}$$

which results in an inside diameter of the insulation of 9.5 mm. The outside diameter of the insulation is given by:

$$OD_{ins} = ID_{ins} + 2 \cdot t_{ins} \tag{4.25}$$

where the insulation thickness t_{ins} is equal to 25.4 mm, resulting in an insulation outside diameter of 60.3 mm. The tube inside diameter is calculated in a similar manner as follows:

$$ID_{tube} = OD_{tube} - 2 \cdot t_{wall} \tag{4.26}$$

where the wall thickness of the tube t_{wall} is 1.6 mm, resulting in an inner diameter of 6.4 mm. The surface area of the insulation exposed to the ambient air is calculated using the length of tubing and the circumference as follows:

$$A_{surf,evap,in} = L \cdot \pi \cdot OD_{ins} \tag{4.27}$$

The tube length for this section is 0.356 m, which results in a surface area of 0.0674 m². Heat transfer between the tube and the ambient is due to natural convection and radiation. For natural convection, the Rayleigh number is calculated as follows:

$$Ra_D = \frac{g \cdot \beta \left(T_{\inf} - T_s\right) OD_{ins}{}^3}{\nu_{air} \cdot \alpha_{air}} \tag{4.28}$$

In the above equation, g is the acceleration due to gravity, β is the volumetric thermal expansion coefficient (0.003348 1/K) at the average temperature between the surface of the insulation and the surrounding air. T_{inf} is the surrounding air temperature of 25.6°C and T_s is the surface temperature of the insulation, which is found to be 25.4°C. The surface temperature is not known prior to simultaneously solving all the equations, but rather determined iteratively. This is due to the fact that the surface temperature depends on the heat transfer from the tube to the insulation surface by conduction as well as the heat transfer to the surrounding air by means of natural convection and radiation. The remaining parameters in the calculation of the Rayleigh number are the kinematic viscosity (1.589×10^{-5} m²/s) and the thermal diffusivity (2.250×10^{-5} m²/s) of the air. From these inputs, the Rayleigh number is calculated to be 4,296. This Rayleigh number is used to determine the natural convection heat transfer from the portion of the refrigerant

line under investigation, assuming quiescent air. The following correlation developed by Churchill and Chu (1975), valid for Rayleigh numbers of up to 1×10^{12}, was used to calculate the natural convection Nusselt number:

$$\overline{Nu}_D = \left\{ 0.60 + \frac{0.387 \cdot Ra_D^{1/6}}{\left[1+\left(0.559/Pr_{air}\right)^{9/16}\right]^{8/27}} \right\}^2 \tag{4.29}$$

With a Prandtl number of 0.707, this correlation yields an average Nusselt number of 3.591. The average convection coefficient is calculated as follows:

$$\overline{h} = \frac{\overline{Nu}_D \cdot k_{air}}{OD_{ins}} \tag{4.30}$$

where k_{air} = 0.0263 W/m-K and the insulation outside diameter is 60.3 mm. The resulting average convection coefficient is 1.565 W/m²-K. The total heat gain to the refrigerant tube due to convection and radiation can be calculated as follows:

$$\dot{Q}_{gain,evap,in} = \overline{h} \cdot A_{surf,evap,in}\left(T_{inf} - T_s\right) + \sigma \cdot \varepsilon \cdot A_{surf,evap,in}\left(T_{inf}^{\ 4} - T_s^{\ 4}\right) \tag{4.31}$$

For this calculation, the emissivity of the insulation is assumed to be equal to one. As the surrounding air temperature is higher than the refrigerant temperature, the heat transfer is from the ambient to the refrigerant, resulting in a calculated heat gain of 0.023 W for this section of the system, i.e., a negligible heat transfer.

As stated earlier, the surface temperature of the insulation is iteratively calculated based on the heat transfer from the air to the insulation and on through to the refrigerant. The heat transferred from the ambient to the surface by radiation and convection equals the heat transfer through the insulation and refrigerant tube by conduction. It is assumed

that the temperature of the interior of the refrigerant tube is equal to the mean refrigerant temperature inside due to the negligible thermal resistance between the refrigerant and the tube wall. The tube wall and insulation resistances are calculated as follows:

$$R_{tube,wall} = \frac{\ln\left(OD_{tube}/ID_{tube}\right)}{2\cdot\pi\cdot k_{tube}\cdot L} \tag{4.32}$$

$$R_{ins} = \frac{\ln\left(OD_{ins}/ID_{ins}\right)}{2\cdot\pi\cdot k_{ins}\cdot L} \tag{4.33}$$

where the outside diameter of the tube and the inside diameter of the insulation are equal to 9.5 mm, the inside diameter of the tube is 6.4 mm, and the outside diameter of the insulation is 60.3 mm. The tube and insulation thermal conductivity are 0.19 W/m-K and 0.04 W/m-K, respectively, and the length of tube is 0.3556 m, which results in a tube wall resistance of 0.9551 K/W, and an insulation resistance of 20.65 K/W. The total resistance is the sum of the two as follows:

$$R_{tot} = R_{tube,wall} + R_{ins} \tag{4.34}$$

The total resistance of the tube and insulation is 21.61 K/W. The heat transfer to the refrigerant across this resistance is given by:

$$\dot{Q}_{gain,evap,in} = \frac{\left(T_s - T_{evap,in}\right)}{R_{tot}} \tag{4.35}$$

with a surface temperature of 25.4°C and a refrigerant temperature of 24.9°C, the heat transfer to the refrigerant is 0.023 W, as computed above using the external convective and radiative resistances.

Similar analyses were conducted for the remaining four locations enumerated above. The corresponding results are shown in Table 4.2 (note that the heat transfer rates shown in parenthesis are heat losses, whereas the others are heat gains).

Table 4.2 Heat Transfer with the Ambient

Tube Location	Internal Fluid Temperature	Surrounding Air Temperature	Heat Gain/(Loss)
Condenser to expansion valve	50.4°C	25.6°C	(1.15 W)
Expansion valve to evaporator	24.9°C	25.6°C	0.023 W
Coolant tank	29.9°C	25.6°C	(0.676 W)
Evaporator to compressor in room air	29.1°C	25.6°C	(0.268 W)
Evaporator to compressor in elevated temperature air	29.1°C	46.0°C	0.207 W

The net heat transfer with the ambient is given by:

$$\dot{Q}_{net,ambient} = -\dot{Q}_{loss,exp,in} + \dot{Q}_{gain,evap,in} - \dot{Q}_{loss,tank} - \dot{Q}_{loss,evap,out} + \dot{Q}_{gain,comp,in} \quad (4.36)$$

which results in a net loss of 1.9 W from the system. This is a relatively small value compared to the overall heat duty of the evaporator of 230 W and does not affect the results significantly.

5. RESULTS

5.1 Cooling System Performance

Results from the tests described in the previous chapters are presented here. As stated before, tests were conducted at three ambient temperatures (37.7, 43.3 and 47.5°C), three evaporator coolant temperatures (26, 28 and 30°C), and three engine speeds (10,500, 12,250 and 13,300 RPM).

Figure 5.1 shows three test conditions that span the overall test matrix on a single pressure-enthalpy diagram.

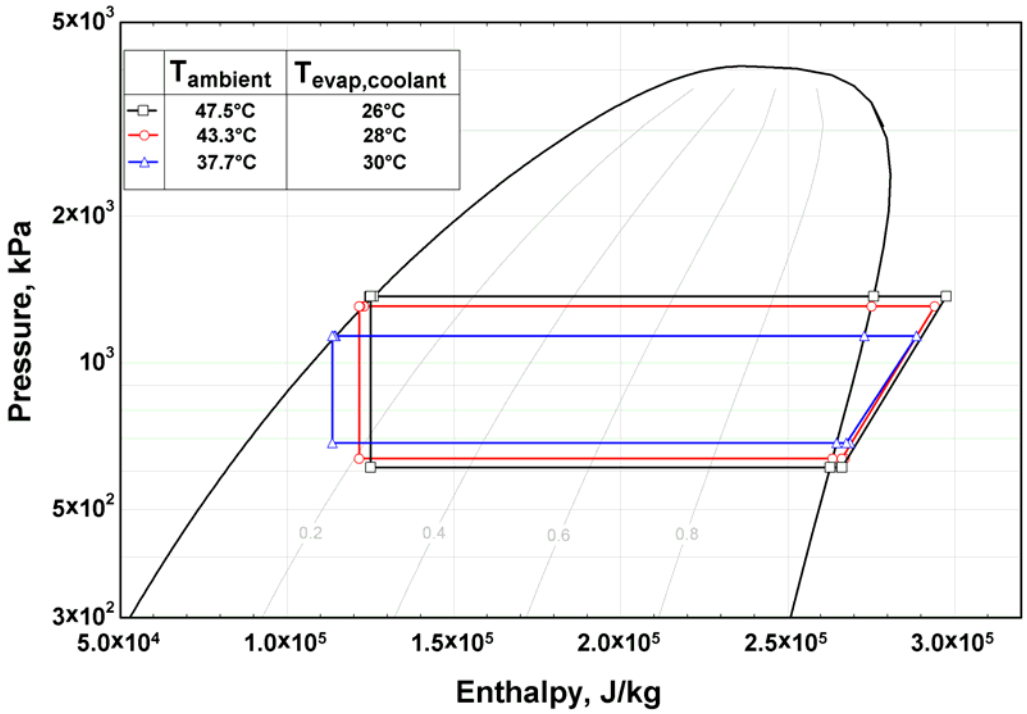

Figure 5.1 Pressure versus Enthalpy Diagrams Across the Test Matrix

The cases selected here for representation on the p-h diagram are all at the same engine speed of 10,500 RPM. These conditions represent the most extreme ($T_{ambient}$ = 47.5°C, $T_{evap,coolant}$ = 26°C), intermediate ($T_{ambient}$ = 43.3°C, $T_{evap,coolant}$ = 28°C), and least extreme ($T_{ambient}$ = 37.7°C, $T_{evap,coolant}$ = 30°C) conditions. Figure 5.1 shows that at increased ambient temperature, the high-side system temperature (and therefore pressure) must be increased to allow heat transfer to the ambient air. Conversely, for a lower coolant temperature, the evaporator temperature (and therefore pressure) must be lowered to allow heat transfer to the refrigerant from the coolant in the evaporator. Both of these influences require increased work input to the system since the compressor pressure differential is greater. These have a negative impact on system performance, as demonstrated by the test results.

Figure 5.2 displays the results of the entire test matrix for comparison purposes; the influence of individual parameters is discussed separately in the following sections.

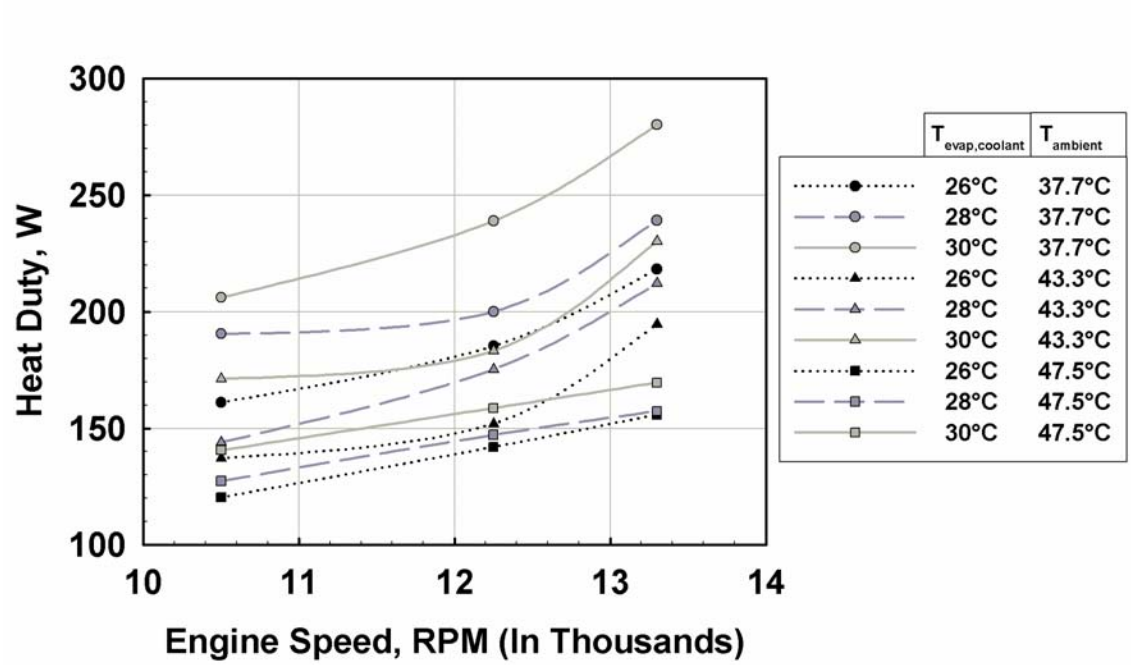

Figure 5.2 Overall Test Results

5.1.1 Performance at Constant Ambient Temperature

The variation of evaporator heat duty as a function of engine speed and evaporator

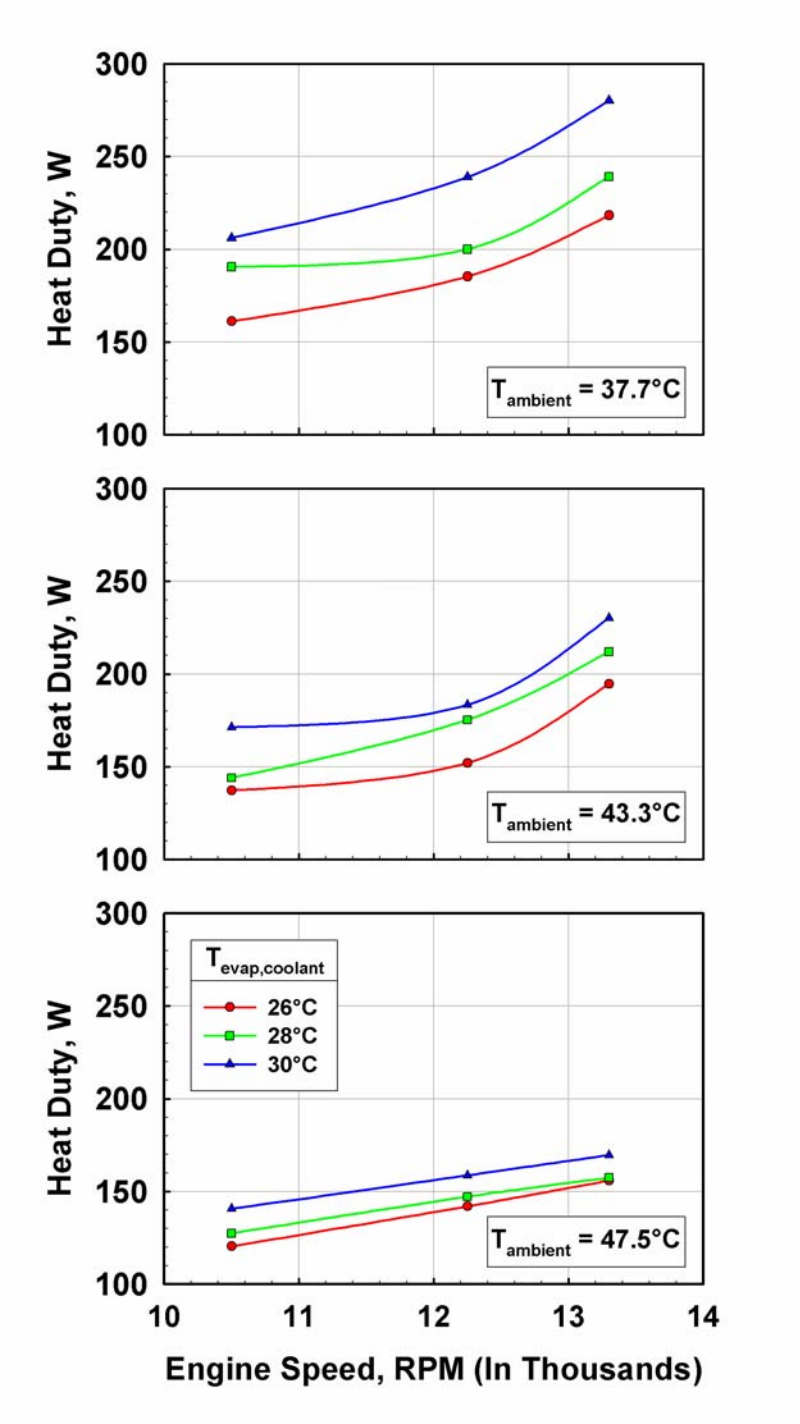

Figure 5.3 Heat Duty versus Engine Speed

temperature, while at a constant ambient temperature, is plotted in Figure 5.3 for three ambient temperature cases. It can be seen that the heat duty of the evaporator increases with increasing engine speed. The increased rotational speed of the compressor leads to greater refrigerant flow rates and therefore, the capability to deliver increased cooling in the evaporator. At the highest engine speed of 13,300 RPM, the evaporator duty was 280 W when tested at the highest coolant temperature (30°C) and lowest ambient temperature (37.7°C). The graph also indicates that the duty decreases when the evaporator coolant temperature is lowered. This is due to the fact that the temperature lift between the low side and high side temperature is increased. The larger the temperature lift, the higher the pressure ratio is in the compressor and the lower the performance of the system. For example, the pressure ratio for the least extreme case ($T_{evap,coolant}$ = 30°C, $T_{ambient}$ = 37.7°C) was approximately 1.7, whereas for the most extreme case ($T_{evap,coolant}$ = 26°C, $T_{ambient}$ = 47.5°C) the pressure ratio was approximately 2.3.

The condenser refrigerant pressure must be increased to accommodate the need for a higher saturation temperature. As the ambient temperatures increased from 37.7°C to 47.5°C, the condenser saturation temperature increased from 44.2°C to 51.5°C, with a corresponding pressure increase from 1136 kPa to 1370 kPa. With higher pressures, the compressor input work is increased, which, in turn, leads to additional heat rejection in the condenser. Finally, with higher ambient temperatures, the system would also have higher heat gains to the evaporator from the surroundings. Therefore, the increased air temperature has a negative effect on the cycle in multiple ways.

The increased compression for a given input power reduces the achievable refrigerant mass flow rates, and therefore the cooling load. For the two cases mentioned above, the

refrigerant mass flow rate decreases from 0.0015 kg/s for the least extreme case to 0.0010 kg/s for the most extreme case for an engine speed of 12,250 RPM.

The graphs show an upward sloped curve of the evaporator duty with increases in engine speeds, indicating a sharp increase in capacity with higher speeds. One potential explanation is the associated increase in condenser fan speed which causes higher airflow rates, leading to increases in condenser heat rejection, refrigerant mass flow rate, and cycle performance for the same compressor power input. Another potential simultaneous effect may be that the compressor isentropic efficiency increases at the higher rotational speeds. These evaporator duty increases may not continue beyond the range of tests performed, additional testing would be required to understand the effect further.

Figure 5.3 shows that the effect of the three different coolant temperatures on the evaporator duty was much less pronounced at the higher ambient temperature (47.5°C). This is because the variation in coolant temperature is much smaller relative to the overall temperature lift between the ambient air temperature and the coolant temperature for this case than in the lower ambient temperature cases. The temperature lifts between the ambient air and evaporator coolant temperatures were 17.5°C, 19.5°C and 21.5°C for the three cases shown. It should be noted that the refrigerant temperature in the evaporator was typically around 3 to 4°C lower than that of the coolant.

5.1.2 Performance at Constant Engine Speed

Figure 5.4 shows the variation of evaporator heat duty with ambient temperature at constant values of engine speed. It should be noted that these data are the same as those shown in Figure 5.3, however, these plots enable a clearer depiction of the effect of ambient and evaporator coolant temperatures.

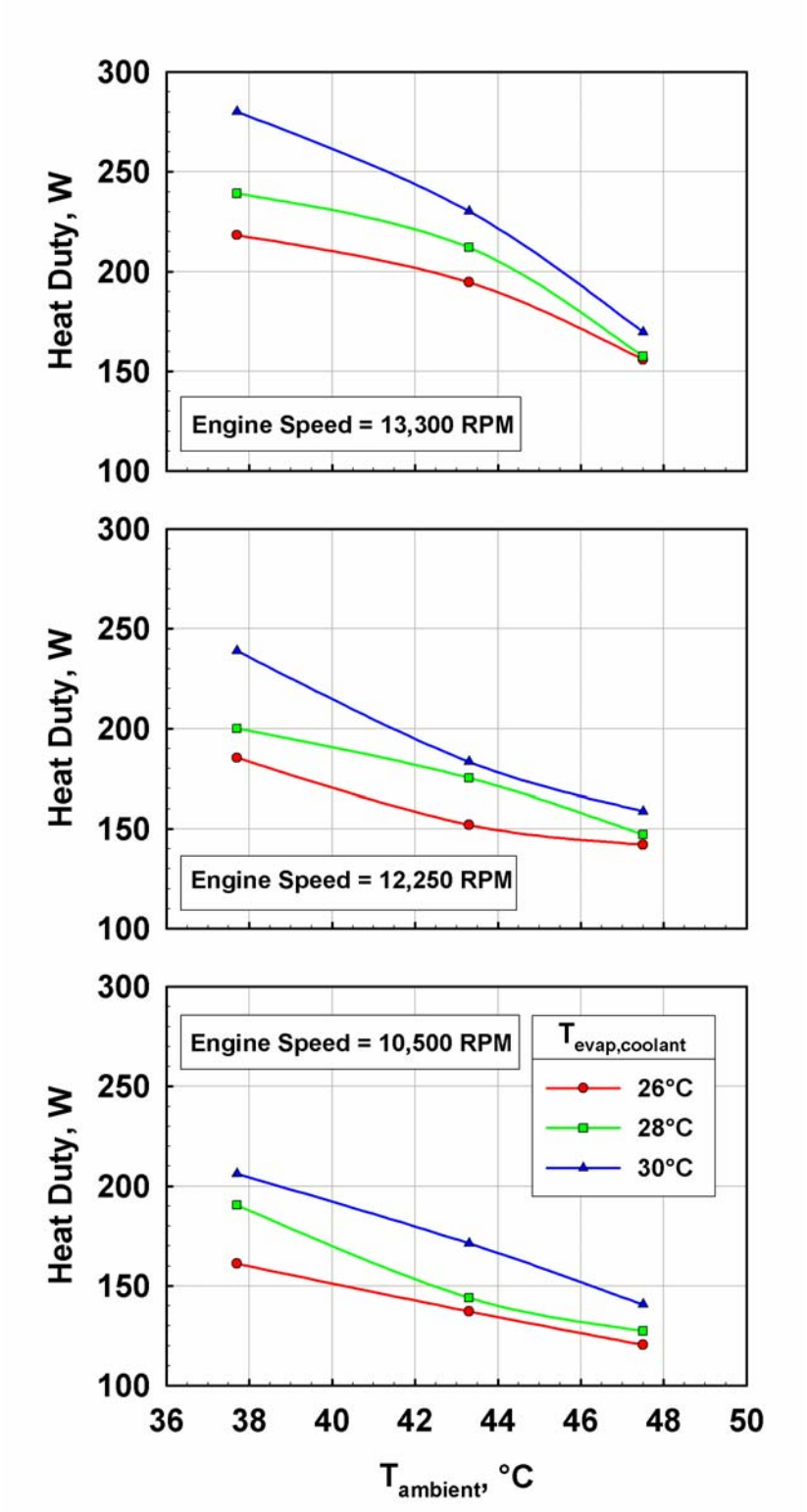

Figure 5.4 Heat Duty versus Ambient Temperature

The top graph in Figure 5.4 (engine speed = 13,300 RPM) shows that the evaporator duty decreases rapidly with increases in ambient temperature. This is most notable in the case with the highest engine speed. Increased ambient air temperature is detrimental to the performance of the system due to the increased difficulty of rejecting heat to the surroundings. The refrigerant temperature in the condenser needs to be sufficiently high to reject heat to the ambient air, causing increased compressor work.

The duties are lower at the intermediate engine speed; however, they do not drop off as rapidly with higher ambient temperatures as in the case of an engine speed of 13,300. This is because the evaporator duty is proportionately lower at the decreased engine speeds. The refrigerant mass flow rate, and therefore the evaporator duty, is dependant on the compressor speed. With proportionately lower duties, the actual change in duty is smaller. Similar trends are shown at an engine speed of 10,500 RPM. It can be seen from these graphs that the change in ambient temperature has the largest impact at higher rotational speeds. Also, the difference in duties due to different evaporator coolant temperatures is relatively constant throughout.

5.1.3 Performance at Constant Evaporator Temperature

The data were also plotted at constant values of evaporator coolant temperature to investigate the effect of varying the ambient temperature and engine speed (Figure 5.5). The difference in heat duty at the three ambient temperatures is significant and increases in engine speed show the expected increase in heat duty. The difference in heat duty due to different values of ambient temperature is less pronounced at the lower values of evaporator coolant temperature. This is due to the fact that as the overall temperature difference between the low and high sides increases, the individual effect of the variation

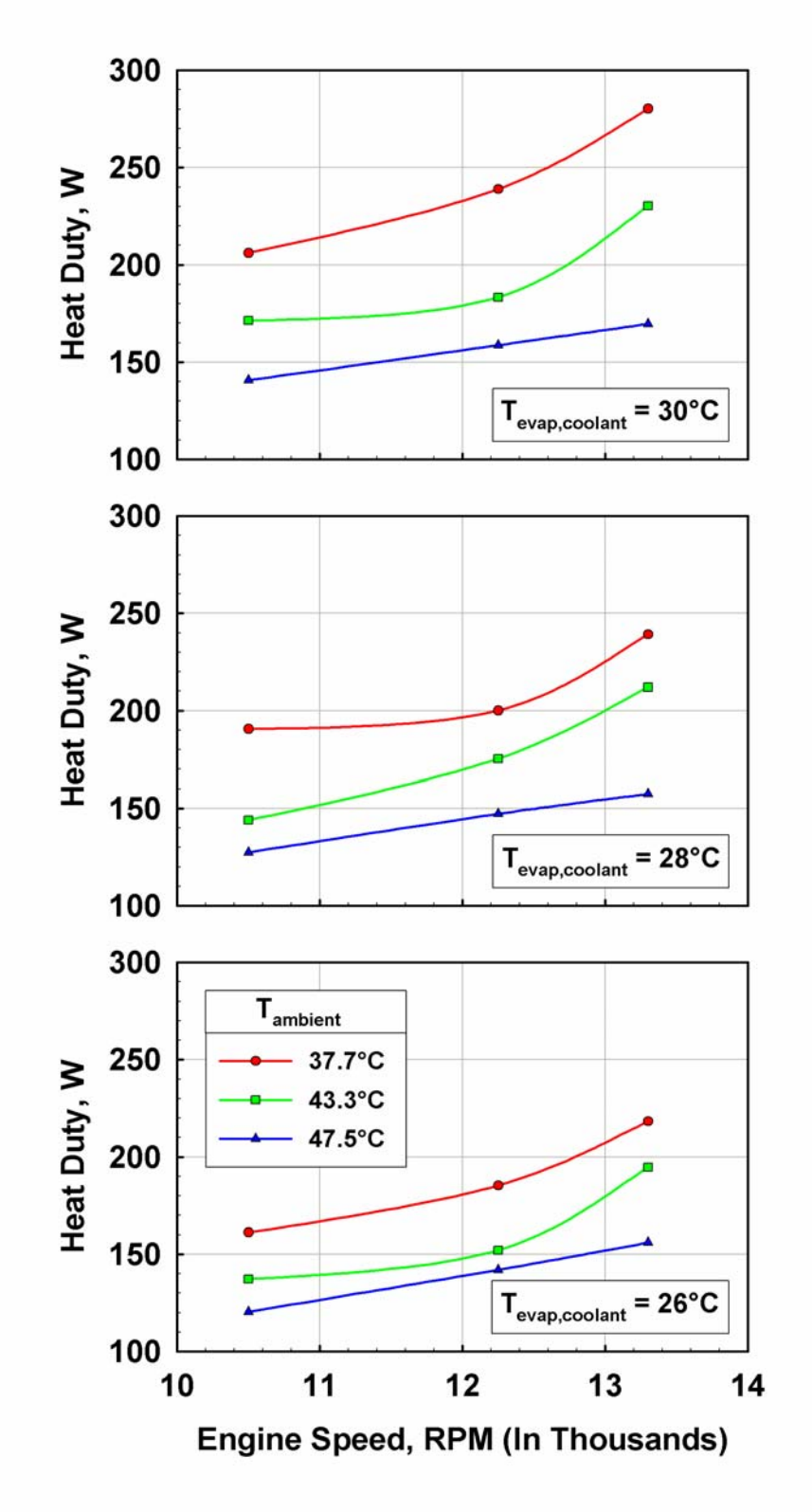

Figure 5.5 Heat Duty versus Engine Speed

of ambient temperature by itself becomes less significant. This is particularly evident in the final graph of Figure 5.5 for the case of the lowest evaporator coolant temperature (26°C).

5.1.4 Effect of Increased Engine Speed

As stated earlier, the testing also included a set of data points outside the original matrix to investigate the performance of the system at higher engine speeds. The drawbacks of the higher engine speeds are an increased fuel consumption rate, more severe loading on the overall system and increased noise.

Figure 5.6 shows the results of the increased engine speed tests. The other variables were held constant at nominal design values: evaporator coolant temperature = 28°C and ambient temperature = 43.3°C. During these tests, the average refrigerant temperature in

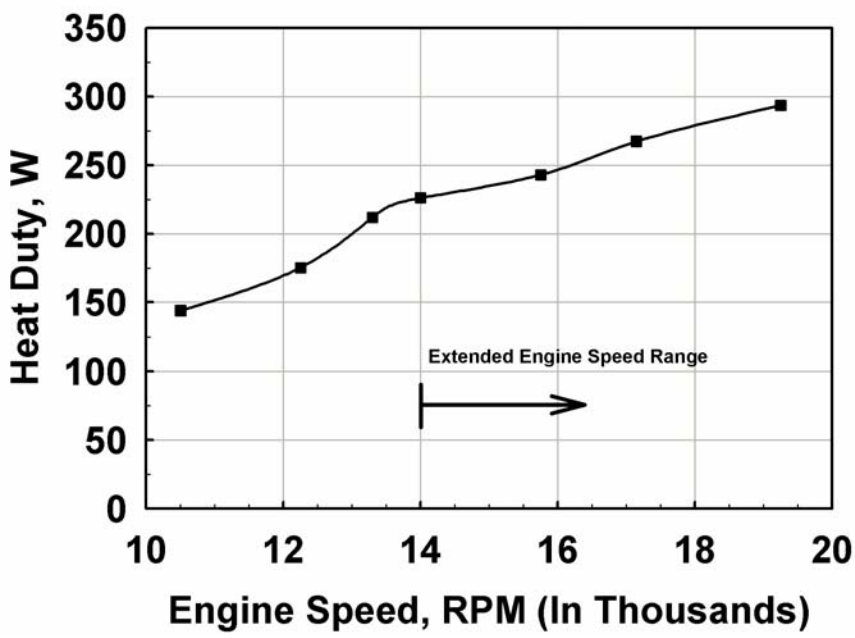

Figure 5.6 Heat Duty versus Engine Speed
($T_{evap,coolant}$= 28°C, $T_{ambient}$ = 43.3°C)

the evaporator was 24.5°C. Figure 5.6 shows that the evaporator heat duty continues to increase as engine speed is increased beyond the originally chosen range, however, the rate of increase is less significant at the higher engine speeds tested.

It should be noted that the system was designed with the intention of producing a portable system that was as light-weight and compact as possible. There is a tradeoff between durability of the system and the overall weight and size. Designs for extended period operation necessitate more massive components. In this study, components were designed to satisfy the pressure and temperature requirements of the system without exceeding them significantly, to avoid excessive increases in system weight. Testing at increased engine speed placed higher levels of stresses on the components for the investigation of potential failure modes and the identification of the weakest components. The higher engine speed testing was terminated when the set screw used to transmit the torque from the input gear to the compressor shaft failed.

5.2 Fuel Consumption

The amount of fuel used during each set of tests was measured to determine the fuel consumption rates of the system during operation. It should be noted that fuel consumption rates were not measured individually for each data point, but for series of tests grouped in sets. The testing was performed in three stages where nine data points each were taken. This was due to the fact that the air handler took an appreciable length of time to start up and stabilize at the desired air temperature. Thus, the air handler was set at the appropriate temperature and then the testing of all data points at that particular temperature was accomplished. After steady state had been reached and allowed to continue for several minutes, the engine speed and the evaporator temperature were

changed to the next data point. During testing, the fuel consumption of the entire set of data points for each ambient temperature was recorded. This gave an overall average for the fuel usage for each ambient air temperature setting. Each value of ambient temperature had the same nine combinations of evaporator temperatures and engine speeds. Figure 5.7 shows a graph of the average fuel consumption at the three values of ambient air temperature.

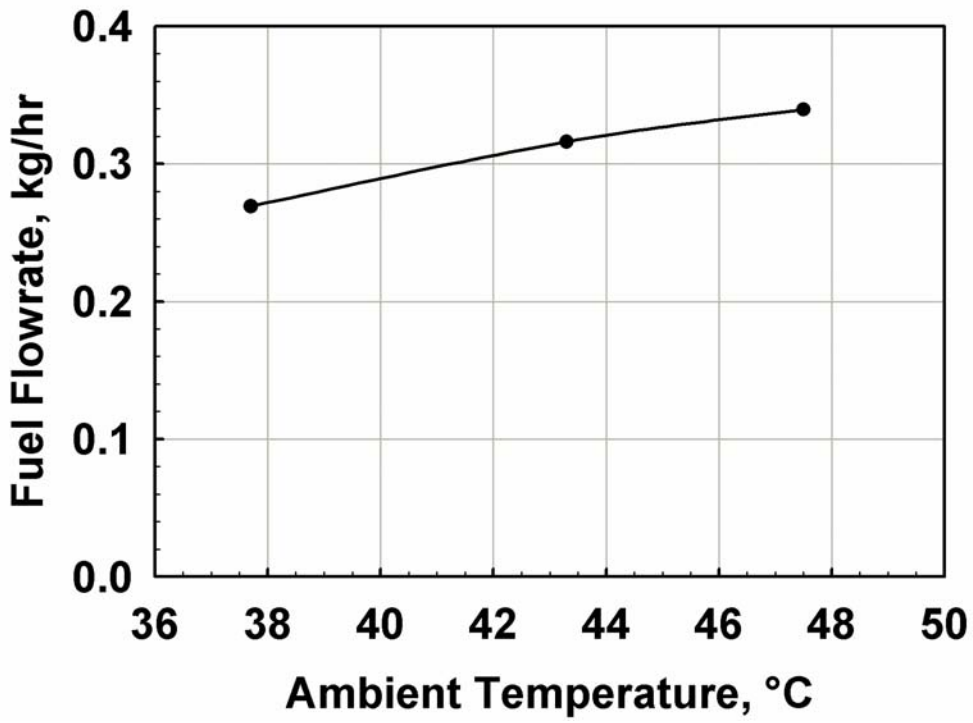

Figure 5.7 Variation of Fuel Consumption Rate with Ambient Air Temperature

Fuel consumption increased with increasing ambient air temperature. This is because the engine had to provide higher input power at the elevated temperatures to achieve the additional compression.

As described in Chapter 4 for the representative test point, the resulting system performance of converting the fuel's energy into evaporator cooling duty was 13.2

percent. It should be noted that although this efficiency is relatively low, the engine-driven system still has a higher energy density than the other methods examined, such as powering with batteries or a fuel cell. Small scale engines typically have a relatively low efficiency in converting fuel's potential energy to usable shaft work. Despite this fact, the system still proved to be the most practical in regards to overall system mass.

Table 5.1 summarizes the volumetric fuel consumption rate as well as the fuel mass flow rate, based on a fuel density of 903 kg/m³. System performance relating fuel energy usage to evaporator cooling duty (η) is also shown.

Table 5.1 Fuel Consumption Rates

Ambient Temperature (°C)	Average Fuel Mass Flow Rate (kg/hr)	Average Fuel Volumetric Flow Rate (L/hr)	Average Evaporator Duty (W)	System Performance (%)
37.7	0.269	0.298	226	15.2
43.3	0.316	0.350	178	10.2
47.5	0.340	0.376	149	8.0

Table 5.1 illustrates the penalty associated with cooling at elevated ambient temperatures. With increased temperature, not only does the fuel flow rate increase, but the evaporator duty also decreases. This would cause an increased fuel storage requirement and an associated increase in system weight to provide cooling for the desired duration at elevated temperatures. With the use of an integrated two liter fuel tank, the system can provide cooling for the three ambient conditions (37.7°C, 43.3°C, 47.5°C) for a period of 6.7, 5.7 and 5.3 hours, respectively, while cooling at a rate of 226, 178 and 149 W, respectively.

Fuel consumption was also measured for the additional testing at increased engine speed with an evaporator coolant temperature of 28°C and an ambient temperature of

43.3°C. During these tests, the average rate of fuel consumption was 0.397 L/hr, which is equivalent to a mass flow rate of 0.358 kg/hr over a range of engine speeds from 14,000 to 19,250 RPM and an average evaporator duty of 268 W.

6. WEARABLE SYSTEM

6.1 Wearable Evaporator

As described in Chapter 3, the evaporator used for testing purposes was significantly different from the cooling garment evaporator. The actual evaporator consisted of a garment worn in contact with the human body to perform the necessary cooling for personal comfort while in a high temperature environment. The wearable evaporator was first modeled to determine the appropriate tube pitch, tube diameter, tube length and foil thickness. After the initial analysis was completed and the thermal system had been tested using the coolant tank test evaporator, a cooling garment was constructed that utilized information garnered from the testing and the analyses.

6.1.1 Wearable Evaporator Modeling

As shown in Figure 6.1, the cooling garment model consisted of three layers which included the insulation, the foil and the refrigerant tube layer.

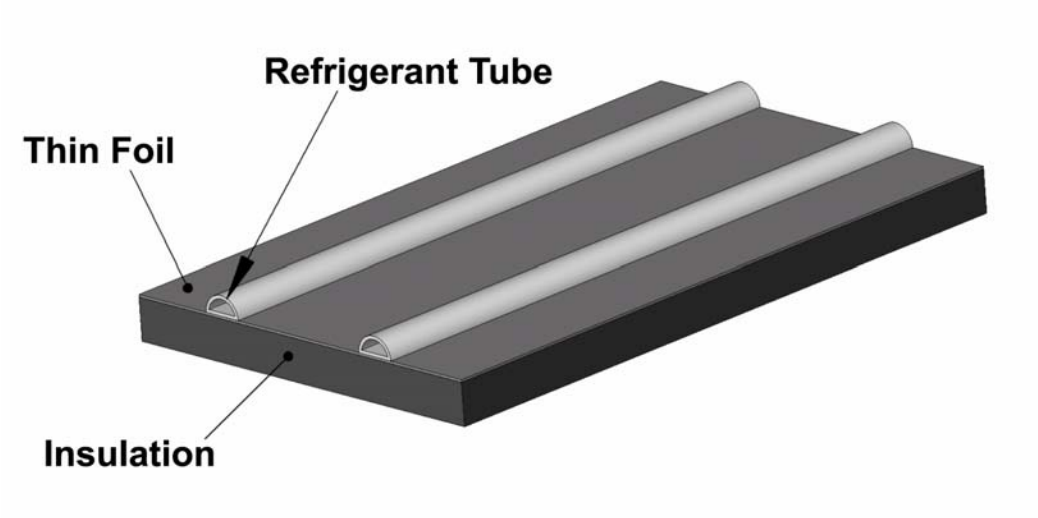

Figure 6.1 Representative Section of Wearable Evaporator Garment

The refrigerant tube side would be worn toward the body, with the insulation layer shielding the cooled interior from the surrounding ambient conditions. The cooling garment model used semicircular tubing that was attached to the thin aluminum foil layer. The semicircular tubing would carry the refrigerant as it removed heat from the body while evaporating. The foil layer would serve as a fin to remove heat from a larger area and transfer the heat energy to the refrigerant tubes. For the analysis, the foil was chosen to be made of aluminum due to its high thermal conductivity and low weight.

An energy balance was performed on a section of the garment to analyze the heat transfer requirements for cooling of a subject during use. The details of this calculation are shown in Appendix C. The analysis was performed assuming the cooling garment encompassed the entire body and uniformly removed heat from the subject. Table 6.1 presents the resulting geometry of the cooling garment used for the model, as well as the dimensions of the actual cooling garment, for comparison.

6.1.2 Cooling Garment Description

After testing of the thermodynamic system using the test evaporator had been successfully completed, the actual cooling garment was fabricated. As mentioned earlier, the test evaporator allowed more accurate measurements of the cooling system's capabilities. However, there was still the need to test the actual evaporator and ensure that it performed as predicted by the model. The major difference between the modeled and actual wearable evaporator was that the latter was constructed to cover only a portion of the body, rather encompassing the entire body. A cooling vest was developed that would remove heat from the torso and chest of the individual. As discussed in Chapter 2,

this is the most effective area to cool on the body (Epstein *et al.*, 1986), since it has the largest surface area and generates a significant amount of heat.

The cooling vest was fabricated using a neoprene wetsuit manufactured by Body Glove Inc., as shown in Figure 6.2. The 3 mm thick wetsuit served as the insulating outer shell of the cooling garment to minimize unwanted heat gain from the surroundings.

Figure 6.2 Cooling Garment Exterior

Figure 6.3 Cooling Garment Construction

Inside the neoprene shell, the aluminum cooling tubes and foil were held in place by using a thin fabric mesh sewn into the neoprene (Figure 6.3).

The tubing outer diameter was 3.2 mm (0.125 inches), the same as the test evaporator. The aluminum foil was 0.0508 m (2 inches) wide and had a thickness of 1.52×10^{-4} m (0.006 inches). Each tube was centered on a strip of foil and ran parallel with it. The thin fabric mesh held the strip of foil and tube in place on the garment. The foil had adhesive on the side toward the tube which held the two bonded together. The garment had a total of four tubing passes in parallel sewn into it (Figure 6.4), each supplied by a flexible hose from the backpack structure.

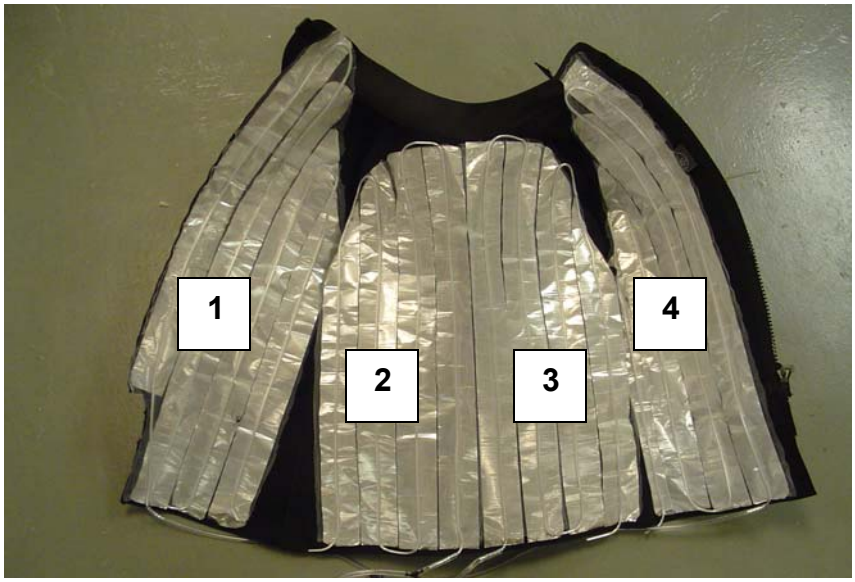

Figure 6.4 Cooling Garment Interior

The individual tubes were 2.44 m (8 ft.) in length, for a total length of tubing in the garment of 9.8 m (32 ft.). Each of the four passes of tubing traversed up and down twice inside the garment before being routed back to the backpack structure in another flexible tube. Figure 6.4 shows the layout of the four sections of tubing in the cooling garment.

Table 6.1 gives a comparison of the full-body evaporator that was modeled, and the actual evaporator that only covered the torso and chest.

Table 6.1 Evaporator Geometry

	Modeled	**Actual**
Tube Length	2 m	2.4 m
Tube Pitch	55 mm	51 mm
Total Surface Area	1.8 m²	0.495 m²
Tube Hydraulic Diameter	1.1 mm	1.9 mm
Tube Wall Thickness	0.5 mm	0.64 mm
Number of Tubes	16	4
Tube Material	Aluminum	Aluminum
Foil Thickness	0.35 mm	0.15 mm
Foil Width	55 mm	51 mm
Insulation Thickness	6.4 mm	3 mm

The wearable evaporator with reduced coverage was intended to serve as a means of testing the performance of the conceptual design prior to constructing an entire cooling suit. System testing (Figure 6.5, top) was performed using the wearable evaporator in an ambient air temperature of 40.5°C (105°F). The system operated satisfactorily by providing cooling to the user while jogging on a treadmill at 7.2 km/hr (4.5 miles/hour). Figure 6.5 (bottom) displays multiple views of the cooling garment and portable cooling system as worn on the back by the user.

Figure 6.5 Portable Cooling System Testing

6.2 System Mass

The individual masses of each component, as well as the overall system (excluding the fuel) are tabulated in Table 6.2. For a volume of two liters, the resulting fuel mass would be 1.8 kg (4.0 lb).

Table 6.2 Component and System Mass

System/Component	Component Mass (SI)	Component Mass (English)
Refrigeration System	**1.76 kg**	**3.88 lb**
Compressor	0.44 kg	0.97 lb
Condenser	1.22 kg	2.69 lb
Expansion Valve	0.10 kg	0.22 lb
Wearable Evaporator System	**0.85 kg**	**1.87 lb**
Insulating Vest	0.32 kg	0.70 lb
Aluminum Foil/Tubes	0.53 kg	1.17 lb
Power Supply System	**1.57 kg**	**3.46 lb**
Engine and Base	0.71 kg	1.56 lb
Battery Pack	0.43 kg	0.95 lb
Gears	0.43 kg	0.95 lb
Support System	**1.13 kg**	**2.49 lb**
Backpack	0.26 kg	0.57 lb
Miscellaneous Structure/ Hardware	0.87 kg	1.92 lb
Overall Total	**5.31 kg**	**11.7 lb**

7. CONCLUSIONS AND RECOMMENDATIONS

7.1 Conclusions

A wearable personal cooling system was designed, fabricated and tested in this study. The main challenges in developing a wearable cooling system are the requirement for an adequate source of input power and the miniaturization of the refrigeration system components. After considering various options for accomplishing the cooling including phase-change materials, absorption and adsorption cooling and others, a vapor compression system was chosen based on criteria such as simplicity, performance, and number of components. Similarly, a liquid fuel-based small-scale engine was chosen based on a higher overall energy density from among options such as fuel cells and lithium-ion batteries to supply power to the vapor compression cooling system. The engine output was used to power the vapor-compression system compressor and the heat rejection condenser fan through appropriate gear trains. Several modifications to an off-the-shelf portable air compressor were designed and fabricated in-house to convert it into a refrigerant compressor required for this application. Detailed tests on a stand-alone compressor test stand were first performed to establish the viability of this compressor for refrigerant compression.

After compressor development was completed, it was integrated into the overall cooling system and system performance was investigated over a wide range of controlled, elevated ambient temperatures, evaporator temperatures and engine speeds. The cooling system was successful at providing cooling at a level equivalent to the heat produced by a typical subject performing work at a level comparable to calisthenics or moderate exercise at elevated ambient temperatures. Thus, the system demonstrated heat removal

rates between 100-300 W at ambient temperatures in the range 37.7-47.5°C (100-117.5°F), engine speeds of 10,500 to 13,300 rpm, and evaporator coolant temperatures of 26 to 30°C. Fuel consumption rates varied from 0.269 to 0.340 kg/hr for this same range of conditions. The cooling duty increased at higher engine speeds, but decreased at higher ambient temperatures and lower evaporator temperatures. Additional testing at higher engine speeds (13,300 < rpm < 19,250) showed that the resulting increase in compressor speed leads to higher cooling capacities.

The backpack mounted wearable cooling system developed in this study had a total mass of 5.31 kg and can provide cooling at the rate of about 178 W for a duration of 5.7 hrs at a nominal ambient temperature of 43.3°C. This eliminates the need to be tethered to a source of input power or cooling fluid, which some systems currently employ for personal cooling. Thus, the system will help reduce the effects of heat exhaustion and fatigue, thereby reducing the stress level on the body, while increasing productivity and safety. This system is expected to benefit hazardous duty personnel such as firefighters, military, or factory personnel who work at elevated temperatures.

7.2 Recommendations

The present study was successful at demonstrating the feasibility of a completely independent, wearable cooling system. The demonstrated cooling capacity of 300 W was, however, somewhat lower than the desired performance 400 W at an ambient temperature of 43.3°C. Some modifications to the cooling system developed here that may enable increased performance are proposed below.

7.2.1 Engine and Gear Train Modifications

The engine used for this study was one commonly used for powering remote control cars and airplanes. It provided the desired input power; however, certain aspects made it undesirable such as high sound levels and exhaust. Furthermore, testing at increased engine speed resulted in a commensurate increase in noise level. Noise levels could be reduced by using an engine developed specifically for this type of system.

Since the engine was a two-stroke model, lubrication of the moving parts came from the fuel itself as there was no oil reservoir in the crankcase. The fuel contained a mixture of castor oil that provided the necessary lubrication to the engine. A small trace of oil was expelled along with the exhaust as it remained unburned during combustion, which was an undesirable characteristic of this type of engine. The oil also added additional weight to the fuel that was not used for producing power. An engine with an oil reservoir that lubricates the moving parts of the engine would eliminate the need for oil in the fuel, which would reduce fuel consumption rates and also eliminate the expulsion of oil from the exhaust. Such engines are not readily available, but could be designed specifically for this application if deemed appropriate.

The engine would also benefit from a better exhaust system to reduce engine noise. Although backpack structure modifications to dampen the noise level to the surroundings as much as possible can be considered, certain areas must remain unobstructed, and would therefore provide a path for sound to propagate without being dampened. One such path is the air for condenser heat rejection, which also provides engine and compressor cooling. This air stream requires an open path from the engine and compressor to the surroundings, as the air enters through the condenser and is expelled

out the sides. The engine and the compressor are the two loudest components of the system, but shielding opportunities appear to be limited due to the simultaneous heat rejection requirements. The best option, therefore, appears to be the design of quieter small-scale engines and compressors.

Another avenue for power system modifications is in the potential development and use of small-scale gasoline engines rather than engines that run on model aircraft fuel. The additional energy density of gasoline would considerably extend the mission duration or reduce fuel payload requirements for a given duration. Also, engines with speeds tailored closer to the requirements of the intended application, and modification of the gear train to potentially use fewer (and perhaps spoked) gears, would reduce the weight of the gear train, and therefore the overall system.

7.2.2 Compressor Modifications

Improvements in the performance of the system may also be possible from modifications to the compressor subassembly. The measured compressor efficiency in this study was typically between 45-55 percent. The intake and exhaust valves remained unmodified from the original air compressor that was used as a starting point to develop the refrigerant compressor. Valves designed specifically for this application may yield a higher compressor efficiency. It may also be possible to use a larger compressor because in the finalized system, there was sufficient room for a slightly larger compressor, as the compressor was not the component that dictated the overall size of the system. A larger compressor typically has a higher efficiency because the ratio of heat generated from friction with the cylinder wall compared to the work required for compression of the refrigerant decreases with increasing compressor size, thus increasing compressor

efficiency. The use of a larger compressor may require a different gear train and increased engine speed to deliver the necessary input power.

7.2.3 Condenser Modifications

The condenser offers another potential opportunity for redesign. In the configuration tested in this study, the condenser dictated the overall system envelope as it had the largest width and height. The current configuration also added significantly to the overall system depth as the condenser needed to be inline with the axial flow fan for proper airflow. The fan blades that spanned the entire condenser require being placed in a different plane as compared to the engine and compressor, resulting in a stack up of three subsystem planes (condenser, fan and shroud, and engine and compressor). One potential option to reduce this overall system depth is the use of a condenser arrayed around the perimeter of the system instead of a rectangular slab as in the present case. With such a configuration, the fan would draw air in from the periphery of the system and expel it out the back. While eliminating the condenser plane from the depth stack up, this arrangement might add slightly to the overall width and height of the system; although not substantially because the condenser in the current design has the largest height and width among all components. The optimum tradeoff between overall system depth, height and width will depend on the particular application for this system. One other aspect of condenser design is the further optimization of tube and fin geometry and tube-side pass arrangement. The condenser used in the present study was ultimately picked because of its ready availability from Modine Manufacturing Company, also based on initially estimated refrigerant and air state points and fan flow rates. With the knowledge gained from this study, more accurate operating conditions can be specified and a more

rigorous optimization between system mass, fan flow rate and power, and mission duration can be conducted to result in a condenser suited specifically for this application.

Further development efforts on this system should first identify the components that affect overall system mass most dramatically, since it is likely that system mass will be of the greatest importance for most applications. While further improvements in system efficiency would result in decreased fuel mass, this may not change the overall system mass significantly. As was stated, for a mission duration of approximately 6 hours, the fuel mass constitutes 25 percent of the total mass when filled with 2 Liters of fuel. Slight improvements in system efficiency would not affect the overall mass significantly. Therefore, further weight reductions should consider the components most likely to lead to reductions in mass; this may include the use of lighter weight materials, redesigned components or changing the overall layout.

7.2.4 User Comfort Characterization

The main focus of the present study was to demonstrate the feasibility of the wearable cooling system, which was accomplished successfully. Implementation of such a system in the actual elevated temperature, hazardous duty applications will require additional testing and development of the system to address user comfort issues. Additional testing must be conducted with more rigorous measurement of skin temperatures and thermal comfort according to well established guidelines. This testing will yield insights into the specific cooling requirements for the different anticipated use scenarios, and establish the evaporator duties more accurately. It will also assist in the design of integrated evaporator and cooling jackets with the intention of minimizing thermal resistances and ensuring maximum cooling to the most appropriate regions of the body.

APPENDIX A - THERMODYNAMIC CYCLE ANALYSIS

A.1 System Inputs

The program written on the EES platform to analyze the thermodynamic cycle served as a means of determining the state points, heat duty and required sizes of the components in the vapor compression system. The key variables used in this program are shown in Table A.1, along with the values chosen for the initial analysis. As the research project progressed, some variables were changed in value, based on the results of the ongoing analyses and experimental results. There were also changes in the method of calculation based on information acquired during the research. However, Table A.1 shows the initial values used to aid in determining preliminary system power requirements, sizing and heat duty.

Table A.1 Thermodynamic Cycle Inputs

Ambient temperature (T_{amb})	37.7°C
Desired temperature of cooling near the body (T_{skin})	29.4°C
Closest approach temperature for the condenser (CAT_H)	3.8°C
Closest approach temperature for the evaporator (CAT_L)	3°C
Amount of superheating in the evaporator ($T_{superheat}$)	2.78°C
Amount of subcooling in the condenser ($T_{subcool}$)	1.67°C
Compressor efficiency (η_c)	0.4
Heat rejection from the body (Q_{body})	400 W
Fan work (W_{fan})	22 W
Duration/operating time (time)	8 hours
Thermal conductivity of insulating material (k)	0.03 W/m-K
Thickness of insulating material (t)	6.4 mm
Body surface area (A)	1.8 m²
Activity level (M) (Kuehn *et al.*, 1998)	5.17 MET

The ambient temperature has a significant impact on the performance. With higher ambient temperatures, heat rejection must take place at higher temperatures, which leads to a lower efficiency. Higher ambient temperatures also have an associated increased rate of heat gain through the insulation, resulting in a higher evaporator duty. Comfort levels for the human body dictate the temperature near the skin: the temperature should be slightly lower than that of the human body to enable heat rejection to the evaporator, but not so low as to cause discomfort to the user.

The closest approach temperature (CAT) represents the smallest temperature difference between the fluids exchanging heat in a heat exchanger. For a system using a pack-mounted condenser, the closest approach temperature is a parameter that can be optimized by varying the geometry of the heat exchanger and the amount of air movement through the condenser.

Heat dissipation requirements for the human body depend on activity level, body size and type. The system was designed for "moderately high" physical exertion which produces approximately 220 W/m²; this is comparable to moving 50 kg (110 pound) bags or jogging at 1.8 m/s (5.9 ft/s) (Kuehn *et al.*, 1998). Assuming the average skin surface area of an adult male is approximately 1.8 m² (Kuehn *et al.*, 1998), the resulting heat dissipation is approximately 400 Watts.

The refrigeration cycle that was initially modeled was a typical vapor compression cycle with the following assumptions:

- isenthalpic expansion valve
- no pressure drop in the refrigerant lines
- refrigerant R-134a as the working fluid

- the refrigerant exits the condenser as a subcooled liquid
- the refrigerant exits the evaporator as a superheated vapor
- the condenser and evaporator surface temperatures are equal to the internal refrigerant temperature (negligible wall resistance)

A.2 Vapor Compression Cycle Analysis

A.2.1 State Points

The refrigeration cycle is shown in Figure A.1 with the state points labeled throughout the cycle. Beginning at the evaporator inlet, the refrigerant enters at state 1 (26.4°C, x = 0.15) and removes heat from the body while evaporating.

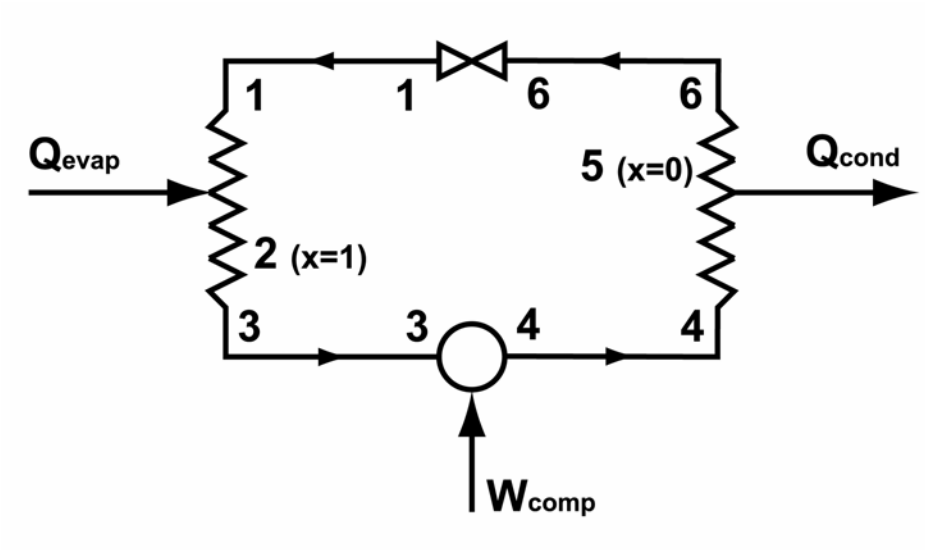

Figure A.1 Simplified Thermodynamic Cycle

This continues until state 2 (26.4°C, x = 1), where the refrigerant is a saturated vapor. The temperature of state 2 is determined by subtracting the closest approach temperature (CAT_L = 3°C) for the evaporator from the desired temperature near the body (T_{skin} = 29.4°C):

$$T_2 = T_{skin} - CAT_L \tag{A.1}$$

The low-side pressure (694 kPa) is then determined from the temperature of state 2, as the refrigerant is a saturated vapor. The refrigerant is then superheated to state 3 (29.2°C) by the amount specified in the program input ($\Delta T_{superheat}$ = 2.78°C). The enthalpy at state 3 can then be determined from the pressure and temperature.

The compressor raises the pressure of the refrigerant from state 3 (694 kPa) to state 4 (1193 kPa), requiring work input from the portable power source. The compressor work constitutes the major portion of the energy input to the system during operation. The isentropic efficiency of the compressor is user-defined (η_c = 0.4), and depends on the type and model of compressor used. The enthalpy at state 4 is calculated using the following equation:

$$h_4 = h_3 + \frac{(h_{4s} - h_3)}{\eta_c} \tag{A.2}$$

where h_{4s} is the enthalpy at state 4 for isentropic compression and η_c is the isentropic efficiency of the compressor.

Refrigerant then enters the condenser as a superheated vapor at state 4 (67.0°C) and dissipates heat to the environment while condensing. The temperature of state 5 (46.1°C, saturated liquid) is determined by adding the closest approach temperature for the condenser (CAT_H = 3.8°C) to the air temperature leaving the condenser (42.3°C):

$$T_5 = T_{air,o} + CAT_H \tag{A.3}$$

At state 5, the refrigerant is fully condensed; this allows the high-side pressure (1193 kPa) to be determined using the temperature T_5. The refrigerant is then subcooled by the

specified amount ($\Delta T_{subcool}$ = 1.7°C) to state 6 (44.4°C) and continues downstream to the expansion valve.

The expansion valve is assumed to be isenthalpic and therefore the enthalpy at state 1 is set equal to the refrigerant enthalpy at state 6, which is at the condenser exit. This determines the state of the refrigerant entering the evaporator, thus completing the cycle.

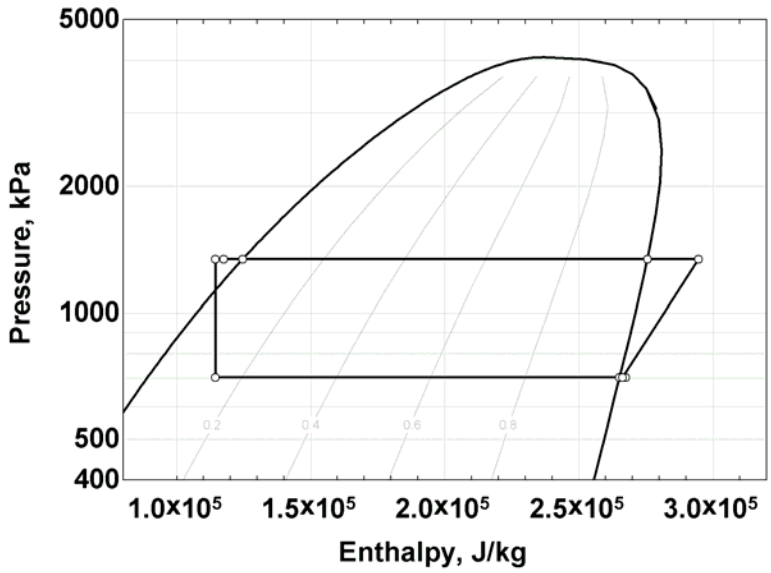

Figure A.2 Pressure-Enthalpy Diagram of Thermodynamic Cycle

The enthalpies and other thermodynamic properties throughout the cycle are calculated using EES based on the pressure and either the temperature, the quality or the entropy. Figure A.2 displays the thermodynamic cycle on a P-H diagram.

A.2.2 Energy and Mass Balances

The heat input to the evaporator determines the overall load on the system and includes both the heat dissipated by the body ($\dot{Q}_{body}$ = 400 W), as well as heat gain from the surrounding environment through the insulation ($\dot{Q}_{gain}$ = 65 W):

$$\dot{Q}_{evap} = \dot{Q}_{body} + \dot{Q}_{gain} \tag{A.4}$$

The heat gain is the summation of the convective and radiative heat transfer from the surrounding environment to the insulation surface, described in Appendix C. The total heat input to the evaporator is $\dot{Q}_{evap}$ = 465 W.

The refrigerant mass flow rate is calculated from the evaporator heat input and the respective enthalpy at the inlet and outlet as follows:

$$\dot{m} = \frac{\dot{Q}_{evap}}{(h_3 - h_1)} \tag{A.5}$$

Once the mass flow rate is known ($\dot{m}$ = 3.04×10^{-3} kg/s), the work input for the compressor (89 W) is determined using the refrigerant flow rate in conjunction with the change in enthalpy across it as follows:

$$\dot{W}_{comp} = \dot{m} \cdot (h_4 - h_3) \tag{A.6}$$

The amount of heat dissipated by the condenser (554 W) is calculated similarly as follows:

$$\dot{Q}_{cond} = \dot{m} \cdot (h_4 - h_6) \tag{A.7}$$

The energy storage requirement (in the form of fuel carried by the user) is then found by multiplying the power requirement ($\dot{W}_{comp}$ = 89 W, $\dot{W}_{fan}$ = 22 W) by the amount of time the system is intended to operate:

$$E_{req} = \left(\dot{W}_{comp} + \dot{W}_{fan}\right) \cdot t \tag{A.8}$$

where t is the mission duration of the system (8 hours), which is user specified. The resulting energy storage requirement E_{req} is 886 W-hr. The coefficient of performance

(COP) of the cycle is found using the total work input of 111 W along with the evaporator heat removal rate of 465 W as shown following:

$$COP = \frac{\dot{Q}_{evap}}{\dot{W}_{total}} \tag{A.9}$$

This resulted in a calculated COP of 4.2.

APPENDIX B – CONDENSER DESIGN

B.1 Condenser Description

The design of the condenser required for the refrigerant heat rejection is described in this Appendix. The required heat duty of the condenser ($\dot{Q}_{cond}$ = 554 W) was determined in Appendix A, which modeled the overall thermodynamic cycle. The required mass flow rate of refrigerant $\dot{m}$ was found to be 3.04×10^{-3} kg/s. A schematic of a section of the condenser used for this analysis is shown in Figure B.1. The condenser consists of microchannel extruded aluminum tubes brazed to multi-louvered fins.

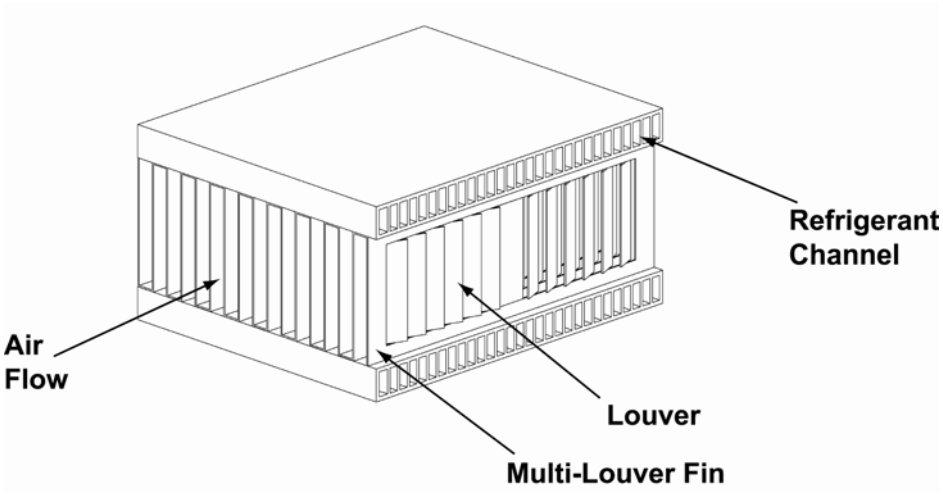

Figure B.1 Representative Condenser Section

The fins were modeled as parallel rectangular channels (Figure B.2) for simplicity in computing the respective flow and surface areas.

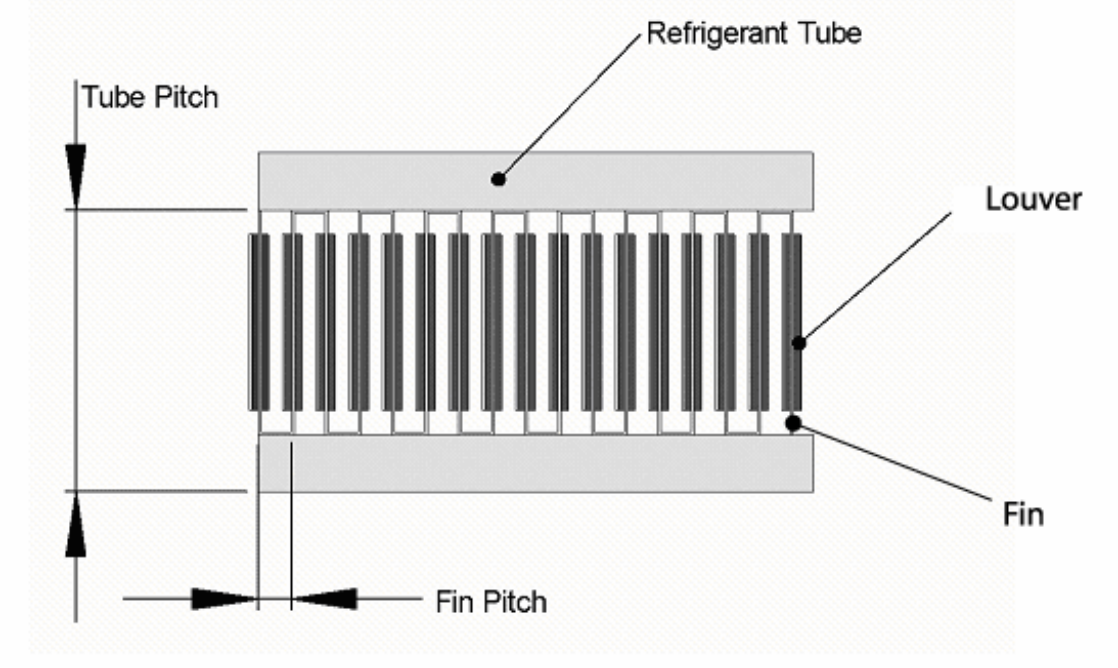

Figure B.2 Condenser Geometry Approximation

B.2 Condenser Geometry

Table B.1 Condenser Geometry

Tube Side		Fin		Louver	
Outside width	15 mm	Fin pitch	1.2 mm	Louver angle	23°
Outside height	2.1 mm	Fin height	8.2 mm	Louver pitch	1.6 mm
Wall thickness	0.5 mm	Fin thickness	0.1 mm	Louver length	6.4 mm
Tube length	0.2 m	Fin depth	15 mm		
Number of tubes	20				
Number of webs	9				
Web thickness	0.3 mm				
Tube pitch	10.2 mm				

The nominal overall width and height were selected for the condenser based on the desired size and the maximum cross-sectional profile of the portable cooling system. The overall width (w_{total} = 0.20 m) and height (h_{total} = 0.19 m) of the condenser can be represented as follows:

$$w_{total} = \left(N_f - 1\right) \cdot F_P \tag{B.1}$$

$$h_{total} = \left(N_t - 1\right) \cdot t_p \tag{B.2}$$

where N_f is the number of fins (167), F_p is the fin pitch (1.2 mm), N_t is the number of tube rows (20), and t_p is the tube pitch (10.2 mm).

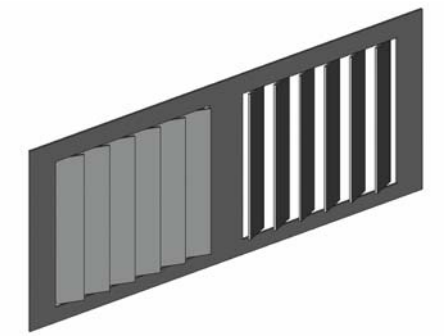

Figure B.3 Condenser Multi-Louver Fin

Figure B.3 shows a single fin with louvers along the direction of air flow, whereas Figure B.4 displays the cross-section of a multi-louver fin along with the geometrical dimensions characterizing the louvers and used in the following equations.

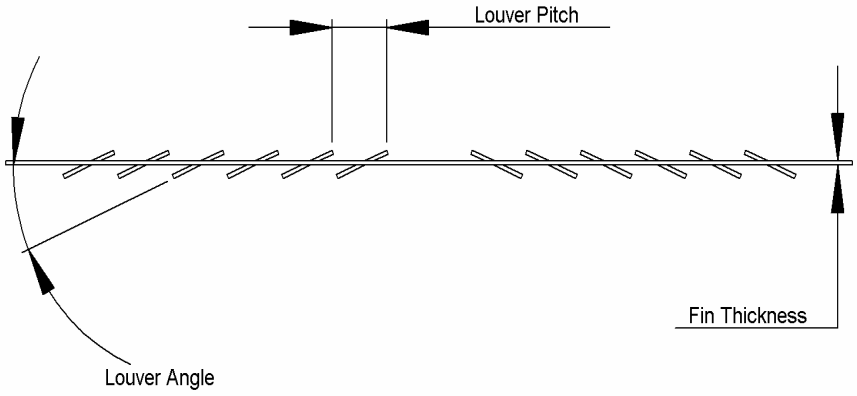

Figure B.4 Multi-Louver Fin Cross-Section

B.3 Air-Side Calculations

The air-side heat transfer area for one unit cell and for the whole heat exchanger are calculated as follows:

$$A_{unit} = 2 \cdot \left(t_p - t_{tube} + F_p - 2 \cdot \delta_{fin} \right) F_d \tag{B.3}$$

$$A_{total} = A_{unit} \cdot \left(N_f - 1 \right) \left(N_t - 1 \right) \tag{B.4}$$

where t_{tube} is the thickness of the refrigerant tube (2.1 mm), δ_{fin} represents the fin thickness (0.1 mm), and F_d is the air flow depth through the condenser (15 mm). The resulting surface area for one unit cell A_{unit} and for the entire condenser A_{total} are 2.75×10^{-4} m² and 0.866 m², respectively. The frontal area of the condenser A_{fr} can be obtained using:

$$A_{fr} = w_{total} \cdot h_{total} \tag{B.5}$$

This resulting frontal area is 0.039 m². The ratio of the frontal air flow area A_{fr} to the free flow area A_c is given by:

$$\frac{A_{fr}}{A_c} = \frac{t_p \cdot F_p}{t_p \cdot F_p - \left(t_{tube} + \delta_{fin} \right) F_p - H \cdot \delta_{fin}} \tag{B.6}$$

where H is the fin height (8.2 mm); resulting in a ratio of 0.72 with a free flow area A_c of 0.028 m². In the above equation, the second and third terms in the denominator account for the area blocked by the tube and the fin. This is used to compute the air flow velocity in the heat exchanger core from the frontal air velocity.

B.3.1 Air-Side Heat Transfer

The following empirical correlations proposed by Kim and Bullard (2002) for the so-called j and f factors were used for the calculation of air-side heat transfer and pressure drop:

$$j_{factor} = \mathrm{Re}_{Lp}^{-0.487}\left(\frac{L_\alpha}{90}\right)^{0.257}\left(\frac{F_p}{L_p}\right)^{-0.13}\left(\frac{H}{L_p}\right)^{-0.29}\left(\frac{F_d}{L_p}\right)^{-0.235}\left(\frac{L_1}{L_p}\right)^{0.68}\left(\frac{t_p}{L_p}\right)^{-0.279}\left(\frac{\delta_f}{L_p}\right)^{-0.05} \quad \text{(B.7)}$$

$$f_{factor} = \mathrm{Re}_{Lp}^{-0.781}\left(\frac{L_\alpha}{90}\right)^{0.444}\left(\frac{F_p}{L_p}\right)^{-1.682}\left(\frac{H}{L_p}\right)^{-1.22}\left(\frac{F_d}{L_p}\right)^{0.818}\left(\frac{L_1}{L_p}\right)^{1.97} \quad \text{(B.8)}$$

where Re_{Lp} is the Reynolds number based on the louver pitch (L_p = 1.6 mm) for an air mass flow rate of 0.12 kg/s, L_α is the louver angle (23°), and L_1 is the louver length from top to bottom (6.4 mm). The resulting f factor and j factor are 0.122 and 0.027, respectively. Re_{Lp} is calculated as:

$$\mathrm{Re}_{Lp} = \frac{V_c \cdot L_p}{\nu_{air}} \quad \text{(B.9)}$$

using the air velocity at the smallest cross-sectional flow area (V_c = 3.8 m/s) in conjunction with the louver pitch and the air viscosity (ν_{air} = 1.74×10^{-5} m²/s) to yield Re_{Lp} = 340. The air velocity V_c in this equation is given by:

$$V_c = \frac{\dot{V}_{air}}{A_c} \quad \text{(B.10)}$$

where $\dot{V}_{air}$ is the volumetric flow rate of the air through the condenser (0.106 m³/s) and A_c is the smallest cross-sectional area for airflow (A_c = 0.028 m², Equation B.6).

The air-side convective heat transfer coefficient h_{air} is calculated from the j factor as follows:

$$h_{air} = \frac{j_{factor} \cdot \rho_{m,air} \cdot V_c \cdot c_{p,air}}{\mathrm{Pr}_{air}^{2/3}} \tag{B.11}$$

where $c_{p,air}$ is the specific heat of air (1007 J/kg-K), Pr_{air} is 0.735 and $\rho_{m,air}$ is the mean density of the air (1.12 kg/m³) flowing through the condenser, evaluated at the mean air temperature of 40°C. This results in an air-side convection coefficient of 145 W/m²-K.

The total fin area A_{fin} and tube area A_{base} used to determine the effective area of the condenser are calculated as:

$$A_{fin} = 2 \cdot H \cdot F_d \left(N_t - 1 \right) N_f \tag{B.12}$$

$$A_{base} = 2 \cdot \left(l_{tube} - N_f \cdot \delta_{fin} \right) F_d \cdot N_t \tag{B.13}$$

where H is the fin height (8.2 mm) and l_{tube} is the length of one tube (0.2 m). This results in a fin area of 0.78 m² and a base area of 0.10 m². The effective area of heat transfer for the condenser is given as:

$$A_{effective} = A_{base} + \eta_{fin} \cdot A_{fin} \tag{B.14}$$

where η_{fin} is the fin efficiency and is modeled as a straight fin with a uniform cross section and an adiabatic tip, which corresponds to the centerline of the fin, and is calculated as:

$$\eta_{fin} = \frac{\tanh mL}{mL} \tag{B.15}$$

where L is half the fin height (4.1 mm) and m is the fin parameter calculated as:

$$m = \sqrt{\frac{h_{air} \cdot P}{k \cdot A_c}} \tag{B.16}$$

where P is the fin perimeter (30.2 mm), k is the thermal conductivity of aluminum (238 W/m-K) and A_c is the cross-sectional area of the fin (1.5×10^{-6} m²). This results in a value of m of 111 m^{-1}, which gives a fin efficiency of 94 percent. Therefore, the resulting effective area of the condenser is 0.83 m², which in turn yields a conductance ($h_{air}A_{eff}$) of 120 W/K.

B.3.2 Air-Side Pressure Drop

The air-side condenser pressure drop ΔP_{air} is obtained using the f factor (f = 0.122) from Kim and Bullard (2002) as follows:

$$\Delta P_{air} = f_{factor} \frac{A_{total}}{A_c}\left(\frac{\rho_{m,air} \cdot V_c^{\,2}}{2}\right) \tag{B.17}$$

where V_c is the velocity of the air flowing through the condenser (3.8 m/s), A_c is 0.028 m² and A_{total} is 0.866 m². The resulting pressure drop is 30.5 Pa, which is used to calculate the required input work for the fan as follows:

$$\dot{W}_{fan} = \frac{\dot{V}_{air} \cdot \Delta P_{air}}{\eta_{fan}} \tag{B.18}$$

where η_{fan} is the fan efficiency, assumed to be 0.15 for this calculation. The resulting fan input work is 22 W. The effect of varying the fan efficiency was examined using the system model and was found to have negligible effect on the value of the optimum air flow rate required. The system model predicted that the optimum air flow rate increased slightly with increasing fan efficiency, as would be expected. A low fan efficiency was assumed in order to account for the flow constriction leading up to the fan and lack of smoothed edges inherent to the shroud fabricated in-house.

B.4 Refrigerant-Side Heat Transfer and Pressure Drop

Due to the use of the microchannel geometry for the condenser refrigerant side, the relative heat transfer resistance of the internal two-phase refrigerant flow is minor compared to the air-side resistance, as shown in the following section.

The two-phase heat transfer coefficient h_{tpm} for the refrigerant flowing through the condenser channels is calculated using the Shah (1979) correlation. The mass flux of refrigerant (247 kg/s-m²) is given by:

$$\dot{m}_{flux} = \frac{\dot{m}}{A_{channel}} \tag{B.19}$$

where the mass flow rate of refrigerant is 3.04×10^{-3} kg/s, as determined in Appendix A.

The hydraulic diameter D_h is given by:

$$D_h = \frac{4 \cdot A_{channel}}{P_{channel}} \tag{B.20}$$

where $A_{channel}$ and $P_{channel}$ are the individual channel flow area (1.2×10^{-6} m²) and perimeter (4.44×10^{-3} m), respectively. The resulting hydraulic diameter is 1.1×10^{-3} m. The Reynolds number Re_{Liq} is for the refrigerant flow, assuming the entire flow is in the liquid phase and is given by:

$$\mathrm{Re}_{Liq} = \frac{\dot{m}_{flux} \cdot D_h}{\mu_L} \tag{B.21}$$

This results in a Reynolds number Re_{Liq} of 1844. The corresponding liquid-phase coefficient h_L is calculated as follows:

$$h_L = \frac{0.023 \cdot \mathrm{Re}_{Liq}^{\ 0.8}\, \mathrm{Pr}_L^{\ 0.4}\, k_L}{D_h} \tag{B.22}$$

where Pr_L and k_L are the liquid phase Prandtl number (Pr_L = 3.16) and thermal conductivity (k_L = 0.072 W/m-K), respectively. The average heat transfer coefficient was determined by setting the quality equal to 0.5 for this order of magnitude analysis as follows:

$$h_{tpm} = h_L \cdot \left[(1-x)^{0.8} + \frac{3.8 \cdot x^{0.76} \cdot (1-x)^{0.04}}{p_r^{0.38}} \right] \tag{B.23}$$

where h_L is the heat transfer coefficient (974 W/m²-K) with the entire refrigerant flowing as a liquid and p_r is the ratio of the refrigerant pressure to the critical pressure (p_r = 0.2934). This results in a mean two-phase flow convection coefficient of 3945 W/m²-K.

Using the calculated internal two-phase flow heat transfer coefficient (3945 W/m²-K) and the total internal tube area (0.177 m², assuming a fin efficiency of 100 percent), the tube-side conductance ($h_{tpm}A_{total,int}$) is 698 W/K, compared to the corresponding air-side conductance of 120 W/K. Thus, the condenser size is determined primarily by the air-side thermal resistance.

The internal frictional pressure drop for the condenser (22.5 kPa) can be estimated using the following correlations from Lockhart and Martinelli (1949):

$$\Delta p_{cond} = \left(\frac{\Delta p_F}{\Delta z} \right) \cdot L_{cond} \tag{B.24}$$

In this approximate analysis, the pressure gradient is assumed to be constant throughout the length of the condenser (L_{cond} = 4.0 m) and is given as:

$$-\frac{\Delta p_F}{\Delta z} = \phi_L^{\,2} \cdot \left(\frac{\Delta p_F}{\Delta z} \right)_L \tag{B.25}$$

where ϕ_L^2 is the two-phase multiplier to the single-phase liquid pressure drop (ϕ_L^2 = 49.4) and is calculated as follows:

$$\phi_L^2 = 1 + \frac{C}{X} + \frac{1}{X^2} \tag{B.26}$$

C is a constant based on the type of flow (C = 12), whether turbulent or viscous, for the liquid and gas phases and X is calculated as:

$$X = \left(\frac{\left(\frac{\Delta p_F}{\Delta z} \right)_L}{\left(\frac{\Delta p_F}{\Delta z} \right)_G} \right)^{1/2} \tag{B.27}$$

This results in a value of X of 0.31. The liquid pressure gradient and gaseous pressure gradient are then calculated using the following equations:

$$-\left(\frac{\Delta p_F}{\Delta z} \right)_L = \frac{2 \cdot f_L \cdot \dot{m}_{flux}^2 \cdot (1-x)^2}{D_h \cdot \rho_L} \tag{B.28}$$

$$-\left(\frac{\Delta p_F}{\Delta z} \right)_G = \frac{2 \cdot f_G \cdot \dot{m}_{flux}^2 \cdot x^2}{D_h \cdot \rho_G} \tag{B.29}$$

where x is the quality of the refrigerant, taken here as 0.5 to represent the entire condenser. The friction factors f_L and f_G are given by:

$$f_L = \frac{16}{\mathrm{Re}_L} \tag{B.30}$$

$$f_G = 0.079 \cdot \mathrm{Re}_G^{-0.25} \tag{B.31}$$

The laminar friction factor expression is used for the liquid phase above because the liquid phase is in laminar flow. The friction factors for the liquid and gaseous phases

were 0.012 and 0.007, respectively. The corresponding Reynolds numbers for the liquid and gas phase flows are as follows:

$$\mathrm{Re}_L = \frac{\dot{m}_{flux} \cdot (1-x) \cdot D_h}{\mu_L} \tag{B.32}$$

$$\mathrm{Re}_G = \frac{\dot{m}_{flux} \cdot x \cdot D_h}{\mu_G} \tag{B.33}$$

The Reynolds numbers for the liquid and gaseous phase were 1356 and 15,464, respectively.

B.5 Condenser Selection

From these analyses, the resulting overall heat transfer coefficient (UA) is calculated as follows:

$$UA = \left(\frac{1}{h_{air} \cdot A_{eff}} + \frac{1}{h_{tpm} \cdot A_{total,int}} \right)^{-1} \tag{B.34}$$

The resulting overall heat transfer coefficient is 100 W/K (neglecting the thermal resistance of the wall). The condenser heat rejection can be calculated as follows:

$$\dot{Q}_{condener} = UA \cdot LMTD \tag{B.35}$$

where LMTD refers to the log-mean temperature difference between the air and the refrigerant and is given by:

$$LMTD = \frac{\Delta T_2 - \Delta T_1}{\ln\left(\frac{\Delta T_2}{\Delta T_1}\right)} \tag{B.36}$$

where ΔT_1 and ΔT_2 are the temperature differences at the condenser inlet (8.3°C) and outlet (3.7°C), respectively, between the refrigerant and the air:

$$\Delta T_1 = T_{refg} - T_{air,i} \tag{B.37}$$

$$\Delta T_2 = T_{refg} - T_{air,o} \tag{B.38}$$

The refrigerant temperature is a constant value (46°C), as it is undergoing phase change at constant pressure (assumed to be constant for this calculation). The air inlet and outlet temperatures are 37.7°C and 42.3°C, respectively. This yields an LMTD of 5.7°C, and results in a total heat rejection from the condenser of 570 W, which is approximately equal to the required heat rejection of 554 W, as determined in Appendix A. For testing purposes, a condenser similar in geometry to the condenser modeled here was selected because it was readily available.

APPENDIX C – EVAPORATOR MODELING

C.1 Evaporator Description

The evaporator consists of a garment worn in contact with the human body to perform the necessary cooling for personal comfort while in a high heat stress environment. As shown in Figure C.1, the garment is made of three layers including the insulation, the foil and the refrigerant tube layer.

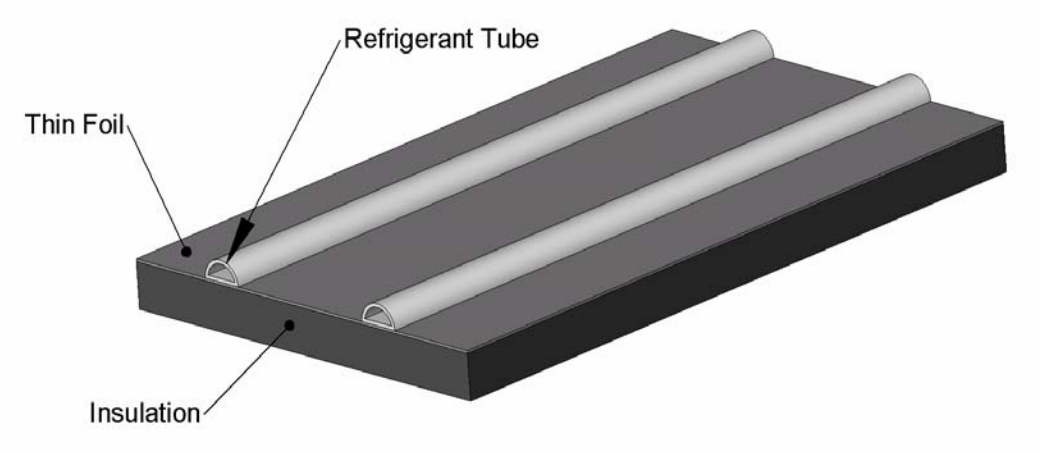

Figure C.1 Representative Section of Wearable Evaporator Garment

The semi-circular tubes carry the refrigerant as it removes heat from the body while it evaporates. The foil layer serves as a fin to remove heat from a larger area and transfer it to the refrigerant tubes. For this analysis, an aluminum foil was chosen due to its high thermal conductivity and low weight.

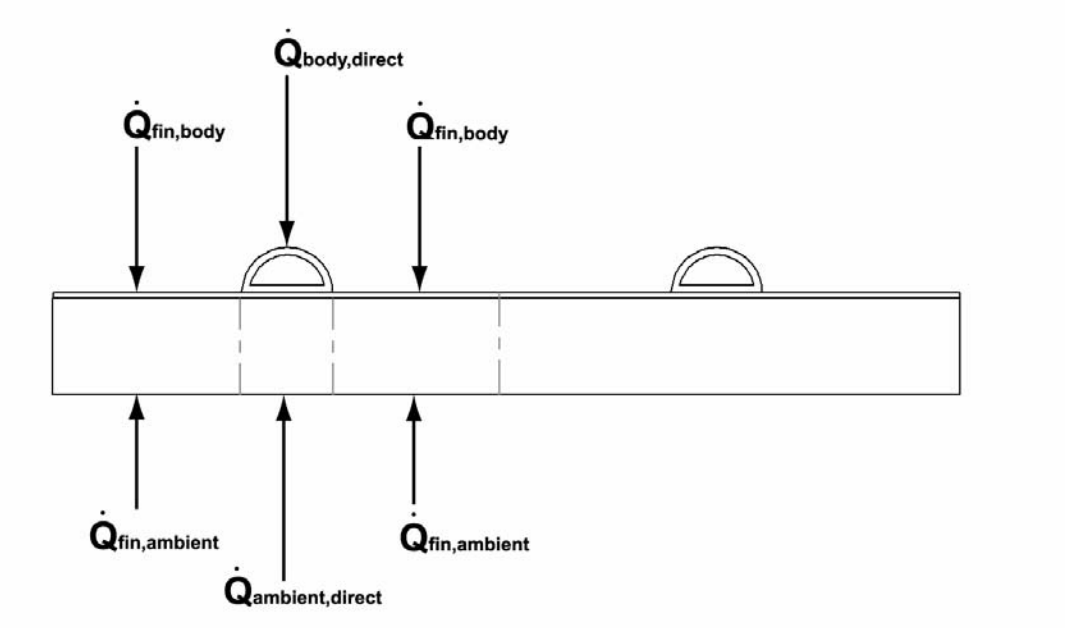

Figure C.2 Heat Transfer to Evaporator

C.2 Energy Balance

As shown in Figure C.2, the total thermal energy absorbed by the wearable evaporator ($\dot{Q}_{evap}$ = 465 W) is the sum of the dissipated body heat ($\dot{Q}_{body}$ = 400 W) and the heat gain from the environment ($\dot{Q}_{ambient}$ = 65 W); both are absorbed by the refrigerant in the tube through two separate routes. One route is the direct transfer to the tube, whereas the other is an indirect route where heat is transferred to the tube via the fin. The heat transfer modes can be written as the sum of the direct heat transfer and the fin heat transfer:

$$\dot{Q}_{evap} = \dot{Q}_{body,direct} + \dot{Q}_{ambient,direct} + 2 \cdot \left(\dot{Q}_{fin,body} + \dot{Q}_{fin,ambient} \right) \tag{C.1}$$

where $\dot{Q}_{body,direct}$ (40 W) and $\dot{Q}_{ambient,direct}$ (5 W) are the heat transfer from the body and the ambient directly to the tube, respectively, and $\dot{Q}_{fin,body}$ (180 W) and $\dot{Q}_{fin,ambient}$ (30 W) are the heat transfer from the body and the ambient to the fin on one side of the tube,

respectively. It should be noted that the control volume extends from the fin centerline to fin centerline between adjacent tubes, hence the multiplication by two for the fin heat transfer modes. One dimensional heat transfer through the insulation layer is assumed, as well as a constant surface temperature for the external surface of the insulation (35.5°C); the surface temperature calculation is shown later.

$\dot{Q}_{body,direct}$ and $\dot{Q}_{ambient,direct}$ are calculated as follows:

$$\dot{Q}_{body,direct} = h_{internal} \cdot A_{tube,proj} \cdot \left(T_{skin} - T_{tube}\right) \tag{C.2}$$

$$\dot{Q}_{ambient,direct} = \frac{k_{ins}}{t_{ins}} \cdot A_{tube,proj} \cdot \left(T_{surface} - T_{tube}\right) \tag{C.3}$$

where $h_{internal}$ (148 W/m²-K) is the effective heat transfer coefficient between the body and the garment interior surface, which is a combination of convection heat transfer and conduction, as the evaporator is in partial contact with the skin. T_{skin} is the surface temperature of the skin (29.4°C), T_{tube} is the temperature of the tube (27.3°C), k_{ins} is the thermal conductivity (0.03 W/m-K) of the insulation, t_{ins} is the thickness of the insulation (6.4 mm), and $T_{surface}$ is the external surface temperature of the insulation (35.5°C) and is assumed to be constant over the entire surface. The tube surface area is modeled as the projected area of the tube exposed to the interior of the cooling garment and is given by:

$$A_{tube,proj} = l_{tube} \cdot D_{tube} \tag{C.4}$$

where l_{tube} (32.9 m) and D_{tube} (4 mm) are the total length and diameter of the tubing, respectively. Using the projected tube surface area of the semi-circular region ($A_{tube,proj}$ = 0.132 m²), the heat transfer is modeled and calculated assuming one-dimensional heat transfer across the resulting area.

The total heat transfer to the foil is calculated by modeling it as a fin with an adiabatic tip (which corresponds to the centerline between adjacent tubes). The fin heat transfer was calculated by solving the differential equation using a differential element as shown in Figure C.3.

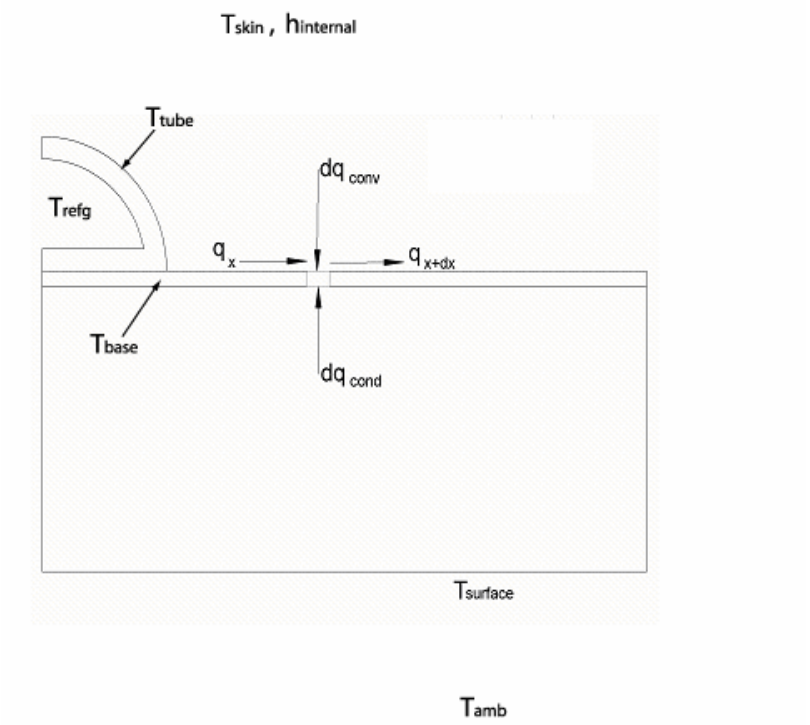

Figure C.3 Differential Element of Evaporator Fin

Each side of the fin has a unique temperature difference, as well as heat transfer mode. On the external side, heat is transferred from the ambient to the insulation first by convection and radiation to the surface, then by conduction through the insulation before reaching the fin. On the internal side, the body gives off heat and it is transferred to the fin by convection and possibly conduction from the body, depending on the amount of contact. The internal portion is given an effective heat transfer coefficient $h_{internal}$ to model this. The resulting equation is:

$$\dot{Q}_{fin} = m \cdot k_{foil} \cdot t_{foil} \cdot l_{tube} \cdot \tanh(m \cdot L_{fin}) \left(T_{eff} - T_{base} \right) \tag{C.5}$$

where m is essentially the square root of the ratio of the resistance of the heat transfer to the fin from the surroundings compared to the resistance of heat transfer through the fin and is given as:

$$m = \left(\frac{k_{ins} + h_{internal} \cdot t_{ins}}{k_{foil} \cdot t_{ins} \cdot t_{foil}} \right)^{1/2} \tag{C.6}$$

and T_{eff} is an effective temperature of the surroundings (29.6°C). An effective temperature has to be used to represent the surroundings because the two sides are at different temperatures and have different heat transfer modes:

$$T_{eff} = \frac{k_{ins} \cdot T_{surf} + h_{internal} \cdot t_{ins} \cdot T_{skin}}{k_{ins} + h_{internal} \cdot t_{ins}} \tag{C.7}$$

L_{fin} (25.4 mm) is the distance from the edge of the tube to the centerline between the adjacent refrigerant tube and t_{foil} is the foil thickness (0.35 mm).

The temperature profile of the fin is given by:

$$T(x) = \left(T_{base} - T_{eff} \right) \left(\cosh\left(m \cdot x \right) - \tanh\left(m \cdot L_{fin} \right) \sinh\left(m \cdot x \right) \right) + T_{eff} \tag{C.8}$$

To determine the total required length of tubing in the evaporator (32.9 m), the following equation was used:

$$l_{tube} = \frac{A_{skin}}{P_{tube,evap}} \tag{C.9}$$

where A_{skin} (1.8 m²) is the internal surface area of the cooling garment and $P_{tube,evap}$ is the evaporator tube pitch (54.8 mm) and is determined by:

$$P_{tube,evap} = D_{tube} + 2 \cdot L_{fin} \tag{C.10}$$

The tube pitch is determined by the foil temperature profile between the tubes. Ideally, the entire fin would be at constant temperature to maximize heat transfer, however due to heat gain from the body and the environment, the foil temperature increases with increasing distance from the nearest tube. The tubes are spaced close enough together to prevent the centerline temperature from reaching too high of a value ($\Delta T \sim 1°C$), which results in a foil width of approximately 0.05 meters. The resulting temperature profile of the foil is shown in Figure C.4.

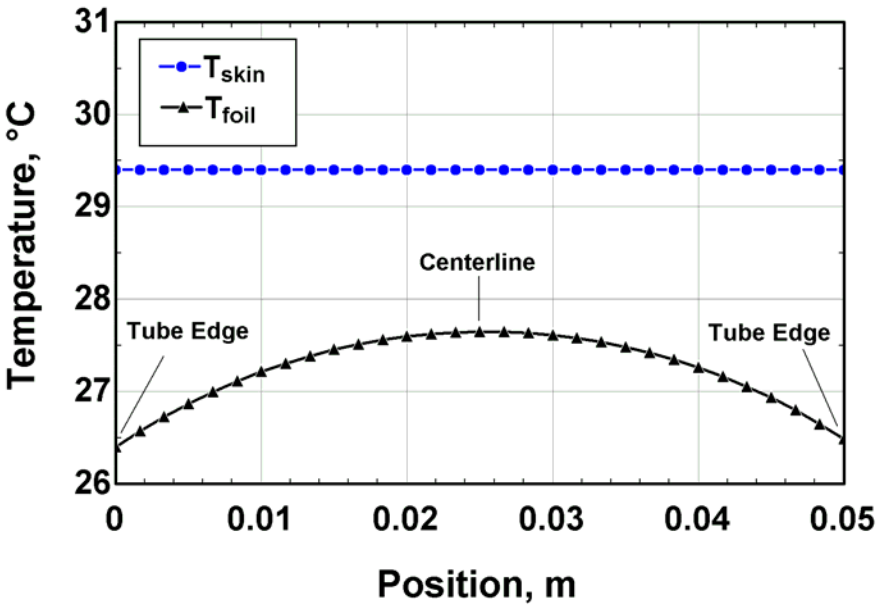

Figure C.4 Foil Temperature Profile

C.3 Heat Gain from the Environment

Performing a surface energy balance on the external surface of the insulation, the total heat gain from the environment to the evaporator is equal to the sum of the radiation and convection heat gains. This can be used to compute the external surface temperature of the insulation in conjunction with the equations for heat gain that are shown later, thus:

$$\dot{Q}_{gain} = \dot{Q}_{gain,rad} + \dot{Q}_{gain,conv} \tag{C.11}$$

where $\dot{Q}_{gain,rad}$ (26 W) and $\dot{Q}_{gain,conv}$ (39 W) are the radiative and convective heat gains, respectively, and can be computed as follows:

$$\dot{Q}_{gain,rad} = \sigma \cdot \varepsilon \cdot A_{skin} \left(\left(T_{amb} + 273.15 \right)^4 - \left(T_{surf} + 273.15 \right)^4 \right) \tag{C.12}$$

where ε is the emmissivity, conservatively assumed to be equal to unity. A_{skin} is the total surface area of the garment exterior (1.8 m²), T_{amb} is the ambient temperature (37.7°C) and T_{surf} is the temperature of the external surface of the insulation (35.6°C). The convection heat transfer is calculated as:

$$\dot{Q}_{gain,conv} = h_{conv,ext} \cdot A_{skin} \left(T_{amb} - T_{surf} \right) \tag{C.13}$$

The convection coefficient ($h_{conv,ext}$ = 10 W/m²-K) is obtained using the correlation suggested by Kuehn et al. (1998) where physical activity levels are related to the convection coefficient of the human body:

$$h_{conv,ext} = 5.7 \left(MET - 0.85 \right)^{0.39} \tag{C.14}$$

where *MET* is a unit of measure that characterizes the activity level of the human body (MET = 5.17). The activity level taken for the design of the portable air conditioner was "moderately high" physical activity, which produces approximately 400 Watts.

To quantify the total heat gain from the environment, the following calculation was used:

$$\dot{Q}_{gain} = \dot{Q}_{gain,direct} + 2 \cdot \dot{Q}_{gain,fin} \tag{C.15}$$

where $\dot{Q}_{gain,direct}$ was shown previously and $\dot{Q}_{gain,fin}$ is calculated using the temperature profile of the fin *T(x)*. The heat gain to the fin ($\dot{Q}_{gain,fin}$ = 30 W) is obtained as follows:

$$\dot{Q}_{gain,fin} = \left(\frac{k_{ins} \cdot l_{tube}}{t_{ins}}\right)\left[T_{surf} \cdot L_{fin} - \left(T_{base} - T_{eff}\right)\left(\frac{\tanh(m \cdot L_{fin})}{m}\right) - \left(T_{eff} \cdot L_{fin}\right)\right] \quad \text{(C.16)}$$

As a result of the calculations done up to this point in the analysis, the required heat transfer coefficient $h_{internal}$ is implicitly computed ($h_{internal}$ = 148 W/m²-K). This is because the closest approach temperature (CAT_L = 3°C) is used to set the temperature of the refrigerant in the tubing based on the desired temperature near the skin:

$$T_{ref} = T_{skin} - CAT_L \quad \text{(C.17)}$$

The actual value of the internal heat transfer coefficient is a function of the physical parameters of the evaporator and the human body, including the distance between the evaporator surface and the skin, the amount of direct contact between the two, and whether an interstitial fabric is used. Also, the level of activity has an impact on its value. It is not a variable that can be easily deduced, as conditions are quite unique to the situation dependant on many variables. The actual system will respond to the fluctuations in the value of $h_{internal}$ by way of changes in the CAT_L. The skin temperature will vary depending on the amount of cooling: with less cooling, the skin temperature will increase. This will then result in increased heat transfer to the refrigerant; however the CAT_L will be higher causing lower cycle performance. If $h_{internal}$ decreases in value, the refrigerant temperature will need to be decreased to allow the required amount of heat transfer from the body, which will yield a larger temperature difference CAT_L. The result of this is a lower COP of the system, because efficiency decreases with lower evaporator

temperatures. It is desirable to design the system to maintain $h_{internal}$ as high as possible, however the maximum value is limited due to the geometry of the body.

C.4 Refrigerant-Side Heat Transfer and Pressure Drop

The mass flux of refrigerant ($\dot{m}_{flux}$ = 93.5 kg/s-m²) is calculated using:

$$\dot{m}_{flux} = \frac{\dot{m}}{A_{tube} \cdot N_{tube}} \tag{C.18}$$

where $\dot{m}$ is the mass flow rate of the refrigerant (3.04×10^{-3} kg/s), A_{tube} is the cross-sectional area of one tube (2.03×10^{-6} m²), and N_{tube} is the number of tubes in parallel. For simplicity, the model assumes the flow is split into 16 equal length tubes, each approximately 2 meters long, to encompass the entire body. Based on approximate area calculations, the legs would each have 3 tubes that run the entire length down and back, the arms each have 2 tubes, and the trunk of the body has 6 tubes. This covers the entire body with tubes that are approximately 50.8 mm (2 inches) apart joined together thermally by the foil.

The internal frictional pressure drop for the evaporator can be calculated using the correlations from Lockhart and Martinelli (1949), as shown in Appendix B for the condenser analysis.

To determine the tube temperature (T_{tube} = 27.3°C), an energy balance was performed on the internal portion of the tube:

$$\dot{Q}_{evap} = h_{tpm} \cdot A_{total,in} \cdot \left(T_{tube} - T_{ref} \right) \tag{C.19}$$

where the mean internal convection coefficient for two-phase flow (h_{tpm} = 1963 W/m²-K) was used along with the inside area of the tube ($A_{,total,in}$ = 0.25 m²) to determine the

temperature of the tube (T_{tube} = 27.3°C) based on the refrigerant temperature (T_{ref} = 26.4°C). This uses the approximation that the refrigerant temperature is constant throughout the evaporator and that the heat transfer is uniform over the entire surface. The tube wall is also modeled as having a uniform temperature throughout, assuming it has negligible conductive resistance. The tube wall resistance was determined to be less than one percent of the total resistance.

The convection coefficient h_{tpm} is calculated using Shah's (1976) correlation for evaporation inside a tube:

$$h_{tpm} = \psi_s \cdot h_L \tag{C.20}$$

where ψ_s (9.01) is a function of the convection number (Co = 0.134) as follows:

$$\psi_s = 1.8 \cdot Co^{-0.8} \tag{C.21}$$

$$Co = \left(\frac{1-x}{x}\right)^{0.8} \left(\frac{\rho_G}{\rho_L}\right)^{0.5} \tag{C.22}$$

and h_L (218 W/m²-K) is the convection coefficient assuming the entire flow is in the liquid phase:

$$h_L = \frac{0.023 \cdot \mathrm{Re}_L^{0.8} \cdot \mathrm{Pr}_L^{0.4} \cdot k_L}{D_h} \tag{C.23}$$

where the fluid properties Prandtl number (Pr_L = 3.3) and thermal conductivity (k_L = 0.082 W/m-K), as well as the Reynolds number (Re_L = 221) are based on the liquid phase. The hydraulic diameter ($D_h = 1.06 \times 10^{-3}$ m) is calculated as:

$$D_h = \frac{4 \cdot A_{tube}}{P_{tube}} \tag{C.24}$$

where A_{tube} and P_{tube} are the tube area (2.03×10^{-6} m²) and perimeter (7.71×10^{-3} m), respectively.

APPENDIX D – ANALYSIS OF A REPRENTATIVE DATA POINT

D.1 Sample Point - Heat Duty Calculation

(Representative point is for Ambient Temperature = 43.5°C, Evaporator Water Temperature = 29.9°C, and Engine Speed = 13,300 RPM)

Table D.1 Measured Data

Refrigerant Cycle:	***SI Units***	***British Units***
Evaporator refrigerant inlet temperature [2]	24.9°C	76.8°F
Evaporator refrigerant outlet temperature [4]	29.1°C	84.4°F
Condenser refrigerant inlet temperature [7]	68.9°C	156.0°F
Condenser refrigerant outlet temperature [10]	50.4°C	122.7°F
Compressor refrigerant inlet temperature [5]	28.3°C	82.9°F
Compressor refrigerant outlet temperature [6]	68.9°C	156.0°F
Expansion valve refrigerant inlet temperature [11]	50.4°C	122.7°F
Expansion valve refrigerant outlet temperature [1]	24.9°C	76.8°F
Low-side refrigerant pressure [5]	663.8 kPa	96.3 psia
High-side refrigerant pressure [6]	1370 kPa	198.7 psia
Condenser Air-Side:		
Condenser air inlet temperature	43.5°C	110.3°F
Condenser air outlet temperature	46.0°C	114.8°F
Engine speed	13,300 RPM	
Evaporator Coolant-Side:		
Evaporator coolant inlet temperature	30.9°C	87.6°F

Table D.1 Measured Data (cont.)

Evaporator coolant outlet temperature	28.8°C	83.8°F
Coolant volumetric flow rate	2.555×10^{-5} m^3/s	0.405 GPM
Heater voltage	58.2 Volts	
Heater amperage	3.86 Amps	
Heater coolant inlet temperature	28.7°C	83.7°F
Heater coolant outlet temperature	30.9°C	87.6°F
Other Variables:		
Coolant	50% Prestone coolant, 50% water	
Coolant specific heat	3412 J/kg-K	Coolant Manual (Prestone, 2001)
Coolant density	1069 kg/m^3	Coolant Manual (Prestone 2001)
Coolant Volume	0.008 m^3	2.11 gallon
Room Air Temperature	25.6 °C	78.1°F

Table D.2 Thermodynamic Cycle Calculations

Eq. No	Equation	Inputs	Outputs	Reference
(1)	$\dot{Q}_{evap,heater} = V \cdot I$	V = 58.2 Volts, I = 3.86 Amps	$\dot{Q}_{evap,heater}$ = 224.7 W	
(2)	$m_{coolant} = \rho_{coolant} \cdot vol_{coolant}$	$\rho_{coolant}$ = 1069 kg/m^3, $vol_{coolant}$ = 0.008 m^3	$m_{coolant}$ = 8.552 kg	
(3)	$\dot{Q}_{storage} = m_{coolant} \cdot c_{p,coolant} \cdot \frac{-dT_{average}}{dt}$	$m_{coolant}$ = 8.552 kg, $c_{p,coolant}$ = 3412 J/kg-K, $\frac{dT_{average}}{dt} = -1.88\times10^{-4} \frac{^{o}C}{s}$	$\dot{Q}_{storage}$ = 5.5 W	
(4)	$\dot{Q}_{evap,total} = \dot{Q}_{evap,heater} + \dot{Q}_{storage}$	$\dot{Q}_{evap,heater}$ = 224.7 W, $\dot{Q}_{storage}$ = 5.5 W	$\dot{Q}_{evap,total}$ =230.2 W $\Delta\dot{Q}_{elec,coolant}$ = 19 W	
(5)	$\dot{m} = \frac{\dot{Q}_{evap,total}}{\left(h_{evap,out} - h_{evap,in}\right)}$	$\dot{Q}_{evap,total}$ = 230.2 W $h_{evap,out}$ = 268,418 J/kg, $h_{evap,in}$ = 124,082 J/kg	$\dot{m}$ = 1.595×10^{-3} kg/s	
(6)	$\dot{Q}_{cond,refrigerant} = \dot{m}\left(h_{cond,in} - h_{cond,out}\right)$	$\dot{m}$ = 1.595×10^{-3} kg/s, $h_{cond,out}$ = 124,082 J/kg, $h_{cond,in}$ = 296,405 J/kg	$\dot{Q}_{cond,refrigerant}$ = 274.8 W	
(7)	$\dot{W}_{comp} = \dot{m}\left(h_{comp,out} - h_{comp,in}\right)$	$\dot{m}$ = 1.595×10^{-3} kg/s, $h_{comp,out}$ = 296,405 J/kg, $h_{comp,in}$ = 267,606 J/kg	$\dot{W}_{comp}$ = 45.93 W	
(8)	$\eta_{comp} = \frac{h_{comp,out,isen} - h_{comp,in}}{h_{comp,out} - h_{comp,in}}$	$h_{comp,out,isen}$ = 282,790 J/kg, $h_{comp,in}$ = 267,606 J/kg, $h_{comp,out}$ = 296,405 J/kg	η_{comp} = 0.5273	

Table D.3 Air-Side Analysis

Eq. No	Equation	Inputs	Outputs	Reference
(1)	$V_{air} = a_0 \cdot rpm_{fan}{}^2 + a_1 \cdot rpm_{fan} + a_2$	$a_0 = 4.40X10^{-8}$ m/s-RPM², $a_1 = 2.19\times10^{-4}$ m/s-RPM, $a_2 = 0.0774$ m/s, $rpm_{fan} = 3800$ RPM	$V_{air} = 1.545$ m/s	Appendix E (Correlation derived from fan airflow testing.)
(2)	$A_{face} = width \cdot height$	width = 0.2223 m, height = 0.2413 m	$A_{face} = 0.05363$ m²	
(3)	$\dot{Q}_{cond,air-side} = V_{air} \cdot A_{face} \cdot \rho_{air} \cdot c_{p,air} \left(T_{air,out} - T_{air,in}\right)$	$V_{air} = 1.545$ m/s, $A_{face} = 0.05363$ m², $\rho_{air} = 1.098$ kg/m³, $c_{p,air} = 1007$ J/kg-K, $T_{air,out} = 46.0$°C, $T_{air,in} = 43.5$°C	$\dot{Q}_{cond,air-side} = 231.8$ W $\Delta\dot{Q} = 43$ W (between two methods of calculating)	
(4)	$rpm_{engine} = rpm_{fan} \cdot ratio_{gear1}$	$rpm_{fan} = 3800$ RPM, $ratio_{gear1} = 3.5$	$rpm_{engine} = 13{,}300$ RPM	
(5)	$rpm_{compressor} = \frac{rpm_{fan}}{ratio_{gear2}}$	$rpm_{fan} = 3800$ RPM, $ratio_{gear2} = 4.4$	$rpm_{compressor} = 863.6$ RPM	

Table D.4 Coolant-Side Analysis

Eq. No	Equation	Inputs	Outputs	Reference
(1)	$\dot{m}_{coolant} = \rho_{coolant} \cdot v\dot{o}l_{coolant}$	$\rho_{coolant}$ = 1069 kg/m^3, $v\dot{o}l_{coolant}$ = 2.555×10^{-5} m^3/s	$\dot{m}_{coolant}$ = 0.02731 kg/s	
(2)	$\dot{Q}_{evap,coolant} = \dot{m}_{coolant} \cdot c_{p,coolant}\left(T_{coolant,in} - T_{coolant,out}\right) + m_{coolant} \cdot c_{p,coolant} \cdot \frac{-dT_{average}}{dt}$	$\dot{m}_{coolant}$ = 0.02731 kg/s, $c_{p,coolant}$ = 3412 J/kg-K, $T_{coolant,in}$ = 30.9°C, $T_{coolant,out}$ = 28.8°C, $m_{coolant}$ = 8.552 kg, $\frac{dT_{average}}{dt}$=-1.88×10^{-4} $\frac{^oC}{s}$	$\dot{Q}_{evap,coolant}$ = 210.7 W $\Delta\dot{Q}$ = 19.5 W (between two methods of calculating)	

Table D.5 System Performance Analysis

Eq. No	Equation	Inputs	Outputs	Reference
(1)	$\dot{E}_{fuel} = \dot{m}_{fuel} \cdot LHV$	$\dot{m}_{fuel}$ = 8.78×10^{-5} kg/s, LHV = 1.992×10^7 J/kg	$\dot{E}_{fuel}$ = 1749 W	
(2)	$\eta = \frac{\dot{Q}_{evap,total}}{\dot{E}_{fuel}}$	$\dot{Q}_{evap,total}$ = 230.2 W, $\dot{E}_{fuel}$ = 1749 W	η = 0.132	

Table D.6 Error Analysis Calculation

Eq. No	Equation	Inputs	Outputs	Reference
(1)	$\dot{Q}_{evap,heater} = V \cdot I$	V = 58.2 V, I = 3.82 A	$\dot{Q}_{evap,heater}$ = 224.7 W	
(2)	$U^2_{\dot{Q}_{evap,heater}} = \left(\frac{\partial \dot{Q}_{evap,heater}}{\partial V} U_V\right)^2 + \left(\frac{\partial \dot{Q}_{evap,heater}}{\partial I} U_I\right)^2$	$\frac{\partial \dot{Q}_{evap,heater}}{\partial V}$ = 3.82 A, $\frac{\partial \dot{Q}_{evap,heater}}{\partial I}$ = 58.2 V U_v = 0.873 V, U_I = 0.0733 A	$U^2_{\dot{Q}_{evap,heater}}$ = 29.16 W²	
(3)	$\frac{\partial \dot{Q}_{evap,heater}}{\partial V} = I$	I = 3.82 A	$\frac{\partial \dot{Q}_{evap,heater}}{\partial V}$ = 3.82 A	
(4)	$\frac{\partial \dot{Q}_{evap,heater}}{\partial I} = V$	V= 58.2 V	$\frac{\partial \dot{Q}_{evap,heater}}{\partial I}$ = 58.2 V	
(5)	$U_{\dot{Q}_{evap,heater}} = \sqrt{\left(I \cdot U_V\right)^2 + \left(V \cdot U_I\right)^2}$	I = 3.82 A, V= 58.2 V, U_v = 0.873 V, U_I = 0.0733 A	$U_{\dot{Q}_{evap,heater}}$ = 5.4 W	

Table D.7 Ambient Heat Gain/Loss Calculation

Eq. No	Equation	Inputs	Outputs	Reference
(1)	$ID_{ins} = OD_{tube}$	OD_{tube} = 9.5 mm	ID_{ins} = 9.5 mm	
(2)	$OD_{ins} = ID_{ins} + 2 \cdot t_{ins}$	ID_{ins} = 9.5 mm, t_{ins} = 25.4 mm	OD_{ins} = 60.3 mm	
(3)	$ID_{tube} = OD_{tube} - 2 \cdot t_{wall}$	OD_{tube} = 9.5 mm, t_{wall} = 1.6 mm	ID_{tube} = 6.4 mm	
(4)	$A_{surf,evap,in} = L \cdot \pi \cdot OD_{ins}$	L = 0.3556 m, OD_{ins} = 60.3 mm	$A_{surf,evap,in}$ = 0.06739 m²	
(5)	$Ra_D = \frac{g \cdot \beta (T_{inf} - T_s) OD_{ins}^3}{\nu_{air} \cdot \alpha_{air}}$	g = 9.8 m/s², $\beta = 3.348 \times 10^{-3}$ 1/K, T_{inf} = 25.6°C, T_s = 25.4°C (T_s determined iteratively) OD_{ins} = 60.3 mm, $\nu_{air} = 1.589X10^{-5}$ m²/s, $\alpha_{air} = 2.250X10^{-5}$ m²/s	Ra_D = 4296	
(6)	$\overline{Nu}_D = \left\{ 0.60 + \frac{0.387 \cdot Ra_D^{1/6}}{\left[1 + (0.559/Pr_{air})^{9/16}\right]^{8/27}} \right\}^2$	Ra_D = 4296, Pr_{air} = 0.707	$\overline{Nu}_D$ = 3.591	Free convection horizontal cylinder-Churchill and Chu (1975)
(7)	$\bar{h} = \frac{\overline{Nu}_D \cdot k_{air}}{OD_{ins}}$	$\overline{Nu}_D$ = 3.591, k_{air} = 0.0263 W/m-K, OD_{ins} = 60.3 mm	$\bar{h}$ = 1.565 W/m²-K	

Table D.7 Ambient Heat Gain/Loss Calculation (cont.)

Eq. No	Equation	Inputs	Outputs	Reference
(8)	$\dot{Q}_{gain,evap,in} = \bar{h} \cdot A_{surf,evap,in}\left(T_{inf} - T_s\right) + \sigma \cdot \varepsilon \cdot A_{surf,evap,in}\left(T_{inf}{}^4 - T_s{}^4\right)$	$\bar{h}$ = 1.565 W/m²-K, $A_{surf,evap,in}$ = 0.06739 m², T_{inf} = 25.6°C, T_s = 25.4°C (T_s determined iteratively), σ = 5.67X10^{-8} W/m²-K^4, ε = 1 (assumed for this calculation)	$\dot{Q}_{gain,evap,in}$ = 0.023 W	
(9)	$R_{tube,wall} = \frac{\ln\left(OD_{tube}/ID_{tube}\right)}{2 \cdot \pi \cdot k_{tube} \cdot L}$	OD_{tube} = 9.5 mm, ID_{tube} = 6.4 mm, k_{tube} = 0.19 W/m-K, L = 0.3556 m	$R_{tube,wall}$ = 0.9551 K/W	
(10)	$R_{ins} = \frac{\ln\left(OD_{ins}/ID_{ins}\right)}{2 \cdot \pi \cdot k_{ins} \cdot L}$	OD_{ins} = 60.3 mm, ID_{ins} = 9.5 mm, k_{ins} = 0.04 W/m-K, L = 0.3556 m	R_{ins} = 20.65 K/W	
(11)	$R_{tot} = R_{tube,wall} + R_{ins}$	$R_{tube,wall}$ = 0.9551 K/W, R_{ins} = 20.65 K/W	R_{tot}= 21.61 K/W	
(12)	$\dot{Q}_{gain,evap,in} = \frac{\left(T_s - T_{evap,in}\right)}{R_{tot}}$	T_s = 25.4°C (T_s determined iteratively), $T_{evap,in}$ = 24.9°C, R_{tot}= 21.61 K/W	$\dot{Q}_{gain,evap,in}$ = 0.023 W	

APPENDIX E – FAN CORRELATION

E.1 Fan Measurements

The heat rejection from the condenser was calculated in two ways. One method used the entering and exiting refrigerant temperatures and pressures along with the refrigerant flow rate, as calculated from the evaporator duty. The second method used the change in the temperature of the air entering and exiting the condenser along with the air flow rate, as measured by the turbine anemometer. The details concerning the measurement of the condenser air flow are provided in this appendix.

The air velocity was measured directly in front of the condenser face using a turbine anemometer capable of averaging the readings over time. The Mannix model DCFM 8906 digital anemometer was moved across the entire face of the condenser manually. Since the anemometer had an averaging mode, the face of the condenser was traversed horizontally in three passes, then vertically in three passes. Both passes were in a serpentine manner as shown in Figure E.1. The use of the averaging feature allowed a single value of air velocity to be obtained for the particular fan speed being tested.

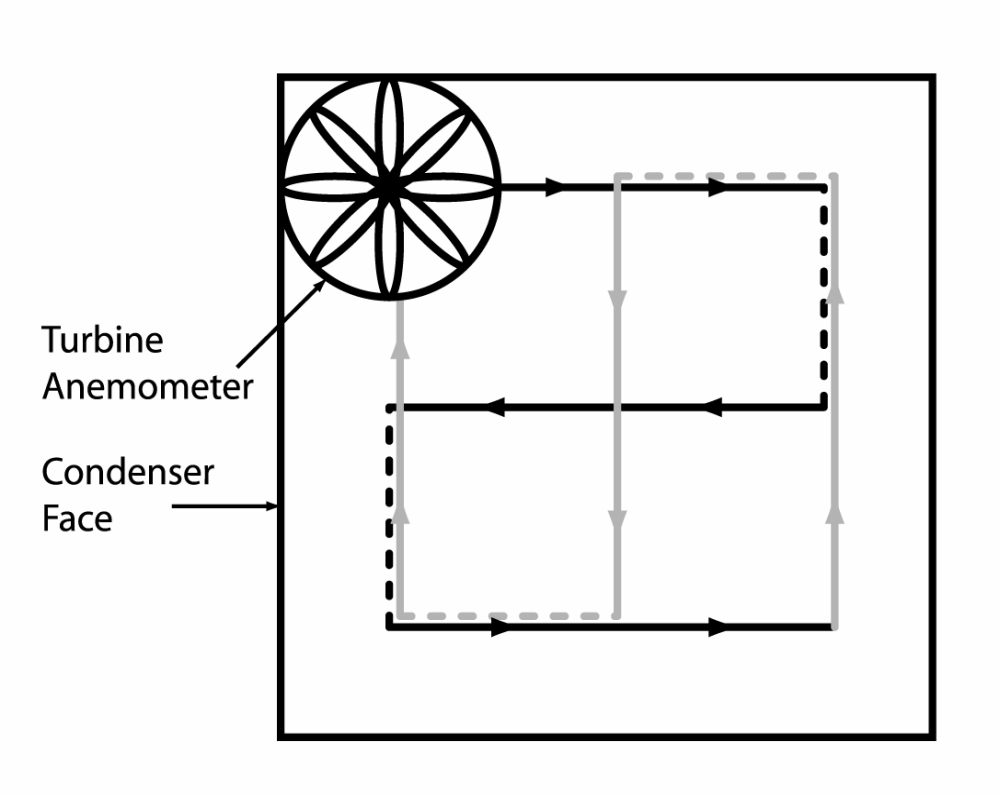

Figure E.1 Turbine Anemometer Path

The anemometer was moved as steadily as possible, taking approximately 4 seconds to traverse across the face in each pass (for a total of 6 passes as shown in Figure E.1). The dashed portions of the path were traversed as quickly as possible to minimize the effect of non-uniform coverage of the condenser face. Each measurement took approximately 24 seconds to cover the entire face area. For each value of fan speed, the measurement was performed five times. This was then averaged to obtain a single value for that particular fan speed. Table E.1 shows the measurements taken at the various fan speeds ranging from 2,400 to 4,000 RPM, which correspond to engine speeds of 8,400 to 14,000 RPM.

Table E.1 Air Flow Readings

Fan Speed (RPM)	Individual Air Velocity Readings (ft/min)					Average Velocity (ft/min)
2400	175	171	167	172	170	**171**
2460	174	179	170	176	173	**174.4**
2600	186	185	183	179	n/a	**183.3**
2800	207	192	210	210	215	**206.8**
2926	209	215	210	211	212	**211.4**
3020	216	226	210	227	223	**220.4**
3200	251	240	240	243	238	**242.4**
3400	255	267	257	276	269	**264.8**
3600	269	288	293	285	286	**284.2**
3800	310	313	311	300	309	**308.6**
4000	325	322	321	318	322	**321.6**

A graph of the average air velocities at the various fan speeds are plotted in Figure E.2. The resulting data points were then curve fit using a second order polynomial equation to

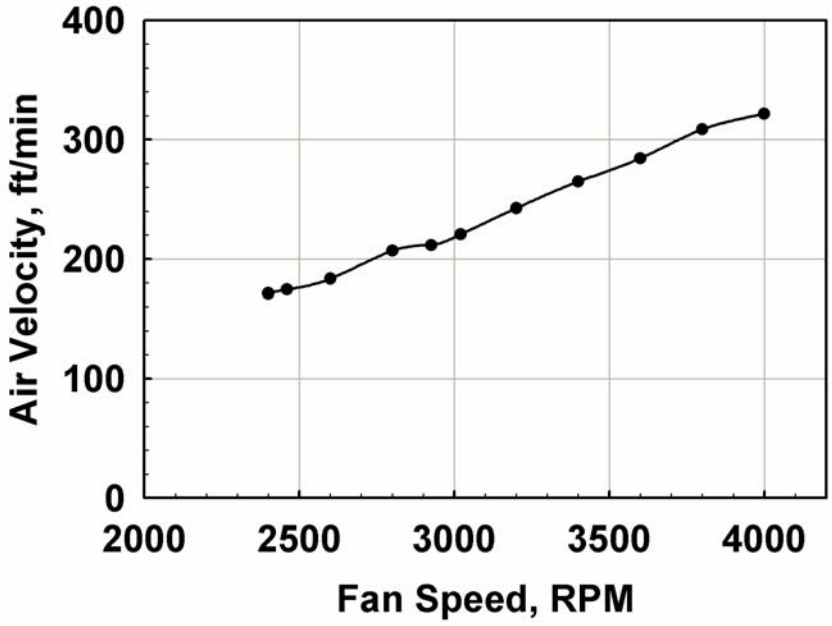

Figure E.2 Condenser Face Air Velocity

develop the following correlation for calculating the condenser air velocity (ft/min):

$$V_{air} = 8.66\times10^{-6} \cdot RPM_{fan}{}^{2} + 0.0431 \cdot RPM_{fan} + 15.24 \quad \text{(E.1)}$$

The corresponding equation for the velocity in meters per second is as follows:

$$V_{air} = 4.40\times10^{-8} \cdot RPM_{fan}{}^{2} + 2.19\times10^{-4} \cdot RPM_{fan} + 0.0774 \quad \text{(E.2)}$$

The correlation coefficient for this equation is 0.996 for air velocity over the range of fan speeds from 2400 to 4000 RPM.

REFERENCES

Bair, S. (2003). *Miniature Scale Engines*, Georgia Institute of Technology, Research Faculty.

Buchmann, I. (2001). *Batteries in a Portable World - Chemistry Comparison*, Cadex Electronics Inc.

Calm, J. M. and G. C. Hourahan (2001), "Refrigerant Data Summary," *Engineered Systems* Vol. 18(11) pp. 74-88.

Chemlink (2004). *Methanol (Methyl Alcohol)*. RC-Trucks. http://www.rc-trucks.org/rc-nitro-fuel.htm, Chemlink Consultants.

Churchill, S. W. and H. H. S. Chu (1975), "Correlating Equations for Laminar and Turbulent Free Convection from a Horizontal Cylinder," *International Journal of Heat and Mass Transfer* Vol. 18 p. 1049.

Drost, M. K. and M. Friedrich (1997), "Miniature Heat Pumps for Portable and Distributed Space Conditioning Applications," *IECEC-97 Proceedings of the Thirty-Second Intersociety Energy Conversion Engineering Conference (Cat. No.97CH6203), 27 July-1 Aug. 1997*, Honolulu, HI, USA, IEEE, pp. 1271-1274.

ElectroChem (2005). *P E M Fuel Cell Stack*, ElectroChem Inc.

Epstein, Y., Y. Shapiro and S. Brill (1986), "Comparison between Different Auxiliary Cooling Devices in a Severe Hot/Dry Climate," *Ergonomics* Vol. 29(1) pp. 41-48.

Grzyll, L. R. and W. C. Balderson (1997), "Development of a Man-Portable Microclimate Adsorption Cooling Device," *IECEC-97 Proceedings of the Thirty-Second Intersociety Energy Conversion Engineering Conference (Cat. No.97CH6203), 27 July-1 Aug. 1997*, Honolulu, HI, USA, IEEE, pp. 1646-1651.

Kim, M.-H. and C. W. Bullard (2002), "Air-Side Thermal Hydraulic Performance of Multi-Louvered Fin Aluminum Heat Exchangers," *International Journal of Refrigeration* Vol. 25(3) pp. 390-400.

Klein, S. (2004). *Engineering Equation Solver*. Madison, WI, F-Chart Software.

Kuehn, T. H., J. W. Ramsey and J. L. Threlkeld (1998). *Thermal Environmental Engineering*. 3rd Ed. Upper Saddle River, N.J., Prentice Hall.

Lockhart, R. W. and R. C. Martinelli (1949), "Proposed Correlation of Data for Isothermal Two-Phase, Two-Component Flow in Pipes," *Chemical Engineering Progress* Vol. 45(1) pp. 39-45.

Nag, P. K., C. K. Pradhan, A. Nag, S. P. Ashtekar and H. Desai (1998), "Efficacy of a Water-Cooled Garment for Auxiliary Body Cooling in Heat," *Ergonomics* Vol. 41(2) pp. 179-187.

Nunneley, S. A. (1970), "Water Cooled Garments: A Review," *Space Life Science* Vol. 2 pp. 335-360.

Pourmohamadian, N., M. L. Philpott and M. A. Shannon (2004), "Novel Connections for Non-Metallic, Flexible, Thin, Microchannel Heat Exchangers," *Proceedings of the Second International Conference on Microchannels and Minichannels (ICMM2004), Jun 17-19 2004*, Rochester, NY, United States, American Society of Mechanical Engineers, New York, NY 10016-5990, United States, pp. 977-981.

Prestone (2001). *Prestone Coolant Manual*, Honeywell International, Inc.

Rahman, M. M. (1996), "Analysis and Design of an Air-Cycle Microclimate Cooling Device," *Transactions of the ASME. Journal of Energy Resources Technology* Vol. 118(4) pp. 293-299.

Shah, M. M. (1976), "New Correlation for Heat Transfer During Boiling Flow through Pipes.," *Proc of Annual Meet, Jun 27-Jul 1 1976* Vol. 82 part 2 pp. 66-86.

Shah, M. M. (1979), "General Correlation for Heat Transfer During Film Condensation inside Pipes.," *International Journal of Heat and Mass Transfer* Vol. 22(4) pp. 547-556.

Shvartz, E. (1972), "Efficiency and Effectiveness of Different Water Cooled Suits - a Review," *Aerospace Medicine* Vol. 43(5) pp. 488-491.

Solidworks (2003). *Solidworks Student Edition*, Solidworks Corporation.

Traxxas (2004). *Traxxas Fuel Information*, Traxxas Inc.

White, M. A., S. P. Glenn, J. Hudnall, C. Rice and S. Clark (1991), "The Effectiveness of Ice- and Freon-Based Personal Cooling Systems During Work in Fully Encapsulating Suits in the Heat," *American Industrial Hygiene Association Journal* Vol. 52 pp. 127-135.